

Curriculum Vitae

Tatiana Claro da Silva

601 S. Fremont Ave. • Baltimore, MD 21230

Phone: (443) 255-8276 (mobile) and (410) 706-7059 (lab) • Fax: 410-706-5017 • E-Mail:

tsilv003@umaryland.edu

LinkedIn: <http://www.linkedin.com/pub/tatiana-claro-da-silva/18/477/610>

Education

Ph.D., Pharmaceutical Sciences Focus: Drug transporters
August 2006 – Present
Graduation October 27th 2011
Department of Pharmaceutical Sciences,
University of Maryland School of Pharmacy, Baltimore, MD
Advisor: Peter W. Swaan, PhD

M.S., Organic Chemistry March 1998 – September 2000
Universidade Federal do Rio de Janeiro (UFRJ)/ Fundação
Oswaldo Cruz (FIOCRUZ), Rio de Janeiro, Brazil
Advisors: André Luis Gemal, PharmD, PhD and Jean-Pierre
Férézou, PhD

Pharmacist March 1993 – September 1997
School of Pharmacy, Universidade Federal do Rio de Janeiro,
Rio de Janeiro, Brazil

Honors and Awards

Pharmaceutical Sciences Merit Award, University of Maryland	2009
Graduate Student of the Month of November, University of Maryland	2009
Teaching Scholarship Award, University of Maryland	2007
Rho Chi Pharmacy Honor Society	2007

Work Experience

Research assistant August 2008 – Present
Department of Pharmaceutical Sciences,
University of Maryland School of Pharmacy, Baltimore, MD
Supervisor: Peter W. Swaan, PhD
Main responsibilities:
Design and conduct experiments to study structure-activity relationships
and protein stability of the human Apical Sodium-dependent Bile Acid
Transporter (hASBT);
Instruct new students and postdocs on the techniques employed in the
lab;
Act as a technical liaison for issues related to the confocal microscope.

Research Technician August 2004 – August 2006
Protein Core Facility and Center for Vaccine Development (dual appointment), University of Maryland School of Medicine, Baltimore, MD
Supervisors: Keith G. Inman, PhD and James P. Nataro, MD, PhD
Main responsibilities:
Laboratory housekeeping; protein purification from native and recombinant systems; column chromatography (gravity and FPLC); tangential flow filtration; ammonium sulfate precipitation; orogastric mice feeding; bacteria plating and counting from culture and from stool; trans epithelial electric resistance measurements of epithelial cell lines (Caco-2, HT-29 and T84).

Research Technician August 2003 – August 2004
Department of Pharmacology and Experimental Therapeutics, University of Maryland School of Medicine, Baltimore, MD
Main responsibilities:
Animal handling (guinea pig) for research on organophosphate pesticides.

Temporary Substitute Teacher August 2002 – August 2003
University of the Vale do Rio Doce (UNIVALE), Governador Valadares/MG, Brazil
Main responsibilities:
Teaching class “Introduction to Pharmacology”.

Staff pharmacist/technical representative September 2001 – June 2002
Hallex Istar Pharmaceutical Industry, Goiânia/GO, Brazil
Main responsibilities:
Proper storage of parenteral solutions; Customer technical support.

Skills

Laboratory skills Tissue culture of various cell lines: COS-1, MDCK, CHO, CHO-Lec, Caco-2; Site-directed mutagenesis, PCR, transformation in competent bacterial cell lines, transient expression of recombinant proteins in various mammalian cell lines; Substrate uptake and kinetics; Protein biochemical modification and stability studies; Immunoblotting, Immunoprecipitation, Immunofluorescence; Trans epithelial electric resistance (TEER) measurements; Confocal Microscopy.

Computer skills Microsoft Windows and Mac OS X; Microsoft Office: Word, Excel, PowerPoint; Curve fitting and statistical analysis: Graphpad Prism 5, Kaleidagraph 4.0; Endnote; Photoshop; Basic knowledge of the Visual Molecular Dynamics (VMD) software; Odyssey imager software for quantification of Western blot bands.

Languages Portuguese (Native); English (Bilingual proficiency); Spanish (Full professional proficiency); German (Limited working proficiency); French (Elementary proficiency).

Publications

Tatiana Claro da Silva, Naissan Hussainzada, Chandra M. Khantwal, James E. Polli, Peter W. Swaan. "Transmembrane Helix I Contributes to Substrate Translocation Events and Protein Stability for the Bile Acid Transporter SLC10A2"
J. Biol. Chem. 2011 Aug 5; 286(31):27322-32. Epub 2011 Jun 6.

Hussainzada N, **Claro da Silva T**, Swaan PW. "The cytosolic half of helix III forms the substrate exit route during permeation events of the sodium/bile acid cotransporter ASBT."
Biochemistry 2009, Sep 15; 48(36): 8528-39.

Hussainzada N, **Da Silva TC**, Zhang EY, Swaan PW. "Conserved aspartic acid residues lining the extracellular loop 1 of sodium-coupled bile acid transporter ASBT Interact with Na⁺ and 7 α -OH moieties on the ligand cholestane skeleton."
J. Biol. Chem. 2008 Jul 25; 283(30):20653-63.

A. Foraker, A. Ray, **T. Claro da Silva**, L. Bareford, K. Hillgren, T. Schmittgen, P. Swaan. "Dynammin 2 regulates riboflavin endocytosis in human placental trophoblasts."
Molecular Pharmacology 2007; 72(3): 553-62

Poster presentations

"Transmembrane Helix I Contributes to Substrate Translocation Events and Protein Stability for the Bile Acid Transporter SLC10A2"

T. Claro da Silva, N. Hussainzada, C. Khantwal, J. E. Polli, P.W. Swaan
Experimental Biology, Washington, DC, April 2011
AAPS Workshop on Drug Transporters in ADME: From the Bench to the Bedside, Bethesda, MD, March 2011

"Intracellular Loop I is involved in bile acid transporter (SLC10A2) degradation by the proteasome"

T. Claro da Silva and P.W. Swaan
Experimental Biology, Washington, DC, April 2011
AAPS Workshop on Drug Transporters in ADME: From the Bench to the Bedside, Bethesda, MD, March 2011

"Amino Acid Residues in Transmembrane Domain I are Critical for the Human Apical Sodium-Dependent Bile Acid Transporter ASBT (SLC10A2) Function"

T. Claro da Silva, N. Hussainzada, C. Khantwal, P.W. Swaan
AAPS Annual Meeting and Exposition, New Orleans, Louisiana, November 2010
Congress for Students and Post Doctoral Fellows, New Orleans, Louisiana, November 2010

“Amino Acids in the Transmembrane Domain I (TM1) of the Sodium-Dependent Bile Acid Transporter ASBT (SLC10A2) are Critical for Function.”

T. Claro da Silva, N. Hussainzada, C. Khantwal, P.W. Swaan

ISSX 16th North American Regional Meeting, Baltimore, Maryland, October 2009

AAPS Workshop on Drug Transporters in ADME: From the Bench to the Bedside, Baltimore, MD, March 2009

“Riboflavin-Specific Receptor-Mediated Endocytosis in Placental Trophoblasts Accounts for 50% of the Active Absorption Mechanism.”

A. Foraker, T. Claro da Silva, A. Ray, L. Bareford, K. Hillgren, T. Schmittgen, P. Swaan

AAPS Workshop on Drug Transporters in ADME: From the Bench to the Bedside, Bethesda, MD, March 2007

Oral presentation

“The Transmembrane Domain I Of The Human Apical Sodium-Dependent Bile Acid Transporter (hASBT; SLC10A2) Contributes to Substrate Translocation Events and Protein Stability” Graduate Research Conference. University of Maryland, April 2010

Professional Associations

Student Member, American Society for Pharmacology and Experimental Therapeutics (ASPET), 2011

Student Member, American Association of Pharmaceutical Scientists (AAPS), 2007 – currently

Extracurricular Activities

Committee member, submission preparation for the AAPS25 award, 2011

Captain, indoor pick-up soccer at the UMAB URecFit gym, winter 2011

Co-captain, Pharmacy United soccer team at the University of Maryland, Baltimore, Spring and Summer 2009

President, Pharmaceutical Sciences Graduate Students Association (PGSA), 2007 – 2008

Reference

Peter W. Swaan, Ph.D.

Professor, Department of Pharmaceutical Sciences

Director, UMB Center for Nanomedicine and Cellular Delivery

University of Maryland, Baltimore

20 Penn Street, HSF2, Rm 621

Baltimore MD 21201

Tel.: (410) 706-0103 Fax. (410) 706-5017

E-mail: pswaan@rx.umaryland.edu

ABSTRACT

Title of Document: UNDERSTANDING STRUCTURE-FUNCTION RELATIONSHIPS AND PROTEIN STABILITY OF THE HUMAN APICAL SODIUM-DEPENDENT BILE ACID TRANSPORTER (ASBT, SLC10A2)

Tatiana Claro da Silva, Ph.D., 2011

Directed By: Peter W. Swaan, Ph.D.
Associate Dean for Research and Graduate Studies,
Professor and Director of the Center for
Nanomedicine and Cellular Delivery
Department of Pharmaceutical Sciences
School of Pharmacy
University of Maryland, Baltimore, USA

The apical sodium-dependent bile acid transporter (ASBT, SLC10A2) is renowned as the major bile acid transporter in the intestine. It utilizes cellular sodium gradient to actively concentrate bile acids in the enterocytes, thereby playing a key role in the enterohepatic circulation of bile acids (EHC). ASBT is a promising target for prodrug approaches aiming at improving drug bioavailability, and for drugs to treat hypercholesterolaemia, since cholesterol metabolism is induced upon bile acid depletion. Moreover, its contributing role in drug-drug interactions is rapidly emerging. Topologically, the human (hASBT) is a glycoprotein that spans the membrane bilayer seven times, oriented with an extracellular N-terminus and a cytoplasmic C-terminus ($N_{\text{exo}}/C_{\text{cyt}}$). Despite its physiological and pharmacological relevance, ASBT remains to be fully characterized at the molecular level. Here, we summarize advances made by our group and others in the quest to understand ASBT's structure-function relationships and its complex mechanism of bile acid transport. We also report our novel findings

regarding protein regions relevant for function and protein stability in the hASBT. Our observations indicate that residues located at the transmembrane 1 (TM1) play a pivotal role in hASBT function, and that Gly⁵⁰, placed at the interface of TM1 with the intracellular loop 1 (IL1), is critical for hASBT stability. Expanding our studies to IL1, we identified a cluster of amino acids comprising Cys⁵¹ – Lys⁵⁷, which are likely involved in hASBT protein stability, whereas residues downstream Lys⁵⁷ appear to be relevant for transport. We have demonstrated that successful mapping of regions implicated in hASBT's transport cycle can be achieved with a combination of site-directed mutagenesis, bile acid uptake and kinetics, sodium-activation assays and the substituted-cysteine accessibility method. Moreover, inhibition of the proteasome with MG132, and of prolyl-peptidyl isomerases with cyclosporine A and FK506, are valuable approaches to reveal the contribution of specific amino acids to hASBT stability. Finally, we integrate our data to propose an overall schematic of hASBT transport, which will contribute to a better understanding on ASBT physiology and, potentially, on other proteins in the SLC10 family.

**UNDERSTANDING STRUCTURE-FUNCTION RELATIONSHIPS AND
PROTEIN STABILITY OF THE HUMAN APICAL SODIUM-DEPENDENT
BILE ACID TRANSPORTER (ASBT, SLC10A2)**

By

Tatiana Claro da Silva

Dissertation submitted to the Faculty of the Graduate School of the
University of Maryland, Baltimore, in partial fulfillment
of the requirements for the degree of
Doctor of Philosophy
2011

© Copyright by
Tatiana Claro da Silva
2011

Dedication

To my beloved family and my dearest boyfriend, Ron Kasl, for their love and constant support.

Acknowledgements

I am highly indebted to my advisor, Dr. Peter W. Swaan, for the opportunity to work in his laboratory and for his commitment to my education and professional growth. As a great mentor, Dr. Swaan encouraged me to be creative, inquisitive and independent. He taught me that excellence is not negotiable; a value that I will take with me in my future endeavors.

I would also like to thank my committee members Dr. James E. Polli, Dr. Hongbing Wang, Dr. Yan Shu and Dr. Shiew-Mei Huang for their time and valuable input on my work. Dr. Polli, Dr. Wang and Dr. Shu always had their doors opened, and were happy to answer any questions I had. I would like to especially thank Dr. Polli for his great help with issues related with transporter kinetics, and for an enduring interest in my scientific progress. I share with Dr. Polli his view that in science, “there is never a dull moment”. I also wish to thank Dr. Huang for accepting our invitation to be a member of my dissertation committee. Her effort to accommodate her busy schedule, and generosity in sharing her knowledge are highly appreciated.

I am grateful to my labmates for providing a pleasant and productive work environment and for insightful scientific discussions. It was always great to wake up in the morning and know that I was not just going to school, but I was actually on my way to meet friends. My current labmates, Brittany Avaritt, Lisa Bareford, Joanna Pak, Dr. Robyn Moore, Dr. Hairat Sabit, Dr. Abhay Andar, Dr. Paresh Chothe and Dr. Yongmei Pan, embody the definition of teamwork, and were always ready to help me as well as each other. I would especially like to thank Robyn for generously sharing with me novels and more efficient ways to perform experiments; Hairat and Paresh for helping me with

any questions regarding drug transporters, and Abhay for giving me a fresh perspective on my work, in addition to valuable scientific and stylistic feedback on this dissertation. Brittany, in addition to my previous lab mate and friend, Dr. Debbie Sweet Goldberg, is an inspiration for excellent work ethics and responsible conduct in the laboratory.

I would also like to thank my previous labmates, Dr. Amy Foraker, Dr. Chandra Khantwal, Dr. Naissan Hussainzada, Dr. Praveen Bahaduri and Dr. Cliff Mason, for welcoming me into the laboratory and for providing a great work environment in my first years. I would like to thank Drs. Foraker and Hussainzada for the opportunity to learn with and share excellent publications with them, and Dr. Foraker for teaching me everything I know about confocal microscopy. Dr. Khantwal was generous with his time and helped me in critical moments of my training, including with troubleshooting and interpretation of intricate results, as well as by being a great friend. I extend my gratitude to Dr. Sairam Mallajosyula, Dr. Yongmei Pan and Dr. Elisabeth Denning for their valuable help with Sybyl and VMD. I appreciate the conversations with my friend Dr. Denning, which were scientifically enlightening and fun.

I wish to thank Drs. C.S. Raman and Sudha Veeraraghavan for their helpful insight on protein folding and repair, as well as membrane protein structure. I also appreciate the encouragement that I received from Dr. Alex MacKerell, who I met before joining school, and was very helpful with clarifications about the Ph.D. program and our school. Several of my great friends in the University of Maryland are current or previous members of his laboratory, including Dr. Pedro Lopes, Dr. Chayan Acharya, Dr. Prabhu Raman, Dr. Kenno Vanommeslaeghe, Dr. Chris Baker, Dr. Ashley Ringer, Dr. Shanthi, Dr. Elisabeth Denning, Jihyun Shim, and Meagan Small. I extend my gratitude

to my fellow students Lidya Stavitskaya, Vidula Kolkhatkar, Xiao Zhu, Sarice Boston, Katherine Joyner, Antonia Tolson, Maura O'Neil, Keely Pierzchalski, Jerry Yap and Zhongqi Dong as well as the post docs Gasirat Tririya, Guyian, Yue Feng, Guoyun Bai, Elisabeth Barbier and Attilio Pingitore, for their precious friendship, which helped me keep sane during the most stressful times in graduate school.

I can't be remiss about all the people that were great inspiration, and affected my decision to pursue a scientific career. Before joining our program, I worked as a lab technician at Drs. Keith Inman's and Dr. James Nataro's laboratories, at the Center for Vaccine Development (CVD). I will be forever indebted to them, especially to Dr. Inman not only for all the science that he generously shared with me, but also for being extraordinarily helpful, patient and encouraging towards my scientific growth, the improvement of my English and finally my decision to join the Ph.D. program. Dr. Nataro was an inspiration through his love for science, which was evident at lab meetings and by his enthusiasm whenever he guided me through an experiment. Dr. Daniel Weinreich, at the Department of Pharmacology and Experimental Therapeutics, and Dr. John Hamlyn, at the Department of Physiology, for helping me when I needed the most, especially with good recommendation letters and precious professional advice, for which I will be forever grateful.

I would like to extend my gratitude to all faculty, staff and fellow students that supported me during my time at the University of Maryland. Particularly, I would like to thank Mrs. Colleen Day, Mrs. Tamara Borisevich, Ms. Nicole Derr and Ms. Liyi Wu for their assistance with business and school-related paperwork, which made graduate school much more pleasurable than it would be without their help.

I extend my immense gratitude to my family, especially mom Creusa dos Reis Claro, and dad, Sérgio Vasconcellos Gonçalves Ribeiro, for their love and encouragement, and for being my safe havens. My siblings, Vanessa Claro Ribeiro, Ligia Guedes da Silva and Vinícius Guedes da Silva, for always being there for me. Also my aunts, especially my aunt Sandra dos Reis Claro for being always present in the big moments of my life, as well as my uncles and cousins. Together, they have always cheered through each landmark in my life.

Finally, I can't thank my boyfriend Ron Kasl enough. In addition to his computer expertise, from which I benefited many times, he was there for me and with me from the beginning, cheering at each accomplishment, and doing anything in his power to help me achieve my goals. His love and dedication were critical during these years, and for that I am more grateful than words can express.

Table of Contents

Dedication.....	iii
Acknowledgements.....	iv
Table of Contents.....	viii
List of Tables.....	x
List of Figures.....	xi
List of Abbreviations.....	xii
Chapter 1 The Apical Sodium-Dependent Bile-Acid Transporter (SLC10A2; ASBT) ..	1
1.1 Introduction and Brief History.....	1
1.1.1 Membrane transporters.....	1
1.1.2 The sodium-dependent bile-acid transporter (ASBT).....	2
1.2 ASBT and the Enterohepatic Circulation Of Bile Acids.....	2
1.2.1 ASBT: Discovery and Initial Studies.....	5
1.2.2 ASBT identification and cloning.....	10
1.2.3 ASBT Regulation.....	14
1.3 Bile Acid Structural Features For ASBT Recognition.....	17
1.3.1 Pharmacophore features of substrates and inhibitors: initial studies.....	17
1.3.2 Pharmacophore Features from prodrug studies.....	20
1.4 Conclusion.....	22
Chapter 2 The Post-ASBT Cloning Era: Structural Studies and the Swaan Laboratory	24
2.1 In Silico ASBT Studies.....	25
2.1.1 ASBT Pharmacophore Models.....	25
2.1.2 Protein-based ASBT Simulations: Homology Model.....	27
2.1.3 ASBT-Bile Acid Docking.....	28
2.1.4 ASBT <i>In Silico</i> Models: Conclusion.....	29
2.2 ASBT Topology: Experimental Methodologies.....	30
2.2.1 ASBT Topology: Divergent Views.....	30
2.2.2 N-glycosylation scanning mutagenesis.....	31
2.2.3 Dual Label Epitope Insertion Scanning.....	32
2.2.4 Cysteine-scanning mutagenesis.....	35
2.2.5 Substituted-Cysteine Accessibility Method (SCAM).....	35
2.2.6 Sodium Activation Experiments: Uncovering Residues Involved in Sodium Transport.....	42
2.3 Summary of hASBT Topology.....	44
Chapter 3 Transmembrane Helix I Contributes to Substrate Translocation and Protein Stability Of Bile Acid Transporter SLC10A2.....	47
3.1 Introduction.....	47
3.2 Experimental Procedures.....	49
3.2.1 Materials.....	49
3.2.2 Site-directed mutagenesis, transfection, cell culture and protein expression... ..	50
3.2.3 Substrate transport and sodium activation of TM1 mutants.....	50
3.2.4 Substrate and sodium kinetics of select TM1 mutants.....	51
3.2.5 Assessment of proteasomal or lysosomal degradation and hASBT folding.....	52
3.2.6 Data Analysis.....	53

3.3	Results	53
3.3.1	Transport activity and membrane expression of TM1 cysteine mutants.....	53
3.3.2	Sodium Activation.....	55
3.3.3	Solvent accessibility of cysteine mutants	57
3.3.4	Substrate Protection Assays.....	58
3.3.5	Kinetic Analysis of Select TM1 Mutants	60
3.3.6	Analysis of select TM1 Mutants against wt-ASBT background.....	61
3.3.7	Residue Gly ⁵⁰ is critical for ASBT folding.....	62
3.4	Discussion.....	67
Chapter 4 Charged Residues At The First Half Of The Intracellular Loop I Are Critical For Protein Stability Of The Apical Sodium-Dependent Bile Acid Transporter (ASBT; SLC10A2), And Respond Specifically To Cyclosporine A		72
4.1	Introduction.....	72
4.2	Materials and Methods.....	74
4.2.1	Materials	74
4.2.2	Site-directed mutagenesis, transfection, cell culture and protein expression ...	75
4.2.3	Substrate transport of IL1 mutants.....	75
4.2.4	Bile acid kinetics of IL1 charged mutants.....	76
4.2.5	Assessment of proteasomal degradation and hASBT folding.....	76
4.2.6	Data Analysis.....	77
4.3	Results.....	77
4.3.1	Taurocholate uptake and protein expression of IL1 mutants	77
4.3.2	Residues Cys ⁵¹ , Glu ⁵⁴ and Lys ⁵⁷ are critical for ASBT stability	82
4.3.3	Cyclosporine A increases wt-ASBT Expression	84
4.3.4	Integrated data on residues important for hASBT stability	86
4.4	Discussion.....	88
Chapter 5 Discussion and Future Directions		90
5.1	ASBT Topology	90
5.2	ASBT Stability.....	91
5.2.1	Misfolding.....	91
5.2.2	Increased wt-hASBT exocytosis.....	92
5.2.3	Altered protein turnover rates or degradation.....	92
5.2.4	CsA effect is indirect	93
5.3	Conclusions	93
Appendix A: Residues Pertinent To ASBT Function Or Stability, As Reported By The Swaan Laboratory		95
Bibliography		101

List of Tables

Table 1. Reported TCA ($[^3\text{H}]$ or $[^{14}\text{C}]$) Uptake Kinetics	16
Table 2. Substrate kinetic parameters for select TM1 mutants ^a	57

List of Figures

Figure 1. Increased level of complexity in ASBT studies.	23
Figure 2. Comparison of the putative 7TM versus 9TM membrane topology model for hASBT	34
Figure 3. MTSET Labeling of the wt-hASBT is Time and Concentration-dependent in Transiently Transfected COS-1 Cells.	42
Figure 4. Sodium Activation/Dependence of the wt-hASBT and C270A in Transiently Transfected COS-1 Cells.	43
Figure 5. Accessibility profile and cooperation among several hASBT regions.....	45
Figure 6. Putative ASBT transport cycle	46
Figure 7. ASBT (SLC10A2) protein secondary structure and sequence conservation across species.	49
Figure 8. [³ H]-TCA uptake and protein expression of TM1 cysteine mutants.	55
Figure 9. [³ H]-TCA uptake ratio under equilibrating (12 mM) vs. saturating (137 mM) sodium concentrations.	56
Figure 10. MTSET labeling of TM1 Mutants.....	58
Figure 11. Effect of GDCA or sodium on uptake recovery from MTSET modification..	59
Figure 12. Effect of mutation on wt-hASBT Function and Sodium Dependence of Select Mutants.	62
Figure 13. Mechanism of G50C Instability.	64
Figure 14. Mechanism of G50A Instability.	66
Figure 15. <i>In silico</i> representation of residues relevant for sodium transport.	69
Figure 16. ASBT (SLC10A2) protein sequence conservation across species.	74
Figure 17. [³ H]-TCA uptake and protein expression of IL1 cysteine mutants.	78
Figure 18. Effect of conservative and non-conservative mutation on wt-hASBT Function and Protein Expression of Select Mutants.	79
Figure 19. Mechanism of Instability of Select Mutants.....	80
Figure 20. Kinetic Parameters of Select IL1 Mutants.....	82
Figure 21. Graphic representation of IL1 amino acids relevant for hASBT function and stability.....	83
Figure 22. Effect of Degradation Inhibitors/Chaperones on wt-hASBT and G50A Cell Surface Expression.....	85

List of Abbreviations

3D-QSAR	3D-quantitative structure-activity relationship
ABC	ATP-binding cassette
ASBT	Apical sodium-dependent bile acid transporter
BBMV	Brush-border membrane vesicles
BR	Bacteriorhodopsin
BSEP	Bile salt export pump
CA	Cholic acid
CDCA	Chenodeoxycholic acid
ChCl	Choline chloride
CoMFA	Comparative Molecular Field Analysis
CoMSIA	Comparative molecular similarity indices analysis
CsA	Cyclosporine A
CyPA	Cyclophilin A
DOC	Deoxycholic acid
EHC	Enterohepatic circulation (of bile acids)
EL	Extracellular loop
ER	Endoplasmic reticulum
ERAD	ER-associated degradation
FKBP	FK506-binding protein
FXR	Farnesoid X receptor
GI	Gastrointestinal
hASBT	Human ASBT
I-BABP	Ileal bile acid binding protein
IBABP	Ileal Bile Acid Binding Protein
IBAT	Ileal Na ⁺ /bile acid cotransporter (ASBT)
IL	Intracellular loop
ILBP	Ileal bile acid binding protein
LacY	Escherichia coli lactose permease
MDR1	Multidrug resistance protein (P-glycoprotein)

MHBSS	Modified Hank's balanced salt solution
MRP2	Multidrug resistance-associated protein 2
MTSEA	2-aminoethyl methanethiosulfonate
MTSES	2-sulfonatoethyl methanethiosulfonate
MTSET	2-(trimethylammonium)ethyl methanethiosulfonate
NTCP	Sodium taurocholate cotransporting polypeptide
OATP	Organic anion transporting polypeptide
Ost	Organic solute transporter
OST	Oligosaccharyl transferase
4-PBA	Sodium 4-phenylbutyrate
PDB	Protein Data Bank
Pgp	P-glycoprotein
PPAR α	Peroxisome proliferator-activated receptor α
RXR	Retinoid X receptor
SCAM	Cysteine-scanning and the Substituted Cysteine Accessibility Method
Se-HCAT	[⁷⁵ Se]-Homocholic acid taurine
SHP	Small heterodimer partner
SLC	Solute carrier family of membrane transporters
SOAT	Sodium-dependent organic anion transporter
TCA	Taurocholic acid
TEA	Tetraethylammonium
TM	Transmembrane domain
TMm	TM model
TMAO	Trimethylamine n-oxide
TS-biotin	Biotin-X ethylenediamine thiosulfate
UPS	Ubiquitin-proteasome system
VDR	Vitamin D nuclear receptor

Chapter 1 The Apical Sodium-Dependent Bile-Acid Transporter (SLC10A2; ASBT)

1.1 Introduction and Brief History

1.1.1 Membrane transporters

Membrane transporters are integral proteins that facilitate the flux of molecules (nutrients, drugs) across the apical or basolateral poles of cells. This flux may occur down a substrate concentration gradient (facilitative diffusion), which is a passive process, or against the gradient, in which case energy is required. In the latter, transport is coupled to ATP hydrolysis, either primarily, *i.e.*, energy from ATP hydrolysis is directly used for transport, or secondarily, whereby the electrochemical gradient of a co-transported ion such as sodium or proton, is employed. This ionic electrochemical gradient is maintained by primary transport, and the energy produced during the flux of ion down its electrochemical gradient is the driving force to transport the substrate, and therefore this process is called secondary transport. Typically, carriers involved in both nutrient and drug transport through the apical or basolateral cellular pole, are members of the ATP-binding cassette (ABC) or the solute carrier (SLC) transporter family, which are, respectively, primary and secondary transporters. The sodium-dependent bile-acid transporter (ASBT) is the SLC10A2 member of the SLC family.

1.1.2 The sodium-dependent bile-acid transporter (ASBT)

The sodium-dependent bile-acid transporter (ASBT, SLC10A2) is largely recognized as the major bile acid transporter in the intestine and plays a pivotal role in the enterohepatic circulation (EHC) of bile acids [4]. Its relevance goes beyond the EHC, as ASBT is also a promising a prodrug target [5-11] and its contributing role in drug-drug interactions is rapidly emerging [4, 5, 12-14]. Numerous reviews compile extensive studies on the role of membrane transporters in the EHC and in pharmacokinetics [15-18], and a particularly noteworthy anthology, focusing on intestinal bile acid transporters, was recently published by Paul Dawson [4]. While the majority of publications mention the putative structure-activity relationships and overall 3D structure for ASBT, a detailed account on the techniques employed to achieve the current progress has not been published in nearly a decade [3]. The current report attempts to fill this gap. Here, we summarize advances made by our group and others in the quest to understand ASBT structure-function relationships and its complex mechanism of bile acid transport. A thorough discussion on the clinical aspects of EHC and its interruption is beyond the scope of this manuscript, and can be found in the aforementioned publications as well as elsewhere [1, 19-25].

1.2 ASBT and the Enterohepatic Circulation Of Bile Acids

The enterohepatic circulation of bile acid (EHC) is a highly efficient mechanism of bile acid (BA) conservation, which relies primarily on the liver, the gallbladder and the intestine to maintain precise levels of circulating BA. Essentially, BAs are taken up from the portal circulation into the liver via the basolateral transporter proteins sodium taurocholate cotransporting polypeptide (NTCP; SLC10A1) and the organic anion

transporting polypeptides (OATP) OATP1B1 (SLCO1B1) and OATP1B3 (SLCO1B3). In the liver, the majority of BAs are conjugated to taurine or glycine, and secreted into bile by the canalicular bile salt export pump (BSEP; ABCB11), for storage in the gallbladder. Similarly, the canalicular multidrug resistance-associated protein-2 (MRP2; ABCC2) and possibly P-glycoprotein (MDR1; ABCB1A) are involved in the efflux of a variety of conjugated and unconjugated BAs into the gallbladder.

In response to a meal, BAs are secreted through the bile duct into the intestine, where they facilitate digestion and absorption of dietary fat-soluble nutrients and vitamins. From the intestinal lumen, BAs return to the portal circulation via passive or active reabsorption. Passive reabsorption occurs throughout the length of the small intestine (primary bile acids) and colon (bacteria-modified, secondary bile acids). In contrast, the active component of BA reabsorption is mostly restricted to the terminal ileum, where ASBT concentrates BAs into the enterocytes using active sodium-coupled secondary transport. ASBT has a much higher affinity for the water-soluble taurine and glycine conjugates, but it can transport unconjugated BAs as well [26, 27]. In the ileum, active uptake is responsible for the vast majority of BA ileal reabsorption [28-30], which underscores the efficiency of ASBT-mediated transport, and the role of ASBT as chief bile acid transporter in the gut. Next, BAs are shuttled to the basolateral membrane of the enterocyte by the Ileal Bile Acid Binding Protein (IBABP; FABP6), a member of the fatty acid binding protein family of protein chaperones, and effluxed into the portal circulation via the heterodimeric organic solute transporter complex Ost α /Ost β . Finally, BAs return to the liver, thereby completing one cycle of EHC.

The EHC ensures that less than 10% of the recirculating BA pool is lost via excretion routes [27], and that lost BAs are replaced by *de novo* synthesis from cholesterol in the liver [27, 31]. Considering the importance of bile acids, not only as lipid solubilizers, but as complex signaling molecules [32], it is not surprising that the body invests so much effort in maintaining BA homeostasis. As an additional effort to prevent BA loss, ASBT is also expressed in renal proximal tubule cells, where it actively reabsorbs BA from the urine. In cholangiocytes, ASBT's role remains undefined, but it allegedly participates in cholehepatic shunt [4], *i.e.*, when biliary bile acids return to the liver for re-secretion into bile [33]. It has been suggested that the cholehepatic shunt may be a physiological adaptation to secure circulating BA levels, especially in pathological conditions such as bile duct obstruction [34].

Defective ASBT function or expression is associated with numerous conditions including gallstone formation, primary bile acid malabsorption (PBAM), idiopathic chronic diarrhea and other diseases [4, 26, 35, 36]. The recent finding that deoxycholic acid (DOC) may induce colorectal carcinogenesis [37] implicitly highlights the importance of ASBT in the prevention of this type of cancer, *i.e.*, since DOC is a secondary bile acid produced by colonic bacteria from cholic acid (CA) dehydroxylation, efficient CA uptake by ASBT should prevent excessive CA from reaching the colon and being metabolized into DOC.

ASBT pharmacological relevance is evidenced by its potential as a drug and prodrug target and its emerging role in drug-drug interactions [12, 14]. The fact that BA are the major cholesterol catabolites in the body renders ASBT inhibition an attractive approach to treat hypercholesterolemia [38, 39]. Notably, new clinical indications are

emerging in this arena, and the ASBT inhibitor A3309, presently on phase II trial, is currently being considered for the treatment of chronic idiopathic constipation [40]. On the other hand, unwanted inhibition by commercially available drugs such as statins, calcium channel blockers and others [12, 14], may result in drug-drug interactions and may potentially underlie some of the side effects exhibited by these drugs. Lastly, ASBT substrates can be used to improve drug bioavailability via BA-conjugated prodrugs [5, 6, 9, 10, 41]. In fact, oral administration of a chenodeoxycholate conjugate with acyclovir increased acyclovir bioavailability by two-fold in rats, compared to acyclovir alone [9].

In view of the clinical and pharmacological significance of ASBT, studies at several fronts (clinical, molecular, computational, etc.) are underway to fully characterize this pivotal transporter and obtain insight on its complex mechanism of BA transport. In the first chapter of this dissertation, we describe the discovery of ASBT and how it guided the initial experiments that lead into a deeper understanding of this transporter's physiology. In the second part, we focus primarily on structural studies performed in our laboratory – but we also recognize the contribution of other authors - in our effort to characterize the ASBT protein and its transport mechanism at the molecular level.

1.2.1 ASBT: Discovery and Initial Studies

1.2.1.1 Active component of bile acid transport occurs in the ileum

By 1960, bile acid absorption throughout the intestinal length and its impact on the EHC had already been well established [42, 43]. It was in that year, however, that a more profound appreciation of the complexity of bile acid absorption in the intestine began to flourish. Baker and Searle demonstrated that bile acid absorption occurred majorly in the small intestine [44], followed by Lack and Weiner who described

taurocholic and glycocholic acid transport as energy dependent and confined to the distal ileum [45]. These landmark discoveries shed new light on this pivotal transport process, and prompted various researchers to pursue the identification of the protein responsible for it.

One of the major approaches employed by Baker and Searle at that time was everted gut sacs (from rat and guinea pig). This method involves surgically removing fresh segments of intestinal tissue, gently everting and suturing them in the form of sacs, and placing the sacs in a suitable medium, with the mucosal side facing the outside environment and the serosal side facing the lumen of the sac. In this “inside-out” intestinal model, vectorial absorption is measured by substrate accumulation inside the serosal compartment, *i.e.*, inside the sacs. Everted gut sacs remains, to date, a valuable method to study intestinal transport [46, 47].

Bile duct cannulation also proved instrumental in revealing the participation of specific regions of the distal ileum in active bile acid transport. As the name suggests, this technique consists in surgically obstructing the cystic duct of intact animals and collecting bile flow from a cannula attached to the common bile duct. Lack and Weiner injected taurocholate (TCA), glycocholate and cholate (CA) salts on isolated regions of the small intestine of guinea pigs, and collected the absorbed bile acids from bile, thereby demonstrating the efficient bile acid transport through the distal ileum, and confirming participation of the distal ileum in the EHC [48]. Curiously, the authors did not employ specifically labeled bile acids, rather, they used the Pettenkofer reaction to identify the injected bile acids. The Pettenkofer reaction occurs between bile acids, sugar and sulfuric acid, resulting in a violet product. According to the authors, this reaction cannot identify

the natural bile acids in guinea pigs, and therefore a distinction between the natural and the injected bile acids could be made [48]. Similarly to guinea pigs, the authors also demonstrated ileal bile acid absorption in mice, hamsters, puppies, monkeys, chickens and pigeons [49], and also inferred a correlation between inhibition of ileal bile salt transport and bile acid diarrhea [50], as well as *in vitro* and *in vivo* decreases in blood cholesterol [51]. Other authors also reported similar observations [19, 20, 52-55], including Henry Buchwald, the pioneer of partial ileal bypass surgery to treat hyperlipidemia [53].

In 1990, Lewis and Root injected radiolabeled TCA in rat jejunum and ileum *in vivo*, and incubated ileal and jejunal tissue with [⁷⁵Se]-homocholic acid taurine (Se-HCAT), a selenium-conjugated taurocholic acid. That way, the authors determined the tissue distribution of TCA binding proteins, and confirmed that the majority of TCA binding occurs in the ileum compared to the jejunum [29].

According to Dietschy, passive ionic and micellar diffusion had a minor participation in bile acid absorption from the gastrointestinal (GI) tract, while active transport and passive non-anionic diffusion are the major contributors [28]. The author also demonstrated that passive permeability decreased for glycine- and taurine-conjugated (at C-24) bile acids, and also with the increased number of hydroxyl groups conjugated at the steroid nucleus (Schiff *et al*) [56].

1.2.1.2 The active bile acid transporter is Na⁺-dependent, obeys Michaelis-Menten kinetics and is electrogenic

In 1964, Holt used everted gut sacs to demonstrate the sodium-dependent nature of active bile acid absorption in rats, as well as its Michaelis-Menten kinetics [54]. Later,

in 1966, he also showed that the transporter could be competitively inhibited by conjugated and unconjugated bile salts [55].

Approximately a decade later, in 1978, Lücke and collaborators reported the need of sodium gradient as prerequisite for optimal TCA transport. The authors measured TCA uptake in brush-border membrane vesicles (BBMV), which are prepared by scraping the mucosal layer of freshly excised ileal segments and treating them under various conditions to afford transport-competent vesicles. Vectorial transport is then measured by substrate accumulation, *e.g.*, radiolabeled bile acid, inside or outside the vesicles. Using this system, the authors also showed that TCA uptake was temperature-dependent, and that replacement of sodium with Li^+ , Rb^+ and Cs^+ failed to stimulate transport [57].

The sodium-dependence of bile acid transport raised the question as to whether sodium and bile acid flux were coupled through the same transporter, and if so, if their fluxes would be electrogenic. Electrogenic transport involves the movement of charge from one side of the membrane to the other, thereby generating electric current and altering the transmembrane electrical potential. In secondary active transport, this movement of charge generates the driving force for substrate translocation.

When Lücke *et al* employed this method to measure TCA transport in BBMVs, they observed that sodium-dependent transport decreased in presence of the electrogenic ionophore monactin (selective for monovalent cations), but increased with valinomycin, a potassium-selective ionophore. These results suggested that sodium-dependent TCA transport was responsive to changes in membrane potential and was directly coupled to sodium in the same transporter. The authors also concluded that TCA transport was electrogenic, with a possible 2:1 cation:taurocholate stoichiometry, and at least one of the

cations being sodium [57]. However, this method has generated incongruent results at different laboratories. For instance, Barnard *et al* [58] and Wilson *et al* [59] indicated that sodium-dependent TCA uptake was electroneutral in BBMVs from rat ileum and rat renal cortex, respectively. In contrast, Wilson and Treanor suggested an electrogenic TCA transport in rat ileum BBMV [60]. Therefore, measurements of substrate flux as a function of the voltage applied has not yielded unambiguous results for sodium-dependent bile acid transport. An alternative method, *i.e.*, electrophysiological measurement of electric current, was technically challenging due to severe background and to the possibility of bile acids altering membrane fluidity due to their detergent properties [61]. Using a third method, whereby TCA uptake was measured at various sodium concentrations in ASBT-expressing COS cells, Paul Dawson and colleagues (Craddock *et al*; [62]) reported a potentially electrogenic transport, with a sodium : bile acid stoichiometry greater than 1 : 1. Finally, Weinman, Carruth and Dawson measured the voltage-dependent changes in accumulation of fluorescent bile acid analogues, and their results suggested that bile acid transport was electrogenic and had a 2:1 sodium : bile acid stoichiometry [63]. To the best of our knowledge, however, no direct measurement of native bile acid transport for the ultimate definition of ASBT stoichiometry has been performed.

Analogously, Lidofsky *et al* showed that active bile acid transport was electrogenic and had sodium : bile acid stoichiometry greater than 1:1 for NTCP [64], the hepatic counterpart of ASBT. NTCP was cloned in 1991 by Hagenbuch and collaborators [65], and is currently known to exhibit striking functional and structural similarities with ASBT. Both proteins share with high amino acid identity and topological similarities

[18], as well as a high affinity for glycine- and taurine-conjugated bile acids [27, 66]. These findings provided additional (indirect) evidence for the electrogenic nature of bile acid transport in the ileum.

1.2.1.3 Sodium gradient is maintained by the $\text{Na}^+\text{-K}^+\text{-ATPase}$

The large body of evidence supporting the active, sodium-dependent bile acid transport in the ileum, prompted researches to ask another question: by which mechanism is the sodium gradient maintained, in order to impart the driving force for active bile acid transport? Wilson and Treanor attempted to answer this question by treating viable rat ileal cells with the $\text{Na}^+\text{-K}^+\text{-ATPase}$ inhibitor ouabain, and with the inducer methylprednisolone. They observed a comparable decrease (with ouabain) and increase (with methylprednisolone) in bile acid uptake, thereby supporting a role for the $\text{Na}^+\text{-K}^+\text{-ATPase}$ in the sodium-dependent bile acid uptake in the ileum [67]. Simon and collaborators further corroborated this hypothesis with the observation that orally administered trihydroxy bile salts induced $\text{Na}^+\text{-K}^+\text{-ATPase}$ activity in rat ileum and liver homogenates. Moreover, this induction was proportional to the sodium demand for bile acid transport and was absent on the jejunum, where bile acid absorption occurs passively [68]. It is presently well recognized that the $\text{Na}^+\text{-K}^+\text{-ATPase}$ is responsible for sustaining the Na^+ electrochemical gradient required for active bile acid transport in the ileum [4].

1.2.2 ASBT identification and cloning

Without unambiguous identification of the ileal bile acid transporter at the molecular level, information on its mechanism of binding and transport was limited. The

following section describes early efforts to identify, isolate and characterize the transporter

1.2.2.1 Several bile acid binding proteins present in the ileum

In 1990, Lin, Kramer and Wilson reported for the first time the use of photoaffinity labeling to detect the ileal bile acid transporter, as well as other proteins involved in bile acid absorption. Photoaffinity labeling exploits the ability of a probe, usually a high affinity photolabeled substrate, to specifically and irreversibly bind the active site of a protein of interest [69]. While substrate binding is typically reversible, in photoaffinity labeling the highly reactive photosensitive moiety attached to the probe ensures covalent binding to surrounding amino acids, by photolysis, before the substrate dissociates from the active site [70]. Typically, the probe is radiolabeled to permit quantification of the amount reacted by radioactive counting. Inhibition of protein function implies successful labeling, and the labeled protein can be identified by immunoblotting. Using enterocytes from ileal brush border and [³H]-7,7-azo-taurocholate as a probe, followed by subcellular fractionation, Lin *et al* detected a 14-kDa protein in the soluble fraction (consistent with the ileal bile acid binding protein, *i.e.*, IBABP or ILBP [71, 72]) and a 99-kDa protein at the brush-border membrane fraction [69]. Later, when Wong *et al* cloned ASBT and showed its molecular mass to be around 38-kDa, they theorized that this 99-kDa protein may possibly be a dimerized or post-translationally modified form of ASBT [73]. Similarly to Lin *et al*, Kramer and colleagues identified a 14-kDa soluble protein, this time in rabbit ileum, which they conjectured to form the Na⁺-bile acid transport system alongside with a 93-kDa membrane protein – an alleged ASBT dimer [4] - also detected in the same tissue. Additionally, Kramer *et al* identified a

84 kDa membrane protein in the jejunum, which they inferred to possibly be involved in jejunal passive bile acid uptake [74].

1.2.2.2 *Xenopus oocytes and Caco-2 cells are suitable models to study the Na⁺-dependent bile acid transport*

Several experimental methods were established to study and characterize the ileal bile acid transporter. Mullins *et al* used BBMVs, as well as expression in *Xenopus laevis* oocytes, to investigate mRNA expression and function of the Na⁺-dependent bile salt co-transporter. The authors measured TCA transport in BBMVs prepared from pig proximal, mid and distal small intestine, from which mRNA was isolated and injected into *Xenopus* oocytes. To their surprise, TCA uptake could be detected from proximal, mid and distal intestine regions in oocytes with comparable kinetics, while in BBMVs it was restricted to the distal region, indicating that although the transporter's mRNA was expressed in various regions of the intestine, it was likely regulated to restrict protein expression to the distal segment [75].

Chandler and collaborators showed that Caco-2 cells were a feasible model to study the ileal active Na⁺-dependent transporter, as [³H]-TCA transport across differentiated (*i.e.*, with brush border expression on the apical surface) Caco-2 monolayers had transport features similar to previously employed techniques such as ileal BBMVs and isolated ileal enterocytes. In this system, Chandler *et al* evidenced the need for apically applied extracellular sodium, since sodium addition to the basolateral side only, failed to significantly stimulate TCA transport [76]. Additional significant contributions from the authors include the modified Hank's balanced salt solution (MHBSS) and the use of tetraethylammonium (TEA) and choline chloride (ChCl) in the buffers used to disrupt sodium-dependent transport. MHBSS is an adaptation of the

Hank's balanced salt solution (HBSS) whereby sodium and KCl are removed to facilitate replacement with other cations. MHBSS became the buffer of choice to investigate ileal bile acid uptake in various laboratories, including ours (*vide infra*). The observation that TEA and ChCl failed to promote TCA transport, which was later confirmed by Wong *et al*, rendered these salts excellent sodium replacement for experiments that evaluate the impact of sodium removal on active bile acid transport.

1.2.2.3 ASBT cloning

Studies aiming to understand the ileal Na⁺-dependent bile acid transport were clearly advancing. However, until the transporter was identified and sequenced, deeper insights on conjectural pharmacophore models, protein structure and mechanism of transport would be curtailed. The breakthrough finally came in 1994, when Dawson and collaborators (Wong *et al*; [73]) cloned, sequenced, and performed the preliminary characterization of the Na⁺-dependent bile acid transporter. The authors generated a cDNA library from the size-fractionated mRNA isolated from hamster ileum, and screened clone pools for [³H]-TCA uptake upon cDNA insertion into pCMV vector and transfection into COS-1 cells. Sequencing and characterization of positive clones showed that the ileal Na⁺/bile acid cotransporter (IBAT; also ASBT, ISBT and ABAT) was comprised of 348 amino acids and had approximately 38 kDa. In addition to hamster ileum, colony hybridization and Northern blot analysis indicated that the same protein was present in hamster kidney and faintly in the jejunum, but was absent in hamster duodenum and liver. Notably, IBAT shared high amino acid sequence identity (35%), similarity (63%), and hydrophathy profile with its hepatic counterpart, the liver Na⁺/bile acid cotransporter (LBAT; also NTCP), formerly identified by Hagenbuch and

collaborators [65]. In the same, highly productive year, Gong and collaborators cloned the 14-kDa ileal bile acid binding protein (I-BABP, ILBP) from rat ileum [77], and Oelker and Dawson cloned ILBP in humans [71].

1.2.3 ASBT Regulation

Bile acid accumulation in cellular compartments is cytotoxic, and is prevented by numerous mechanisms at the transcriptional and post-translational levels, which assist ASBT in its quick response to changes in bile acid demand. In 1993, Lilienau and collaborators reported the bile acid negative feedback inhibition of the bile acid transporter in rodents [78]. This feedback is currently known to be mediated by ASBT inhibition by the farnesoid X receptor (FXR). ASBT expression is tightly regulated at the transcriptional level by nuclear receptors, to which bile acids, cytokines, hormones, and sterols are natural substrates. For example, bile acid binding to the farnesoid X receptor (FXR) leads to FXR association with the retinoid X receptor (RXR), and subsequent activation of the small heterodimer partner (SHP), a repression protein that will inhibit the ASBT positive regulator retinoic acid nuclear receptor, thereby suppressing ASBT transcription. In contrast, the peroxisome proliferator-activated receptor α (PPAR α), the hepatocyte nuclear factor 1 α (HNF1 α) and the vitamin D nuclear receptor (VDR) bind the ASBT promoter and positively regulates expression of the transporter [27, 79, 80].

At the post-translational level, short-term adaptive responses seek to adjust transporter density on the cell surface. Among these responses are modulation of ASBT degradation, insertion in the plasma membrane and turnover. By inhibiting the ubiquitin-proteasome system (UPS) with the selective inhibitors lactacystin and MG132, Xia *et al*

[81] showed that the UPS is the main posttranslational regulator of ASBT availability in the cholangiocytes.

1.2.3.1 ASBT Kinetics: Discrete Parameters in Distinct Systems

ASBT is a high capacity of ASBT bile acid transport, as first demonstrated by Lewis and Root. The authors observed that 82% of TCA injected in rat ileum was absorbed with Michaelis-Menten constant (K_T ; *i.e.*, substrate concentration to achieve half the maximum reaction rate or V_{max}) values for TCA transport in the ileum comparable to TCA concentrations in the intestinal lumen [29]. The authors also reported a K_T of 5.6 mM, however, this value was not a consensus, due to interspecies or experimental differences *in vivo* and *in vitro*, as shown in Table 1. For example, Lewis and Root observed much higher TCA K_T in rat ileum *in vivo* [29] than Schiff and colleagues for *in vitro* perfusion of rat intestinal mucosa [56]. According to Lewis and Root, this discrepancy may possibly be due to bile acid accumulation in the basolateral membrane (trans inhibition) *in vitro*, whereas *in vivo*, absorbed bile acids are rapidly effluxed into the portal circulation, become tightly bound to plasma proteins and are removed from the blood into the liver. That way, bile acid levels in the enterocytes are kept low and transport is stimulated down a concentration gradient (sink effect). Moreover, as noted by Luxon *et al*, albumin binding enhances taurocholate uptake in the liver (while only the albumin-free form of taurocholate is transported through the ileum mucosa) [82], which contributes to an even further decay in bile acid levels in the bloodstream. Lewis and Root as well as Wong *et al*, also proposed an alternative explanation for the *in vivo* vs. *in vitro* disparity, based on the unstirred water layer. This mucous layer is predicted to be thicker *in vivo* than *in vitro* [29] and may serve as a

diffusion barrier in the intact intestine [73], thereby interfering with absorption and affecting kinetics. Using an *in vitro* system, namely, Madin-Darby canine kidney (MDCK) stably expressing ASBT, Balakrishnan and collaborators showed that the aqueous boundary layer may influence K_T and the inhibition constant (K_i ; *i.e.*, inhibitor concentration to achieve half the maximum inhibition) estimates and should therefore be considered in the analysis of kinetics data [83]. Notably, kinetics parameters may also vary in the same model, as illustrated by Candler and Hidalgo's work with Caco-2 cells [76, 84]. These cells are morphologically heterogeneous, and different clones may exhibit distinct features for TCA uptake [85]. These differences should be considered when comparing data obtained from different systems/models (Table 1).

Table 1. Reported TCA ($[^3\text{H}]$ or $[^{14}\text{C}]$) Uptake Kinetics

Ref.	K_T	V_{\max}	System tested
[29]	5.6 mM	$65.5 \text{ nmol}\cdot\text{min}^{-1}\cdot\text{cm}^{-1}$	Rat ileum (<i>in vivo</i>)
[56]	$0.23 \pm 0.07 \text{ mM}$	$1629 \pm 236 \text{ pmoles/min per cm}$	Perfused rat ileum (distal segment; <i>in vitro</i>)
[86]	$36 \mu\text{M}$		BBMV from rabbit ileum
[87]	$37 \mu\text{M}$		BBMV from human ileum
[75]	$40 \pm 3 \mu\text{M}$	$46 \pm 1.2 \text{ pmol/s per mg protein}$	BBMV from pig ileum
[77]	$16 \text{ pmol/h per oocyte}$	$48 \mu\text{M}$ (<i>Xenopus</i>)	<i>Xenopus laevis</i> oocytes (pig ileum mRNA)
[78]	$\approx 65 \mu\text{M}$	$\approx 800 \text{ pmol/min/mg protein}$	Caco-2 cells
[82]	$49.7 \mu\text{M}$	$13.7 \text{ pmol/mg protein/min}$	Caco-2 cells
[75]	$33 \mu\text{M}$	$396 \text{ pmol}\cdot\text{min}^{-1}\cdot\text{mg of protein}^{-1}$	COS-1 cells transiently transfected with hamster ASBT
[86]	11.1 ± 0.4	$300.23 \pm 8.3 \text{ pmol}\cdot\text{min}^{-1}\cdot\text{mg of protein}^{-1}$	COS-1 cells transiently transfected with human ASBT
[87]	$55.6 \pm 5.5 \mu\text{M}$	$547 \pm 48 \text{ pmol/mg protein/min}$	COS-1 cells transiently transfected with mouse Asbt
[64]	$18 \mu\text{M}$	$48 \text{ pmol}\cdot\text{min}^{-1}\cdot\text{mg cell protein}^{-1}$	COS cells transiently transfected with human ASBT
[64]	$18 \mu\text{M}$	$\approx 2,200 \text{ pmol}\cdot\text{min}^{-1}\cdot\text{mg cell protein}^{-1}$	CHO cells stably transfected with human ASBT
[88]	$4.39 \mu\text{M}$	$0.000065 - 0.001 \text{ nmol}\cdot\text{s}^{-1}\cdot\text{cm}^{-2}$	MDCK cells stably transfected with human ASBT
[89]	$8.3 \mu\text{M}$	n/a	HEK293 cells transiently transfected with human ASBT
[90]	$9.4 \pm 1.2 \mu\text{M}$	n/a	HEK293 cells transiently transfected with human ASBT
[90]	$13 \pm 4.3 \mu\text{M}$	n/a	HEK293 cells transiently transfected with mouse ASBT

1.3 Bile Acid Structural Features For ASBT Recognition

1.3.1 Pharmacophore features of substrates and inhibitors: initial studies

Prior to ASBT cloning, the vast majority of studies aiming to understand structure-function attributes of the ileal bile acid transporter, derived mainly from chemical bile acid modifications and their effect on transport. Starting in 1966, Leon Lack and several collaborators began to define some of the main structural requirements for substrate recognition by the ileal transporter. They measured transport of a variety of bile salts and analogues using everted gut sacs (*vide supra*), bile duct cannulation (*vide supra*) and ileal perfusion. In the latter technique, a flow of bile acid solution is infused in the initial segments of the intestine and the outflow is collected at the distal end of the same organ. The authors' results indicated that the following pharmacophoric features were essential for binding: 1) a single negative charge on the non-steroidal moiety (C-24); 2) the number of hydroxyl groups would determine inhibition potency, in the order dihydroxy > trihydroxy > triketo; and 3) conjugated are preferred over unconjugated bile salts [91-93]. Subsequently, Lack published a state-of-the art report where he used the contemporary bile acid structure-activity studies to design a theoretical model of the transporter's binding pocket. His model predicted cooperation among various components of the binding pocket, which was formed by: 1) an interaction site for the bile salt steroidal group; 2) a positively charged moiety that would interact with the negatively charged non-steroidal side chain of the bile salt; and 3) a closely positioned negatively charged region that would interact with sodium. Besides corroborating Lücke and collaborators' findings that Na^+ was irreplaceable [59], Lack also showed that anion replacement was not as critical, since Na_2SO_4 and NaCNS were capable of stimulating

TCA uptake in levels equivalent to NaCl [20]. Additionally, Lack and colleagues investigated the effect of charge on bile acid transport, based on the observation that positively charged or zwitterionic bile acids were inhibitors, but not substrates of the ileal bile acid transporter. The authors replaced the sulfonate (SO_4^{-2}) group in taurochenodeoxycholate with a sulfate (SO_3^-) at the C-24 or the 3α positions, and showed that 3α -conjugation was detrimental for transport and increased urinary excretion of the conjugate, while sulfate replacement did not affect transport [94]. Later, Kihira and colleagues reported that when a C-24 sulfonate conjugate of chenodeoxycholic acid was orally administered to hamsters, it was transported through the ileum, underwent EHC and resisted degradation by colonic bacteria [95]. Additional studies with sulfonated bile acid analogues was published by Miki *et al*, who tested sulfonation as well as the effect of side chain size on chenodeoxycholic analogues, and showed that from the C_{23} - C_{26} (natural bile acids are C_{24}) tested in hamster ileum *in vitro*, only C_{23} and C_{26} were absorbed at rates similar to taurochenodeoxycholic acid [96]. Lillienau and colleagues corroborated these observations with the C_{23} bile acid norursocholic acid (“nor” bile acids have 4 carbons on the side chain, *i.e.*, are C_{23} , rather than the 5 carbons present in C_{24}) and its glycine and taurine conjugates, which showed to be transported by the ileal transporter [97]. The effect of addition of a tyrosine or a glycylytyrosine conjugation at the side chain of $3\alpha,12\alpha$ -dihydroxy bile acids was investigated by Mills and colleagues. The authors measured biliary recovery after injection of ^{125}I or ^{14}C -labeled taurocholate or conjugated bile acids in the ileal lumen of Wistar rats, and showed that tyrosine conjugates were absorbed in the ileum, albeit with lower affinity than the taurocholate control. Addition of the longer glycylytyrosyl- group to the side chain of cholic acid

noticeably decreased absorption, compared to the shorter tyrosyl- analogue, however the authors did not discard the possibility of rapid degradation of the glycyl-tyrosyl- analogue at the intestinal lumen as responsible for this result [98]. Overall, the bile acid transporter accepted sulfonation as well as a variety of lengths at the bile acid non-steroidal side chain.

Walker and collaborators' observation that the absorption rate of 7-ketolithocholate in the ileum and jejunum was comparable to ursodeoxycholate (UDCA) and chenodeoxycholate (CDCA), led the authors to postulate that the 7-OH moiety was not critical for transport [99]. Recently, results from Polli's laboratory (non published data; submitted) indicate that bile acid analogues with a ketone group at the C-7 position were transported by ASBT, but not the ones with an aromatic group. These findings point out to the importance of the moiety size in C-7, but still agree on Walker's findings that a 7-OH group is not essential for ASBT transport.

Schmassmann *et al* showed that cholylsarcosine, a bile acid resistant to bacterial deconjugation, was well absorbed from the ileum of intact rabbits, hamsters and rats, after oral administration. Cholylsarcosine underwent enterohepatic cycling with little biotransformation, and was minimally absorbed from the jejunum or colon [100]. Later, Lillienau and collaborators supported a potential use of cholylsarcosine as a bile acid replacement for the treatment of bile acid deficiency [101].

In 1999, Kramer, Baringhaus and collaborators published a comprehensive map of structure-activity relationships for both ASBT and NTCP, and also demonstrated a rigorous substrate/inhibitor profile for ASBT compared to NTCP [102, 103]. Interestingly, despite ASBT strict substrate requirements, a benzothiazepine molecule,

namely, 2164U90 ((3R,5R)-3-butyl-3-ethyl-5-phenyl-2,3,4,5-tetrahydro-1,4-benzothiazepine 1,1-dioxide), which is structurally distinct from bile acids, was an inhibitor of the mouse, but not human, ASBT, as reported by Hallén *et al.* Remarkably, the authors identified the exact transporter region where this interaction occurred; they showed that replacement of the mouse Thr²⁹⁴ and Val²⁹⁵ with the human equivalents Ser²⁹⁴ and Ile²⁹⁵, respectively, all located in the C-terminal region, abrogated this interaction [90].

1.3.2 Pharmacophore Features from prodrug studies

Targeting the ileal bile acid transporter for drug delivery is an attractive approach to increase drug absorption, and has been subject of a series of studies. Preponderantly, these studies investigate the effect of conjugation of a variety of drugs to bile acid molecules, from which information on bile acid pharmacophore features can be derived. For instance, by coupling the anti-lymphoma drug chlorambucil to the 3 α -OH position in TCA, and demonstrating that the conjugates were inhibitors of the ileal and hepatic bile acid transporters, Kramer and collaborators showed that absence of a hydroxyl group at the C-3 position does not preclude interaction with the transporter. The tested chlorambucil-TCA compounds were conjugated or not with a glycine, taurine or methoxy (OMe) group at the non-steroidal side chain. In rabbit ileum BBMV's and freshly isolated rat liver hepatocytes, the conjugates inhibited the transporter dose-dependently [104]. Chlorambucil coupling to the 7 α and 12 α positions also inhibited the transporter in rabbit ileal BBMV [104].

Cholic acid conjugation at the 3 α -OH and C-17 positions with HMG-CoA reductase inhibitors [3], and at the C-3 position with small peptides [105] or renin-

inhibitory peptides [106], afforded inhibitors of the ileal and hepatic bile acid transporters. The conjugates with renin-inhibitory peptides were inhibitors, but were not substrates of the ileal transporter [106]. In Øie's laboratory, the ability of several bile acid compounds to inhibit TCA uptake was tested in Caco-2 cells. Swaan and colleagues coupled cholic acid with peptide molecules at the C-24 position [40, 107] or replaced one or all three hydroxyl groups in the steroidal skeleton with an amine, keto or formyloxy group, or simply a hydrogen atom [107], and Kågedahl *et al* generated cholic acid-amino acid conjugates with potential inhibitory activity against HIV-protease [108]. Integrated, the main observations reported by the authors include: *i*) peptide conjugates with 4 amino acids are substrates for the intestinal bile acid transporter; *ii*) a negative charge at position 24, as well as hydroxyl groups at positions 3, 7 and 12, are critical for affinity with the transporter; *iii*) conjugates with a single negative charge at C24 – C29 are strong inhibitors of the transporter, but a second negative charge at this region is detrimental to affinity; *iv*) bulky chains are well tolerated at position 24, but showed reduced affinity when attached to the steroid nucleus. Several of these results were corroborated by Balakrishnan and colleagues, who also indicated that binding may be the rate-limiting step of hASBT-mediated transport [88, 109].

James E. Polli and collaborators have been remarkably active in studying ASBT-targeting bile acid conjugates for prodrug approaches [1, 2, 5, 6, 9, 11] as well as ligand-based drug-design models of this transporter [81, 88, 110-114]. The authors conjugated the antiviral drug acyclovir to chenodeoxycholic acid via a valine linker, and showed a two-fold increase in acyclovir bioavailability, compared to acyclovir alone, upon oral administration in rats [5]. Using a combination of transport and inhibition measurements

and *in silico* simulations, Polli's group and collaborators have recently shown that: *i)* the prodrug candidate valylchenodeoxycholate is a substrate for ASBT; *ii)* CDCA-glutamyl-pyridine or CDCA-glutamyl-phenol conjugates are potent ASBT inhibitors, with monoanionic conjugates being more potent inhibitors than neutral ones [109]; *iii)* dianionic CDCA-glutamyl-anilinyll conjugates are strong inhibitors of hASBT, and intramolecular hydrogen bonding between the anylyl aromatic ring and the 3 α and 7 α hydroxyl groups favored binding affinity [114]; *iv)* a single negative charge around C-24 but not dianions and zwitterions, hinder activity [113]; *v)* monoanionic bile acid conjugates with gabapentin are hASBT substrates – and hence, are promising prodrug candidates [2]; *vi)* dianionic gabapentin conjugates inhibit the transporter but are not translocated [2]; *vii)* several commercially available drugs are hASBT inhibitors and could potentially be involved in drug-drug interactions [11, 115].

1.4 Conclusion

The sodium-dependent bile-acid transporter is critical for the EHC and for cholesterol homeostasis, and is a promising target for therapeutical approaches. In this chapter, we have briefly reviewed ligand-based studies that shed light in pharmacophore requirements for ligand recognition by the transporter, as well as the initial efforts to identify and characterize ASBT that culminated with its cloning in 1994 [75]. In Figure 1, we highlight the increasing complexity of information obtained for ASBT throughout the years. Similarly to many authors, we have also benefited from ASBT sequencing as a starting point for our protein-based studies, which we will discuss in the next chapter.

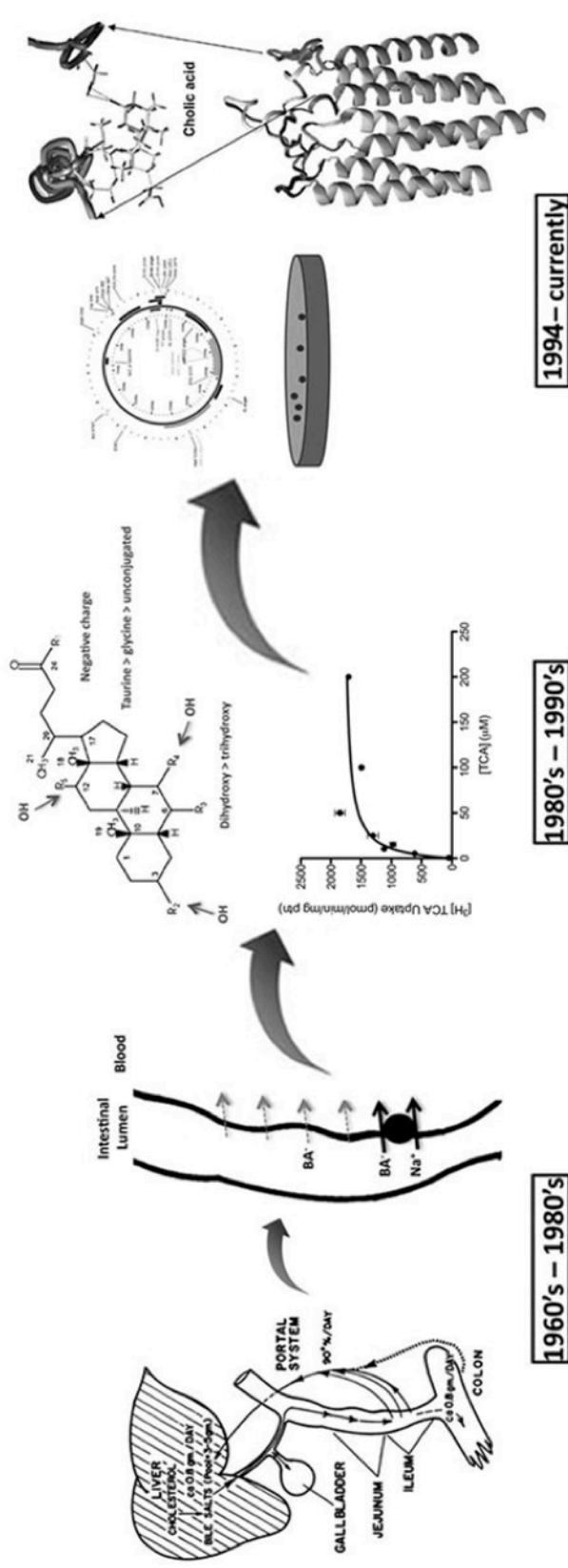


Figure 1. Increased level of complexity in ASBT studies.

1) 1960's – 1980's. The first 20 years were marked by the findings that active bile acid transport was sodium-dependent and restricted to the distal ileum (EHC scheme reproduced with permission from *Environmental Health Perspectives* [1]). 2) 1980's – 1990's. Scientists determined that ASBT exhibits Michaelis-Menten kinetics (represented as an uptake graph). Several pharmacophore features for bile acid substrates were also revealed at that time (indicated by a bile acid structure, with possible hydroxyl groups indicated by arrows). Pharmacophore features are also described. 3) 1994 - currently. Cloning (illustrative vector map designed on PlasMapper 2.0 [2]) in 1994 facilitated several ASBT studies at the molecular level and *in silico* protein-based structural models (represented as *in silico* rendering of the ASBT putative 3D structure and binding pocket (extracted from [3]) is shown).

Chapter 2 The Post-ASBT Cloning Era: Structural Studies and the Swaan Laboratory

To gain insight on the physiology of the apical sodium-dependent bile-acid transporter (ASBT) and to take full advantage of its potential as a pharmacological target, a better understanding of this transporter at the molecular level is a prerequisite. ASBT cloning and sequencing by Paul Dawson and collaborators [75] paved the way to a more profound examination of ASBT structure-function and transport mechanism, as well as to the development of mechanistic models that will potentially serve as paradigm to comprehend ASBT and other SLC10 proteins. Despite considerable progress, ASBT remains to be fully characterized at the molecular level.

For most polytopic proteins, crystal structures are notoriously difficult to obtain, partly because of their heterogeneous biological environments, *i.e.*, the hydrophobic membrane bilayer, hydrophilic cytoplasm and extracellular milieu. Publication of high resolution structures are expected to accelerate structural and mechanistic knowledge about a particular protein. However, from the over 50,000 proteins of known structure deposited at the Protein Data Bank (PDB), less than 1 % are membrane spanning proteins [117]. Not surprisingly, at the time of this writing, there was no crystal structure available for ASBT. Fortunately, biochemical, computational and molecular biological approaches are valuable alternatives to unveil critical protein features. In our laboratory, we have developed *in silico* models for ASBT that served as topological framework for simulations of substrate binding domains, mutation analysis and numerous *in vitro* and *in*

silico studies [86, 116, 118-124]. These studies assisted us in understanding ASBT structure-activity requirements and the contribution of specific amino acids to function and overall mechanism of transport. In 2002, Eric Zhang *et al* [16] and Sean Ekins *et al* [125] published comprehensive accounts on experimental and computational methods, respectively, used to study ASBT. Since then, we [81, 86, 116, 118-124, 126, 127] and others [87, 128-131] have made considerable progress in this regard, which we discuss in this chapter, focusing on the work performed in our laboratory.

2.1 *In Silico ASBT Studies*

2.1.1 ASBT Pharmacophore Models

Ligand-based pharmacophore modeling is a valuable tool to define structural features in a ligand that may be relevant for interaction with a target protein. Because the model is derived from a correlation between the ligand's physicochemical properties (molecular descriptors) such as lipophilicity, polarizability, steric parameters, substituent moieties, etc, and its biologic activity, this approach is particularly useful when information about the target protein is limited. The method consists in aligning various ligands in virtual space and submitting them to molecular dynamic simulations to yield their low energy conformations. A similarity index is obtained thereof, and represents a snapshot of common structural features shared by the tested ligands, and that are expected to be involved in interactions with the target protein. Tested ligands should presumably bind to the same protein, putatively in the same manner and with same relative geometry [132]. In our laboratory, we have employed Comparative Molecular Field Analysis (CoMFA), a 3D-quantitative structure-activity relationship (3D-QSAR) method that maps electrostatic and steric fields around the ligand's molecule, to identify

regions in bile acids and analogues that may putatively interact with ASBT. We have also employed comparative molecular similarity indices analysis (CoMSIA), in collaboration with Polli's laboratory [109]. While also a 3D-QSAR model, this method differs from CoMFA on the statistical methods to predict binding, and is also expected to have better predictive power, as it accommodates additional molecular descriptors [133].

Ligand-based *in silico* methods have assisted us and others [102, 109, 134] in predicting potential ASBT ligands, as well as in rationally designing drug and prodrug candidates that target ASBT [1, 2, 5, 6, 9, 11, 81, 88, 107, 110-113, 135]. With 3D-QSAR methods, we have unveiled critical aspects of pharmacophore requirements for ASBT ligands, and corroborated major findings from the joint laboratories of Kramer and Baringhaus [102], such as the need for: *i*) one hydrogen bond donor [102], which could possibly be a negative group, either a carboxylate or a sulfate moiety around position C-24, as identified by Swaan *et al* [107]; *ii*) one hydrogen bond acceptor [102], perhaps one of the hydroxyl groups in steroid nucleus. These hydroxyl groups should be oriented in the same direction, thereby forming a hydrophilic region relevant for binding [107]; *iii*) three hydrophobic features [102], possibly with participation of the methyl moieties opposite to the hydroxyl groups, forming a well-defined lipophilic region [107].

Ligand-based models are indisputably useful in the absence of target protein information. However, they are also limited in that they are indirect measures of structure-activity relationships, and should therefore, be complemented with other methods, such as protein-based *in silico* and *in vitro* experimental approaches, in order to produce a more comprehensive picture of ASBT transport.

2.1.2 Protein-based ASBT Simulations: Homology Model

Protein-based *in silico* models rely on available information about the three-dimensional (3D) structure of the target protein or its binding pocket. This information is typically obtained from X-ray crystallography, NMR or, in the absence of those, homology or topology modeling. As mentioned above, the dismal number of PDB entries for membrane proteins illustrates the challenges encountered in obtaining high resolution structures for this class of proteins. Fortunately, collaborative efforts such as the Protein Structure Initiative [136-138], have ensured that newly solved structures are easily accessed from online protein libraries such as the PDB, thereby increasing the chances of finding proteins that are similar in sequence and topology. In our search, ASBT did not show sequence homology with any of the proteins of known structure, but it did exhibit topological homology with bacteriorhodopsin (BR) [116], a seven-transmembrane protein that had been recently crystallized [139]. Additionally, remote-threading revealed that the 3D structure of the pheromone ER-2 from *Euplotes Raikovi* (1ERD) and the diptheria toxin repressor (1DTR) were appropriate scaffolds for ASBT flexible regions, and in addition to BR, these proteins were used as templates to develop the ASBT homology model [75, 116]. The advantage of using remote threading here is that it employs statistical methods to relate the amino acid sequence of the query protein with the folding pattern of the known protein, and therefore does not require homology between the two proteins. It uncovers folding similarities between a protein of unknown structure (query) and other proteins deposited in the PDB. Finally, we tested the quality of the model using PROCHECK, an algorithm that aligns an input sequence with related available structures and calculates an all-atom model, *i.e.*, where protein backbone and

side chains are included. The model was validated by *in silico* mutagenesis with the P290S polymorphism, which corroborated the loss of activity observed in carriers of the P290S mutation, as well as *in vitro* site-directed mutagenesis, which confirmed Glu²⁸² critical role in ASBT function. Remarkably, our model also predicts a β -turn in the C-terminus (Asn³⁴⁰-Phe³⁴³), consistent with the same structure reported by Suchy and collaborators (Sun *et al*; [129]), shown to be required for ASBT sorting to the apical membrane. Suchy *et al* examined this protein region with NMR and site-directed mutagenesis, and their results provided further experimental and inter-laboratory validation of our *in silico* model.

2.1.3 ASBT-Bile Acid Docking

Our validated homology model empowered us to predict the putative hASBT binding pocket. We probed the protein space with the natural substrate cholic acid, using docking; a molecular modeling technique that predicts three-dimensional structural interactions between the target protein and its ligand. In this method, the chemical space in the protein is probed with the ligand and submitted to molecular dynamics simulations and energy minimizations, to ultimately indicate regions in both the ligand molecule and the protein that may participate in protein-ligand binding.

In addition to using cholic acid as the probe, we utilized the NMR structure of the cytosolic bile acid binding protein ILBP as the positive control, since it also binds bile acids specifically, during the EHC [140]. Using this approach, we identified binding sites in the extracellular loop 3 (EL3), the N-terminus and a binding pocket formed by an opening (or “cleft area”) between the N-terminus and EL3. According to our model: *i)* Glu²⁸² and Leu²⁸³, located in EL3, form dynamic hydrogen bonds (H-bond) with the bile

acid 12 α -hydroxyl moiety; *ii*) Leu²⁸³ engages in additional H-bond with the 7 α -hydroxyl group; *iii*) hydrophobic residues in EL3 putatively stabilize the methyl groups at positions 18 and 19 of the bile acid steroidal backbone; *iv*) the negatively charged carboxylic acid in the bile acid could possibly interact with Arg²⁵⁴ and Arg²⁵⁶ or alternatively, with Val²¹ and Asn²⁷ in the N-terminus; *v*) Asn², Ala¹¹ or vicinal residues in the N-terminus would form dynamic H-bonds with either the 3 α - or 7 α -hydroxyl group in the ligand [116].

2.1.4 ASBT *In Silico* Models: Conclusion

As illustrated above, protein-based *in silico* models can be validated by experimental methods, and vice versa. Identification of disease-associated mutations such as L243P, T262M and P290S [15, 141-144] served as a framework for mutagenesis studies and *in silico* models. In turn, *in vitro* and *in silico* studies indicated defects in protein structure or stability that may underlie such disease conditions. For instance, our *in silico* model suggests a mechanism for the bile acid malabsorption observed in carriers of the P290S mutation, whereby a serine at position 290 would close a cleft area between the N-terminus and EL3. This area should reputedly be opened to allow cholic acid binding [116]. We have also shown that Cys replacement of Ala¹⁷¹ did not affect ASBT function [123], consistent with the functionally silent nature of the A171S polymorphism, found in high frequency among several ethnic populations in the United States [144].

Despite strong evidence for the robustness of our model, it is worth remembering that it remains a model and as such, requires constant inspection, optimization and validation with experimental data. A crystal structure would be the ultimate corroboration of our model, if and whenever it becomes available. In the meantime, we continue working towards a better ASBT representation, with a combination of biochemical and

molecular biological methods to identify residues crucial for ASBT structure, function and stability. The following part of this manuscript briefly describes our main findings.

2.2 *ASBT Topology: Experimental Methodologies*

2.2.1 ASBT Topology: Divergent Views

Due to the physiological and pharmacological relevance of ASBT, understanding this pivotal protein at the molecular level became one of the major interests in our laboratory. One of the first challenges was to define ASBT topology, which at the time was controversial, *i.e.*, two divergent transmembrane models were recognized based on experimental evidence as well as hydropathy analysis [75, 89, 90, 145]. One model supported the presence of seven membrane-spanning domains, while the other predicted nine transmembrane domains (TM)¹. Although both models agreed on an uneven number of transmembrane domains and in the location of the extracellular N-terminus and the cytoplasmic C-terminus (N_{exo}/C_{cyt}), a definitive conclusion on ASBT transmembrane topology was yet to be reached.

For Hallén and collaborators, hydropathy analysis and membrane insertion scanning supported the nine TM model (9TMm)². Their model predicted a short extracellular loop 1 (2 amino acids long) connecting the second (TM2) and third (TM3) segments, and TM3 and TM4 comprised of 9 – 10 amino acids [90, 145]. Notwithstanding, in order to adhere to this prediction, TM3 and TM4 would have to assume a β -sheet conformation, resulting in a combination of α -helices and β -sheet at the membrane-spanning regions, which is unusual in eukaryotic polytopic membrane

¹ TM = transmembrane domain

² TMm = transmembrane domain model

proteins, as indicated by careful inspection of available protein folds at the scop database (scop@mrc-lmb.cam.ac.uk). In contrast, the 7 TM model (7TMm) predicted a typical alpha helical arrangement, with 21-23 amino acids per TM, and loops comprised of least 12 amino acids [75, 146]. To determine ASBT topology unambiguously, we examined protein regions that were controversial in each model, namely, the extracellular loop (EL)1, TM3 and TM4, using a variety of experimental and computational approaches (described below). Our results indicated that ASBT obeys the 7TM model and adheres to the “positive-inside” rule.

2.2.2 N-glycosylation scanning mutagenesis

N-glycosylation of integral membrane proteins in eukaryotes is confined to the endoplasmic reticulum (ER) compartment, hence it can be used as a tool to define the position of amino acid segments relative to the membrane bilayer. During co-translational translocation, polytopic proteins are inserted into the ER membrane in the same orientation that they will assume at the plasma membrane, *i.e.*, segments facing the ER lumen will later face the extracellular environment in the plasma membrane. Thus, protein topology is defined at the ER level [147]. N-glycosylation occurs concomitantly to this co-translational process, with the enzyme oligosaccharyl transferase (OST) attaching oligosaccharide chains to asparagine residues in the consensus sequence, or sequon, Asn-X-Ser/Thr (X can be any amino acid except proline). Since the OST catalytic side faces the ER lumen, N-glycosylation is restricted to extracellular segments in polytopic proteins [147, 148]. Its compartmentalized nature, combined to the fact that efficient N-glycosylation is only achieved when the sequon is located about 12-14 amino acids away from the ER membrane [148], renders N-glycosylation an attractive cellular

process to be exploited in topologic studies. Detection of N-linked oligosaccharides in a protein segment is a strong indication that the segment being examined is located extracellularly.

In N-glycosylation scanning mutagenesis, engineered sequons are introduced by site-directed mutagenesis at specific locations in the protein, followed by determination of protein expression at the cell surface. Notably, before introduction of glycosylation motifs, all endogenous sequons should be removed to prevent interpretation issues. In the human ASBT (hASBT), we have identified Asn10 as the sole native glycosylation site [116]. Next, we generated the aglyco, functional, N10D mutant, and used it as template for insertion of the glycosylation motifs. Finally, we investigated the protein regions that were controversial in the 7TM versus the 9TM topology models (*vide supra*). We introduced the sequons at positions 113-118 and 266-272, which had been assigned, respectively, as part of EL1 and EL3 (7TMm) or IL2 and TM8 (9TMm). While in the 7TMm these regions would face the extracellular environment, in the 9TMm they would either face the cytoplasm or be located within TM8, and would therefore be unavailable to the glycosylation machinery. Surface labeling with the membrane-impermeable NHS-SS-biotin detected the glycosylated protein in the mutants, but not in the aglyco control, thereby supporting the 7TMm [116].

2.2.3 Dual Label Epitope Insertion Scanning

Detection of the glycosylated protein in N-glycosylation scanning mutagenesis supported the extracellular location for amino acid segments associated with the 7TMm. Nonetheless, lack of detection in regions predicted in the 9TMm was not enough evidence to irrefutably reject this model. The nature of the amino acid sequence flanking

the introduced sequon, or steric hindrance due to proximity to the ER membrane, may affect the efficiency of, or even prevent, glycosylation. Moreover, the possibility of long loops such as EL1 and EL3 reentering the membrane, as occurs with the glutamate transporters GLT1 [149, 150] and EAAT1 [151] and the $\text{Na}^+/\text{Ca}^{+2}$ exchanger NCX1 [152], could hypothetically permit both the 7TMm and the 9TMm to co-exist. Thus, unambiguous topological information by N-glycosylation scanning is restricted to positive results, and is limited to extracellular regions [116].

Membrane insertion scanning (*vide supra*) was another widely used approach that proved instrumental in uncovering important aspects of ASBT structure [145]. However, results from this method are deduced from the truncated protein, and as such, may incur interpretation issues and contradictory models, as reported by Kast and colleagues for P-glycoprotein [153].

In an effort to achieve a more comprehensive depiction of ASBT structural determinants and circumvent the aforementioned limitations, we complemented our investigations with epitope insertion mutagenesis. This method allows examination of intracellular and extracellular regions using the full-length, active protein, followed by detection of strategically inserted epitope tags with specific antibodies. Additionally, it capitalizes on the impermeability of intact plasma membrane to antibodies, to reveal intra/extracellular orientation of introduced tags, *i.e.*, by treating cells under membrane permeabilizing (*e.g.*, detergents) versus nonpermeabilizing conditions. To increase the chances of obtaining functional mutant proteins that are properly inserted in the membrane, we have employed dual label epitope insertion mutagenesis, whereby distinct tags, varying in physicochemical characteristics, are added to the protein. Accordingly,

we introduced the negatively charged FLAG (DYKDDDDK) and the relatively neutral hemagglutinin (HA; YPYDVPDYA) into regions predicted as IL, EL and N- and C-terminal in each model. After verifying that protein stability, trafficking and function were preserved in the tagged mutants, we detected the inserted epitopes under permeabilized (saponin) vs. nonpermeabilized conditions. More specifically, this approach empowered us to confirm extracellular location for insertion sites III-92, IV-116, V-120, VII-186, X-270 and XI-284; intracellular placement for II-56, VI-156 and VIII-221, and the N-terminal orientation with I-16 as well as C-terminal with XII-319 (Figure 2) [118]. Calculated charge distribution of protein segments indicated an (-4/+4) out/in charge ratio, and that the 7TM model strictly adheres to the “positive-inside” rule. Globally, we provided compelling evidence that hASBT topology conforms with a seven-transmembrane topology, has extracellular N-terminus and cytosolic C-terminus, and its charge distribution adheres to the “positive-inside” rule.

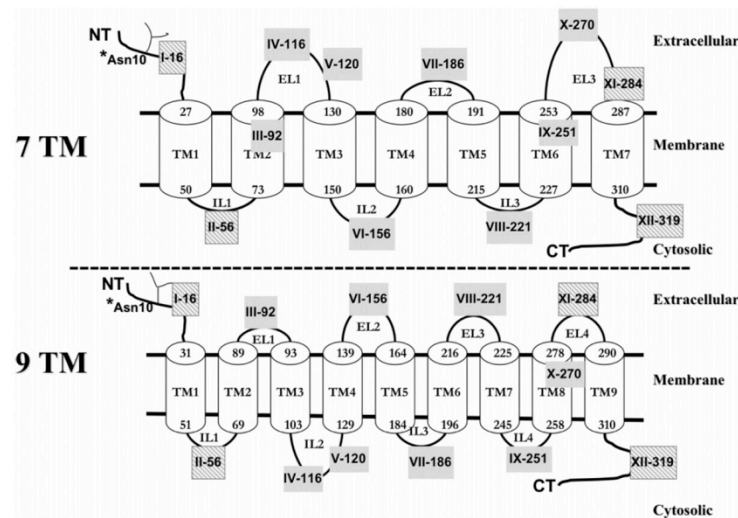


Figure 2. Comparison of the putative 7TM versus 9TM membrane topology model for hASBT

Reproduced with permission from [118] (Copyright 2006 American Chemical Society). Strategically inserted FLAG and HA epitopes are illustrated by roman numerals followed by the amino acid position immediately preceding the epitope insert. Transmembrane helices are represented as cylinders, and numbers indicate the amino acids at the interface of the TMD (transmembrane domain) and the extramembranous environment. *Asn10 represents the sole glycosylation site on hASBT. Hashed gray boxes indicate epitope sites that are conserved between both topologies. NT, N-terminus; CT, C-terminus.

2.2.4 Cysteine-scanning mutagenesis

After successfully establishing the hASBT reputed protein topology, we set out to elucidate the contribution of specific protein regions to transporter structure and function. Our validated topology model provided a framework for mutation of specific amino acids, located at putative extracellular, intracellular and membrane-spanning regions. A variety of conservative and non-conservative mutations, as well as cysteine (Cys) replacement, empowered us to identify relevant amino acid segments (Appendix A). The advantage of using Cys replacement of endogenous residues is the relatively nonbulky nature of cysteines, alongside with their concomitantly hydrophilic and hydrophobic characters at physiologic pH (side chain pKa 8.02). Thus, Cys are likely to be well tolerated in most insertion positions in the membrane [148] as well as in protein loops, without causing significant changes in protein structure. Cysteines are also versatile, in that they can be used as scaffold for further studies such as the substituted-cysteine accessibility method (SCAM).

2.2.5 Substituted-Cysteine Accessibility Method (SCAM)

Membrane protein topology and the placement of specific amino acid residues, potentially located in ligand binding pockets or the substrate translocation pathway, can be revealed using SCAM. This approach relies on the specific reactivity of sulfhydryl-modifying reagents towards cysteine thiols, especially the ionized thiolate (S^-), which reacts 5×10^9 times faster than the unionized form (SH) [154]. A key assumption in SCAM is that the ionized form will only occur when the Cys is accessible to water-filled (the “solvent”) compartments such as the extracellular environment or within a hydrophilic pocket or translocation pathway. Conversely, when the Cys side chain faces

the membrane bilayer or other regions of low dielectric constant, its thiol group is inaccessible to the solvent; it assumes the unionized (SH) form, and cannot efficiently react with the labeling reagent. Consequently, Cys locality relative to the membrane bilayer or hydrophilic environments will dictate Cys “accessibility” to the reagent, and its consequent “labeling” (disulfide formation). Because in most cases, Cys replacement alone is unlikely to perturb the local or global protein conformation [148], solvent-accessibility of introduced cysteines can generally be extrapolated to the original/mutated residue. Notably, the use of functional Cys mutants is critical in SCAM, due to the conceivable notion that structural abnormalities might underlie functional defects, and conclusions derived from dysfunctional mutants may not reflect the physiological scenario.

Thiosulfonates are a class of extensively employed thiol-modifying reagents that provide a wide range of labeling possibilities, due to the distinct charges (*e.g.*, MTSES, MTSET) and functional head groups (*e.g.*, fluorescent, radioactive, biotin groups) that can be attached to their side chains. Typically, cells expressing the protein of interest are incubated with thiosulfonates, washed with buffer to remove the reagent, and finally submitted to functional assays to appraise labeling. The use of functional assays relies on the well-accepted notion that introduction of bulky/charged groups from the thiosulfonate side chain is expected to alter protein structure and activity, and is therefore likely to result in decreased function. Nonetheless, it is worth noting that while successful thiol modification can be clearly detected by altered function, lack of functional changes may not unequivocally signify absence of reactivity (*i.e.*, due to inaccessibility). In such case, the possibility of functionally silent reactions should be considered, and therefore,

negative results should be interpreted with caution. Biotinylated thiosulfonates are a convenient alternative – or complement - to functional assays, especially when negative results are involved. It permits “visual” (rather than “functional”) identification of labeled proteins by immunoblotting, after their pulled-down with streptavidin.

SCAM has been instrumental in providing structural insight for several membrane transporters and receptors, including the Glut1 glucose transporter [155], the dopamine D2 receptor [156], the glutamate transporter GltT [157] and others [158-160]. It also has uncovered protein segments that form the substrate pathway for the human anion exchanger 1 (AE1) [158], the voltage-gated Na⁺ channel [159] and the Na⁺/dicarboxylate cotransporter 1 (NaDC1) [160], as well as for hASBT [119-124, 127]. In the most comprehensive SCAM study performed to date, Kaback and collaborators replaced each individual amino acid in the protein sequence of the Escherichia coli lactose permease (LacY) with cysteines, and used SCAM to successfully define key aspects of LacY structure-activity relationships and putative transport mechanism [161, 162]. Several of their observations were subsequently confirmed on a LacY high-resolution structure, which further validated their SCAM results [163, 164].

2.2.5.1 C270A as Background for hASBT SCAM Studies

Kaback and collaborators observed that none of the eight cysteines in LacY was essential for function. Since removal of all endogenous cysteines was well tolerated, Cys mutations were introduced on an ideal Cys-less template [165]. In many cases, however, a functional Cys-less background is unachievable or unnecessary. As shown for NaDC1 [160], the dipeptide transporter hPepT1 [166, 167], the CB2 Cannabinoid Receptor [168] and others [166, 169, 170], as long as some or all of the endogenous cysteines are

insensitive to MTS modification, and mutation of the sensitive ones preserves activity, the use of a Cys-less template is redundant. Likewise, in our laboratory, a functional Cys-less hASBT mutant was unattainable. Nonetheless, we, as well as Hallén *et al* [89], observed that Cys²⁷⁰ is responsible for wt-hASBT sensitivity to thiol modification, and its replacement with alanine conferred resistance to thiol labeling, while retaining full wild-type function and virtually unaltered kinetics [86]. Also as shown by us [86, 119] and Hallén *et al* [89, 90], Cys²⁷⁰ is not essential for ASBT function, despite its high level of inter-species conservation and alleged location within the substrate-binding region. It became evident that C270A was an excellent scaffold for Cys scanning mutagenesis and that mutation of most native Cys residues was not critical for our SCAM studies. Inaccessibility to thiol-modifiers was further evidenced by C270A treatment with the cysteine-specific reagent MTSEA-biotin, which labeled the wt-hASBT but not C270A, whereas the lysine-specific reagent NHS-SS-biotin detected both proteins [119]. It is worth noting that C270A is resistant to charged, membrane impermeable MTS reagents such as MTSET and MTSES, but not to membrane semi/permeable thiosulfonates such as Allyl-MTS, which can cross the plasma membrane and modify membrane-bound or intracellular cysteines from the trans side [86].

2.2.5.2 Substrate Effect on Thiol-labeling: Mapping hASBT Binding Pocket and Translocation Pathway

In SCAM studies, successful thiol labeling implies solvent-accessibility of the introduced cysteine. While suggestive of a potential role in substrate interactions for the probed amino acid, solvent-accessibility is not irrefutable proof that a residue interacts with the substrate or lines the translocation pathway. The ability of substrates to interfere with MTS labeling can be useful as a tool to disclose this possibility. To that end, we

employed labeling with MTS-bile acid conjugates, or thiosulfonate in presence vs. absence of bile acid or sodium, which we discuss next. In both approaches, COS-1 cells transiently expressing hASBT or mutants were pre-incubated with the MTS reagent/conjugate, and protein function was subsequently assessed with [³H]-TCA uptake.

2.2.5.3 Bile Acid-MTS Conjugates to Map the Binding Pocket

Loo and collaborators have successfully mapped the P-glycoprotein (Pgp) binding site with MTS-verapamil and MTS-rhodamine [171, 172]. Similarly, we have shown that MTS-bile acid conjugates react specifically and dose-dependently with cysteines introduced at the bile acid binding site [86, 126]. In agreement with previous findings [86, 89, 90], we corroborated Cys²⁷⁰ location in a region sensitive to bile acid interactions, and demonstrated that bile acid conjugation with MTS is a promising tool to map ligand binding and translocation regions in hASBT, that can potentially be applied to other bile acid carriers, such as BSEP and NTCP.

2.2.5.4 Substrate Protection/Interference Assays

For specific hASBT mutants, the presence of bile acid in the thiosulfonate pre-incubation buffer or the removal of sodium from it, prevented labeling and restored substrate uptake, often times to the same levels of untreated controls [121-124, 127]. We have thereby, disclosed protein regions in hASBT that are putatively involved, either directly or indirectly, with substrate interactions. We were careful in our results interpretation, as substrate protection may at first suggest that the substrate is competing with the thiosulfonate reagent for the introduced cysteine, however, the mechanism underlying function restoration may vary. For instance, while the substrate itself may

directly block access of the thiosulfonate to the introduced cysteine (and thereby confer “protection”), long-range conformational changes elicited by substrate binding and translocation may alter Cys accessibility, and “hide”/“expose” the Cys side chain from/to the solvent. Hence, the substrate may either “protect” or “unprotect” the Cys from thiol modification, and restored uptake may simply mean that the introduced Cys is placed in a conformationally sensitive region, rather than being directly involved in substrate interactions. For instance, Cys²⁷⁰ (wt-hASBT) reactivity with MTSET increases in presence of sodium, whereas removal of this co-transported cation prevents reaction and restores wt-hASBT uptake. This “protection” in absence of sodium clearly denotes the involvement of conformational events, since there is no substrate to physically “block” access of the MTS reagent to the cysteine. In contrast, co-incubation with the natural substrate glycodeoxycholic acid (GDCA) prevents wt-hASBT labeling by MTSET, suggesting a more direct implication of the substrate in the mechanism of protection, as well as Cys²⁷⁰ location in a region involved in bile acid binding or translocation. Interestingly, MTSET accessibility alternates upon co-incubation with GDCA in presence vs. absence of sodium, which further corroborates location of this residue in a conformationally-sensitive region that is involved in bile acid interactions [120].

It is possible to distinguish between these two mechanisms, *i.e.*, protection conferred by direct occlusion of the Cys or by long-range conformational effects, experimentally, by exploiting the temperature-dependence of transport [151, 173-175]. Molecular motions have to overcome large energy barriers and tend to slow down at 4°C, whereas substrate binding should remain unaffected under these conditions. For instance, at the sodium-dependent glutamate transporter EEAT1, L-Glu transport was significantly

reduced at temperatures approaching 0 °C, without severely affecting substrate binding, as reported by Seal and colleagues [151]. By pre-incubating the thiosulfonate reagent, with or without substrate, at 4 °C versus higher temperatures (typically 22°C), we identified a conformationally sensitive region in TM1 encompassing Leu³⁴ and Leu³⁸. Remarkably, while both L34C and L38C mutants were significantly protected by GDCA, protection levels at 4°C increased for L38C, but decreased for L34C, suggesting that these residues may possibly sense opposite forces during bile acid translocation, and that they are placed in a TM region of intense conformational activity.

To ensure that pre-incubation at low temperature would not interfere with thiosulfonate labeling itself, we tested this protocol with wt-hASBT, using MTSET as the labeling agent. Our preliminary experiments indicated that temperature did not affect wt-hASBT labeling (Figure 3), and that no changes in MTSET pre-incubation would be necessary at the tested temperatures [127]. Since there are reports of increased MTSET concentration [174] or incubation time [173] at low temperatures, or equivalent conditions [175] at both low and high temperatures, this result suggests that the effect of temperature in thiol labeling may be protein-specific. Globally, our observations illustrate the value of the SCAM approach in providing insight on static as well as dynamic processes during the transporter cycle.

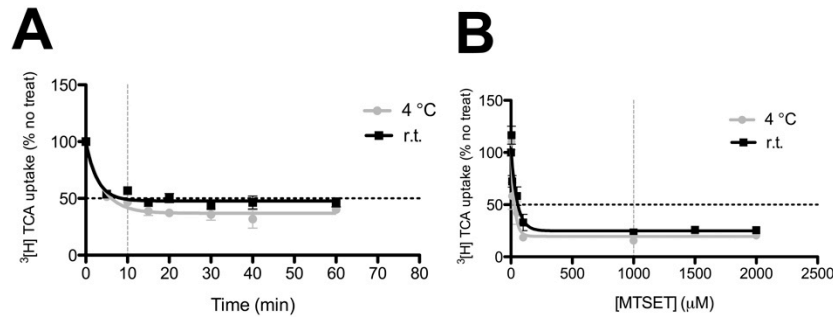


Figure 3. MTSET Labeling of the wt-hASBT is Time and Concentration-dependent in Transiently Transfected COS-1 Cells.

COS-1 cells transiently transfected with the wt-hASBT were pre-incubated at 4 °C or r. t. with A) 1 mM MTSET for various time points or B) 10 min at various MTSET concentrations, followed by washes, and [³H]-TCA uptake.

2.2.6 Sodium Activation Experiments: Uncovering Residues Involved in Sodium Transport

As a secondary active transporter, ASBT harnesses energy from the inward ion (sodium) gradient to concentrate bile acids within the cell interior. Sodium translocation is coupled to bile acid through the same transporter, and active transport does not occur in absence of sodium. While ASBT-mediated transport is optimal under a sodium gradient, *i.e.*, $[Na^+]_{out} > [Na^+]_{in}$ (out = extracellular; in = intracellular), lack of a gradient does not preclude transport. In fact, Lücke and colleagues reported bile acid transport under equilibrative sodium concentrations, *i.e.*, $[Na^+]_{out} \approx [Na^+]_{in}$, albeit with reduced efficiency [59]. TCA transport was 11-fold higher at $[Na^+]_{out} > [Na^+]_{in}$, and 4-fold higher at $[Na^+]_{out} \approx [Na^+]_{in}$, compared to absence of sodium. Likewise, we observed that the wt-hASBT retained approximately 30 % of its function under 12 mM (equilibrative) extracellularly applied sodium, relative to 137 mM (the “physiological” sodium gradient), in transiently transfected COS-1 cells (Figure 4). This protocol has proven valuable to uncover amino acid residues that are highly implicated in sodium transport. Mutation of such residues will incur functional defects that may not be immediately evident under the high

extracellular sodium concentrations ($\approx 137 - 140$ mM) applied in a typical functional assay (“initial rates” of uptake). In contrast, under equilibrative conditions uptake will likely be deficient, and the relevance of the mutated residues will be revealed. The reduced function observed for wt-hASBT under this protocol suggested that mutations on the wt-hASBT background may be further detrimental for activity, and uptake for sodium sensitive mutants may not be measurable. This limitation was circumvented by the use of C270A, which retained approximately 80% of its activity under equilibrative $[\text{Na}^+]$ (Figure 4 and [119]). The minimal sodium-sensitivity exhibited by C270A, combined to the fact that Cys²⁷⁰ is not essential for function [89, 120], rendered C270A an attractive background for our sodium dependence (also called “sodium activation”) experiments [119, 120, 122, 123, 127]. We provide a list of sodium-sensitive residues in Appendix A.

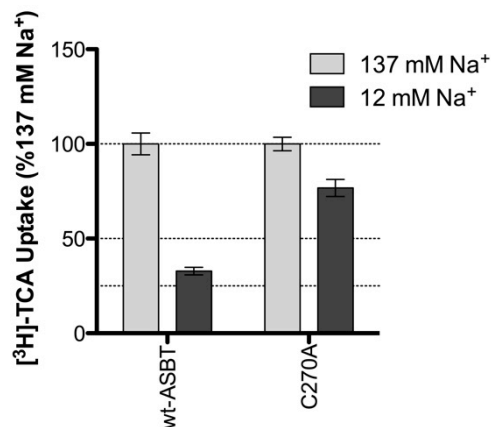


Figure 4. Sodium Activation/Dependence of the wt-hASBT and C270A in Transiently Transfected COS-1 Cells.

COS-1 cells transfected with wt-hASBT or C270A plasmid, were incubated with $5\mu\text{M}$ TCA (spiked with $[\text{3H}]\text{-TCA}$) in buffer containing 12 mM or 137 mM sodium. Uptake is expressed in pmoles $[\text{3H}]\text{-TCA}$ internalized per minute per milligram of protein. Bars represent the S.E.M. of three independent experiments, each performed in triplicates.

2.3 Summary of hASBT Topology

We have demonstrated that successful mapping of regions implicated in hASBT transport cycle can be achieved with a combination of SCAM, kinetics evaluation, sodium activation experiments, and a continuous cross-validation between experimental and *in silico* results. In SCAM, we have systematically mutated individual amino acids comprising entire putative protein segments and evaluated their solvent accessibility with a variety of MTS reagents (MTSET, MTSES, MTSEA, MTSEA-biotin or TS-biotin) and protocols.

Integrated, our observations suggest: *i*) a potential cooperativity between TM6, EL3 and TM7 during bile acid translocation. The TM7 exofacial side and the EL3 transversing segment (where Cys²⁷⁰ is located), exhibited striking solvent accessibility and substrate protection [120]; *ii*) the proline- and glycine- enriched TM6 may possibly function as a conformational switch that facilitates local and global conformational changes in EL3 and TM7, during translocation [122] (Figure 5A); *iii*) hydrophilic cavities in TM3 and TM7, and the presumed presence of proline-induced distortions in their respective helices, also support a collaborative motion between these helices during substrate exit into the cytoplasm [124] (Figure 5B); *iv*) TM1 is involved in translocation of one of the two allegedly transported sodium ions [127], and may potentially collaborate with TM7 and EL1 during this process. *v*) also based on the reputed 2:1 sodium : bile acid stoichiometry, sodium sensors Asp¹²² (EL1) and Glu²⁶¹ (EL3), as well as Phe²⁷⁸ (TM7) and Glu²⁶¹ (EL3), which are putatively responsible for sodium stabilization via cation π interactions, are reputed participants in sodium transport. In summary, we revealed participation of EL1 and EL3 in sodium and bile acid binding;

TM1, TM6 and TM7 in lining the sodium and bile acid pathways and finally, TM3 and possibly TM4 in participating in the substrate exit route into the cytoplasm [119-124, 127]. We present an overview of our observations and a schematic representation of the ASBT transport cycle in Appendix A and Figure 6, respectively. Investigations on the role of TM2 and TM5 in hASBT transport are underway.

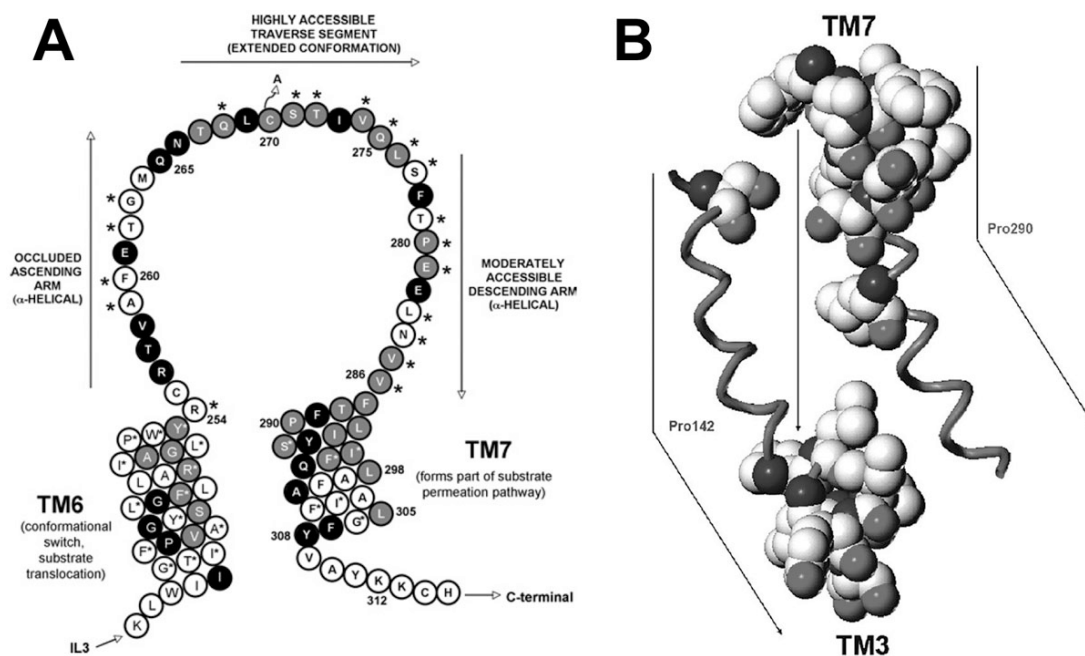


Figure 5. Accessibility profile and cooperation among several hASBT regions.

Reprinted with permission from [124] (Copyright 2009 American Chemical Society) and [120]. A, Solvent accessible regions at TM6, EL3 and TM7. Black circles represent amino acids that exhibit functional loss upon cysteine substitution; light grey circles denote MTS-sensitive mutants. * represent Na^+ -sensitive mutants. B, Relative orientation of TM7 and TM3, based on their solvent-accessibility profiles, with the putative translocation pathway formed between TM7 and TM3. Arrows indicate putative distortions induced by Pro¹⁴² and Pro²⁹⁰, and the space-filled format depicts amino acids.

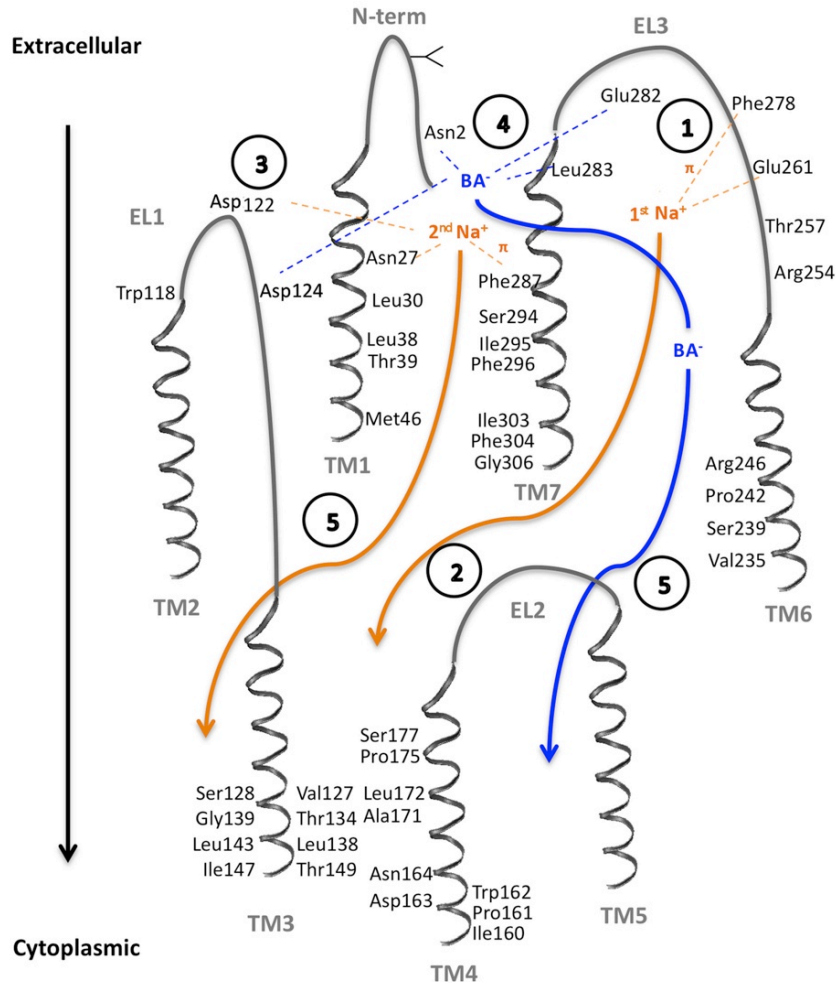


Figure 6. Putative ASBT transport cycle

This research was originally published in [127]. Reprinted with permission. Proposed mechanism based on the established 7 transmembrane domain topology [116] and putative 2:1 sodium : bile acid stoichiometry [65], as well as current and previous publications. Direct interaction of sodium (orange) or bile acid (blue) with amino acid residues is denoted as dotted lines, while translocation through reputed substrate pathways is shown as full arrows. Transmembrane domains (TM1-7) and extracellular loops (EL1-3) are shown in gray, and amino acid residues involved in substrate interactions or that line the substrate pathway are visualized. Intracellular loops were omitted for clarity. Circled numbers describe each proposed step: (1) Stabilization of the 1st Na^+ ion within EL3 via the negatively charged sodium sensor Glu261 [120, 121, 130] and cation- π forces with the Phe278 aromatic ring [120]; (2) Na^+ binding triggers conformational changes that will facilitate its own permeation and (3) simultaneously favor binding of the sodium sensor Asn122 [121, 130] to the 2nd Na^+ ion, which is further stabilized by amino-aromatic/cation- π interactions with Phe287 and the amide proton in Asn27. (4) Structural changes induced by binding/stabilization of the 2nd Na^+ will render the binding pocket formed by Glu282, Leu283 and Asn2 [116], and possibly Asp124, available to interact with the bile acid (BA^-), leading to coupled Na^+ and BA^- translocation through translocation pathways in TM1 (current manuscript), TM6 [122] and TM7 [119], and exit into the cytoplasm through TM3 [124] and TM4 [123](5). Participation of TM2 and TM5 in substrate/ion binding or translocation is currently under investigation.

Chapter 3 Transmembrane Helix I Contributes to Substrate Translocation and Protein Stability Of Bile Acid Transporter SLC10A2³

3.1 *Introduction*

Enterohepatic recirculation is a highly efficient mechanism for conserving the body's total bile acid pool. Whereas the majority of bile acids are reabsorbed passively throughout the small intestine, active reabsorption occurs in the distal ileum by the apical sodium-dependent bile acid transporter (ASBT; SLC10A2). As a high-capacity, high-affinity co-transporter, ASBT effectively reclaims the vast majority of bile acids, such that less than 5% of the circulating bile acid pool is lost through fecal elimination [26]. Defective ASBT transport is associated with various disease conditions [25, 34, 35]. Further, ASBT constitutes a pharmacologic target for improving oral drug bioavailability [5, 6, 108] as well as hypocholesterolemic agents, since cholesterol metabolism is induced upon bile acid depletion [37, 38]. To elucidate the structure-function relationship of ASBT, our laboratory has previously employed cysteine scanning mutagenesis and site-directed alkylation techniques [116, 118] to determine structural requirements for substrates and their turnover [116, 119, 120, 122, 176, 177]. We demonstrate that residues lining TM6 [122] and TM7 [119] participate in substrate recognition and protein

³ This research was originally published in the Journal of Biological Chemistry. Authors: T Claro da Silva, N Hussainzada, CM Khantwal, JE Polli, P Swaan. Title: "Transmembrane helix I contributes to substrate translocation and protein stability of bile acid transporter SLC10A2". *Journal of Biological Chemistry*. 2011; Vol: 286 (31), 27322 - 27332. © the American Society for Biochemistry and Molecular Biology.

entry from the exofacial matrix, while the cytosolic half of TM3 mediates substrate release into the cytosolic milieu [124], putatively in conjunction with TM4 [123]. Moreover, the extracellular loop (EL) 1 [121] and EL3 [120] regions mediate initial substrate and sodium recognition and binding and may facilitate movement of ligands in solvent accessible pockets situated deeper into the protein core, for ultimate translocation along membrane spanning domains. A number of groups have corroborated the functional importance of key residues identified in ASBT transport and function [130, 131].

The present study extends our analysis to TM1 based on: (i) its high degree of amino acid conservation among a wide range of ASBT orthologs (3) (Fig. 7B), in particular the sodium-dependent organic anion transporter (SOAT; SLC10A6) [178], and Ntcp (SLC10A1) [15]; (ii) the relatively amphipathic nature of TM1, which would facilitate passage of charged substrates during permeation events; and (iii) the spatial proximity of TM1 to other regions of functional importance, specifically EL1 and TM7 [116, 118]. Based on these facts, we hypothesized that TM1 plays a pivotal role in ASBT's substrate translocation process.

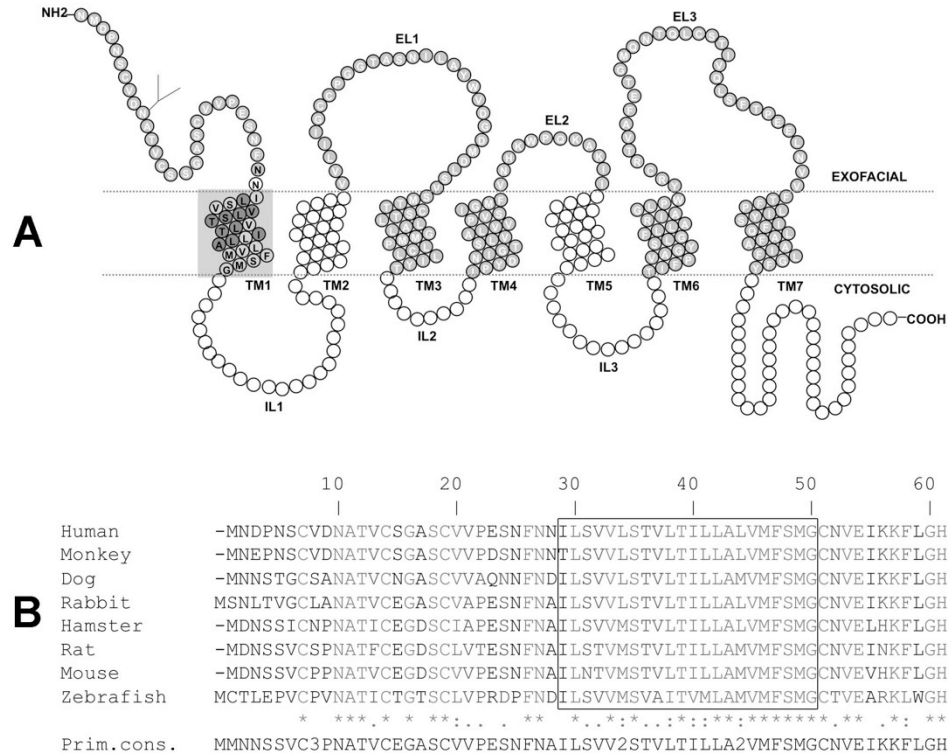


Figure 7. ASBT (SLC10A2) protein secondary structure and sequence conservation across species.

A, Secondary structure of ASBT based on our validated topology model [126]. Circles represent single amino acid residues; dotted lines indicate the lipid-aqueous interface, with large-scale protein features (*i.e.* extracellular loop (EL), intracellular loop (IL) and transmembrane (TM) regions); dark-shaded circles indicate residues previously submitted to Cys-scanning mutagenesis and thiol modification. Residues comprising the TM1 region are encircled by a light gray square and contain their single-letter amino acid designation in black. B, TM1 (Ile²⁹-Gly⁵⁰) is indicated by a box. Sequences were aligned with ClustalW [179], and the levels of conservation are highlighted, with asterisks (*) representing identical residues, colons (:) demonstrating strongly similar residues, and a period (.) denoting weakly similar residues.

3.2 Experimental Procedures

3.2.1 Materials

[³H]-Taurocholic acid (0.2 Ci/mmol) was purchased from American Radiolabeled Chemicals, Inc, (St. Louis, MO); taurocholic acid (TCA) and glycodeoxycholic acid (GDCA) from Sigma (St. Louis, MO); MTS reagents from Toronto Research Chemicals, Inc, (North York, ON, Canada); immobilized streptavidin from Pierce Biotechnology, Inc. (Rockford, IL); pepstatin from Research Products International Corp. (Mt. Prospect, IL); MG132 from Cayman Chemical (Ann Harbor, MI); WST-1 reagent from Roche

Diagnostics GmbH (Mannheim, Germany); cell culture media and supplies were obtained from Invitrogen (Rockville, MD). All other chemicals were of the highest purity available commercially.

3.2.2 Site-directed mutagenesis, transfection, cell culture and protein expression

The MTS-insensitive hASBT C270A construct was used as a scaffold for cysteine point mutations as described previously [86, 119], while the wt-ASBT was the template for Ala mutations, as well as N27D and N27Q. Mutants were verified by sequencing and transiently transfected in COS-1 cells as described [177]. Protein expression at the cell surface was determined by biotinylation with the membrane impermeable EZ Link NHS-SS-Biotin (Pierce, Rockford, IL) followed by Western blot as previously described [177] and detailed in the figure legends. An Odyssey imaging system (Licor, NE) was used to visualize protein bands. This approach permits comparative measurement of expression levels for both the glycosylated (41 kDa) and unglycosylated (38 kDa) ASBT protein species, with a custom-designed rabbit polyclonal anti-hASBT antibody (1:1,000) [116]. Labeling selectivity to cell surface proteins was confirmed by the absence of a 90 KDa band for the ER protein calnexin (mouse anti-calnexin; Sigma; 1:1,000), and presence of a 140 KDa band for the cell surface marker pan-cadherin (mouse anti-cadherin; 1:1000; Abcam). Blots are representative of two independent experiments.

3.2.3 Substrate transport and sodium activation of TM1 mutants

Transiently transfected COS-1 cells were incubated at 37 °C for 12 min in Modified Hanks' balanced salt solution (MHBSS), pH 7.4, containing 5.0 µM cold TCA spiked with 1 µCi/mL [³H]-TCA. Uptake was halted by washing cells with ice-cold

DPBS containing 0.2% fatty acid-free BSA and 0.5 mM TCA. Cells were lysed in 350 μ L 1N NaOH, and substrate incorporation was measured by liquid scintillation counting, using a LS6500 liquid scintillation counter. Rates of uptake were calculated as pmols of [3 H]-TCA internalized per min per mg of protein using the Bradford assay for total protein quantification. The influence of sodium on transport function was determined by [3 H]-TCA uptake under equilibrating (12 mM) versus physiological (137 mM) sodium concentrations, as described previously [177]. Choline chloride (ChCl) is used as a replacement for sodium and added to the 12 mM sodium solution to maintain osmolarity. The ratio of uptake at 12 mM Na⁺ versus 137 mM Na⁺ was calculated for each mutant transporter and normalized to the C270A control ratio. An uptake ratio equal to one implies minimal participation of that residue during sodium interaction or binding events, while fractions above or below one suggest a putative role during sodium co-transport events.

3.2.4 Substrate and sodium kinetics of select TM1 mutants

Substrate kinetics were determined for a select group of TM1 cysteine mutants using a wide range of bile acid (0 – 200 μ M TCA) and sodium (0 – 200 mM NaCl) concentrations as described previously [121]. Kinetic parameters were derived by nonlinear regression using GraphPad 5.0 software (San Diego, CA) as described [121].

MTSET inhibition and substrate protection studies– Transiently transfected COS-1 cells were pre-treated with 1 mM MTSET for 10 min at room temperature (r.t.), and evaluated for [3 H]-TCA uptake, as previously described [121, 177]. Control cells (without MTSET) were treated identically and run in parallel. For each mutant, MTSET inhibition of transport activity was calculated as the ratio of uptake for the MTSET-

treated cells versus the control cells. Each ratio was then normalized to the C270A ratio. Additionally, the influence of sodium or the endogenous substrate glycodeoxycholic acid (GDCA; 200 μ M) on MTSET (1mM) labeling rates was evaluated as described [177]. Briefly, cells were pre-treated with 1 mM MTSET in the absence or presence of GDCA or Na⁺ for 10 min at r.t. and incubated in MHBSS buffer at 37 °C for 15 min, followed by [³H]-TCA uptake as described above. To evaluate the effect of temperature on substrate protection, pre-incubations with 1 mM MTSET in the absence or presence of GDCA or Na⁺ were performed for 10 min at r.t. vs. 4 °C. Inhibition was determined for each mutant by calculating the ratio of mutant uptake at each experimental condition versus its respective unmodified control. Mutant ratios were then normalized to the C270A ratio calculated in the same manner.

3.2.5 Assessment of proteasomal or lysosomal degradation and hASBT folding

Transiently transfected COS-1 cells were treated 24 – 48 hrs post-transfection with the following inhibitors (final concentrations in antibiotic-free, 10% FBS DMEM, *i.e.*, AB-free DMEM): NH₄Cl, leupeptin/pepstatin, MG132, cyclosporine A (CsA), and cholic acid (CA), at concentrations listed in the figure legend. After 8h (MG132, NH₄Cl and leupeptin/pepstatin) or 24h (CsA and CA), cells were washed twice in ice-cold PBS, lysed and processed as described above, or reagents were replaced with AB-free DMEM for 30 min prior to experiment, followed by biotinylation as described above. Protein concentrations were determined by the Bradford assay, with equal gel protein loading (7 μ g/lane), except for G50C samples, which were loaded at a slightly higher concentration (8.5 μ g/lane), to permit band visualization. Densitometric analysis later accounted for this difference, since both the loading control cadherin, as well as the protein bands were

normalized to the amount loaded per well. This method allowed us to make comparisons of different treatments for the same mutant, as well as between mutants. To ensure that the treatments did not cause cytotoxicity, cell viability was examined with the WST-1 reagent (Roche Applied Sci, IN) per manufacturer's instructions.

3.2.6 Data Analysis

One-way analysis of variance (ANOVA) with Dunnett's post-hoc test, or the two-tailed unpaired Student's t-test was employed when appropriate, using GraphPad 5.0 or Kaleidagraph 4.0. Differences were considered statistically significant (*) at $p \leq 0.05$. Bars represent the standard error of the mean (SEM) for $n \geq 3$.

3.3 *Results*

3.3.1 Transport activity and membrane expression of TM1 cysteine mutants

Individual cysteine substitutions were incorporated along the TM1 helix (Ile²⁹-Gly⁵⁰; Fig. 7A) using our previously validated C270A scaffold as the mutagenic template [86, 119]. The polar residues Asn²⁷ and Asn²⁸ were included since they are positioned at the putative exofacial membrane-aqueous boundary. Each mutant was transiently transfected in COS-1 cells and evaluated for functional activity and protein cell surface expression. Parallel measurements of total protein levels in whole cell lysates were performed to distinguish between mutants with alterations in protein synthesis or degradation rate versus membrane targeting defects due to cysteine substitution.

After normalizing uptake rates to membrane expression, the majority of TM1 cysteine mutants (71%; 18 of 24 mutants; Figure 8), demonstrated significantly altered uptake rates for the prototypical substrate taurocholic acid (TCA) compared to C270A

control. Activity for mutant G50C was severely diminished (<10% control activity) as was its overall expression, suggesting that mutation caused protein misfolding or instability leading to rapid degradation. The other TM1 cysteine mutants demonstrated measurable expression levels both in whole cell lysate fractions as well as at the cell surface (Figure 8). Interestingly, N27C had ~20% residual transport activity whereas neighboring N28C remained largely unaffected. In contrast, mutant L38C exhibited increased uptake rates. degradation rate versus membrane targeting defects due to cysteine substitution.

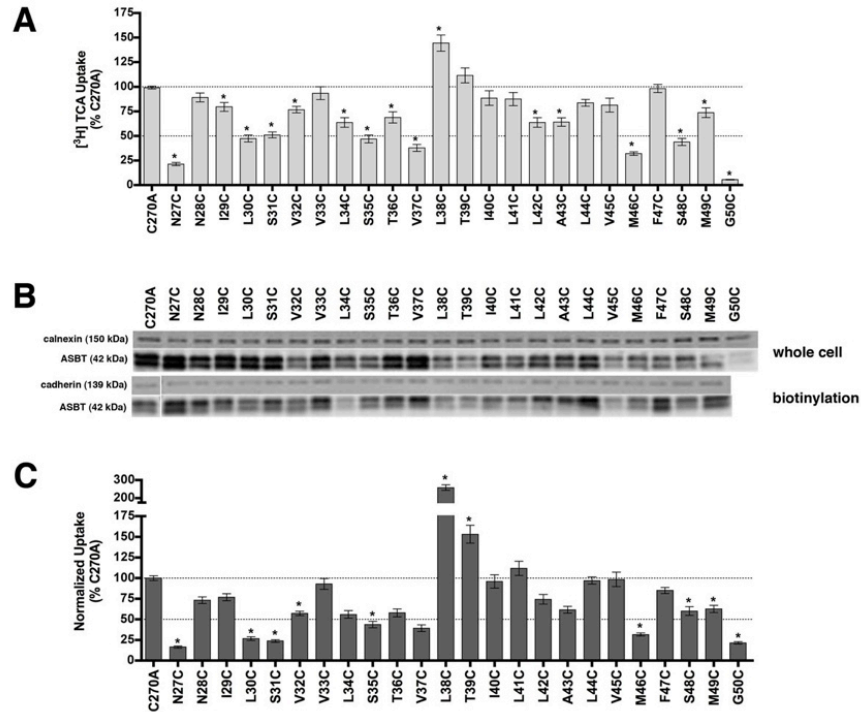


Figure 8. [³H]-TCA uptake and protein expression of TM1 cysteine mutants.

A, COS-1 cells were transfected with C270A or mutant plasmids as described in Methods. Rates of uptake were expressed as a percentage of the parental transporter, C270A, in pmoles [³H]-TCA internalized per minute per milligram of protein. Bars represent the S.E.M. of three independent experiments, each performed in triplicate. ANOVA with $p < 0.05$ (*) indicates significant mean differences. B, Total (whole cell) and cell surface (biotinylation) protein expression of Cys mutants. Equal amounts of protein (7 μ g/lane) were loaded on a 12.5% denaturing polyacrylamide gel, and hASBT protein was identified using a custom anti-hASBT antibody (1:1,000). Labeling selectivity to cell surface proteins was confirmed by the absence of a 90 KDa band for the ER protein calnexin (mouse anti-calnexin; 1:1,000), and presence of a 140 KDa band for the cell surface marker pan-cadherin (mouse anti-cadherin; 1:1,000). Mature glycosylated hASBT visualizes as the 41kDa band while the lower, 38kDa band (not indicated) represents the unglycosylated species. Blots are representative of two independent experiments. C, Rate of uptake expressed as a percentage of the parental transporter, C270A, normalized to ASBT cell surface expression (from B, lower panel). Since levels of glycosylated (41 KDa) and unglycosylated (38 KDa) protein were tightly correlated, only glycosylated protein bands were considered for densitometric analysis.

3.3.2 Sodium Activation

ASBT actively concentrates bile acids within the cell interior by harnessing energy from the inward sodium gradient [65]. To investigate the involvement of TM1 in sodium translocation, we assayed each mutant for TCA transport at physiological and equilibrating extracellular $[Na^+]$ (12 mM), *i.e.* $[Na^+]_{out} \approx [Na^+]_{in}$. Theoretically, this strategy can identify residues that are sensitive to extracellular levels of sodium and that

may participate, either directly or indirectly, during sodium transport steps. For each mutant, we calculated the ratio of transport at 12 mM vs. 137 mM $[Na^+]$ and then normalized values to the C270A ratio. Our previous studies confirm minimal sodium sensitivity of the C270A parental template under equilibrative extracellular Na^+ conditions [119]. N27C, L30C, L38C, T39C and M46C demonstrated significant differences in sodium sensitivity (Fig. 9 and Table 2) compared to C270A control.

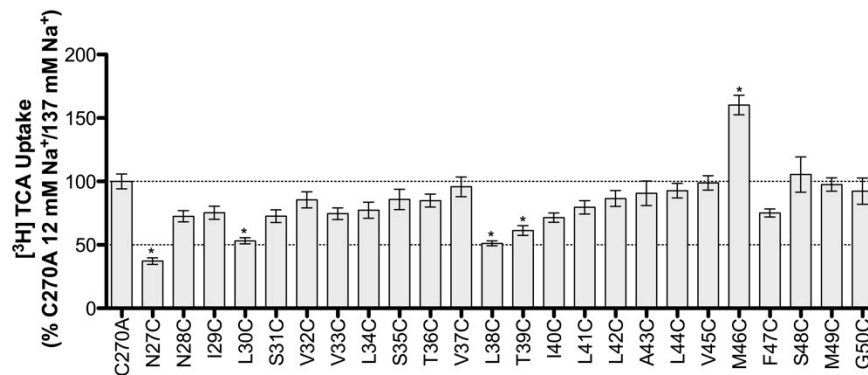


Figure 9. [³H]-TCA uptake ratio under equilibrating (12 mM) vs. saturating (137 mM) sodium concentrations.

Uptake of 5 μ M TCA (spiked with [³H]-TCA) in COS-1 cells transfected with C270A or mutant plasmid, in pmoles [³H]-TCA internalized per minute per milligram of protein, calculated as the ratio of uptake at 12 mM/137 mM sodium concentrations, and further normalized as a percentage of the parental C270A ratio. Bars represent the S.E.M. of three independent experiments, each performed in triplicates. ANOVA with $p < 0.05$ (*) indicate significant mean differences.

Table 2. Substrate kinetic parameters for select TM1 mutants^a.

	Na ⁺ Kinetics		TCA Kinetics	
	J _{max} (pmol/min/mg protein)	K _{Na} (mM)	J _{max} (pmol/min/mg protein)	K _{TCA} (μM)
C270A	380.3 ± 16.8	8.9 ± 1.6	892.8 ± 57.7	9.7 ± 2.4
N27C ^{1,2}	93.4 ± 8.2	*34.0 ± 8.3	312.5 ± 28.7	21.5 ± 6.2
N28C	347.7 ± 25.1	5.5 ± 2.0	1469.0 ± 55.6	17.7 ± 2.2
L30C ^{1,2,3}	198.1 ± 8.2	*19.5 ± 2.6	1047.0 ± 183.5	*59.8 ± 25.0
L34C ^{1,3,4}	178.4 ± 6.9	7.5 ± 1.2	592.7 ± 23.3	11.6 ± 1.7
S35C ^{1,3}	270.3 ± 9.4	11.3 ± 1.5	389.5 ± 35.6	5.7 ± 2.6
T36C ^{1,3,4}	336.5 ± 16.7	9.9 ± 1.9	801.8 ± 37.1	8.6 ± 1.6
L38C ^{2,3,4}	716.6 ± 54.7	*24.1 ± 5.6	*1507.0 ± 32.2	10.6 ± 0.9
T39C ^{2,3}	406.9 ± 17.5	*16.4 ± 2.4	553.5 ± 70.0	6.3 ± 3.6
M46C ^{1,2}	164.2 ± 8.4	* 1.3 ± 0.8	239.2 ± 25.2	8.4 ± 3.3
F47C	297.6 ± 13.0	12.8 ± 2.0	453.8 ± 64.6	6.5 ± 4.0

¹decreased uptake due to mutation, ²sodium sensitive, ³MTSET inhibition, ⁴substrate protection

^aCOS-1 cells transiently transfected as described in "Experimental Procedures". Uptake measured at substrate concentrations ranging from 0 - 200 μM for TCA, or 0 - 200 mM for NaCl (measured in triplicate). Kinetic data analyzed using Graphpad Prism software, with constants determined via nonlinear regression, and one-way ANOVA for significance. Parameters significantly different from the C270A control are indicated, *p ≤ 0.05.

3.3.3 Solvent accessibility of cysteine mutants

Membrane-impermeant MTSET is highly selective for ionized sulfhydryl groups, which predominantly occur on Cys residues exposed to an aqueous environment [154, 180]. Thus, pre-incubation with MTSET followed by evaluation of functional activity can theoretically identify residues that lie within binding pockets or translocation pathways. Our data reveal significant decreases in functional activity upon MTSET treatment for mutants L30C, V33C, L34C, S35C, L38C and T39C (Figure 10). These sites are situated predominantly along the exofacial half of the helix. Interestingly, L30C, L34C, and L38C are most affected by MTSET modification and roughly display a-helical periodicity. While we expect inhibition of [³H]-TCA uptake for residues that line an aqueous substrate permeation pathway, functionally silent modifications may occur that cannot be identified under these experimental conditions.

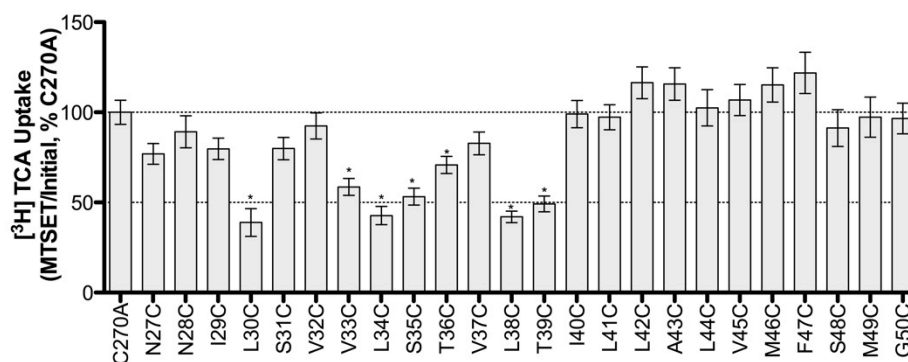


Figure 10. MTSET labeling of TM1 Mutants.

Transiently transfected COS-1 cells were pre-incubated with 1 mM MTSET for 10 min, at r.t., followed by washes, and [³H]-TCA uptake. The ratio of uptake in absence vs. presence of MTSET (*i.e.* MTSET/Initial rates of uptake) was expressed as a percentage of MTSET/Initial ratio of the parental C270A. Bars represent the S.E.M. of three independent experiments, each performed in triplicates. ANOVA with $p < 0.05$ (*) indicate significant mean differences.

3.3.4 Substrate Protection Assays

To determine whether ASBT substrates interact with solvent accessible residues identified above, MTSET was co-incubated with glycodeoxycholic acid (GDCA, $K_T \sim 2.0 \mu\text{M}$). “Substrate protection” afforded under these conditions was calculated as a percentage of the uptake under untreated conditions. Only residues affected under these conditions are shown (Figure 11). Native wt-ASBT protein was included as a positive control, since it displays significant substrate protection from MTSET modification in presence of GDCA (Figure 11A). Substrate protection was observed only for mutants L34C, T36C and L38C (Figure 11A); complete restoration of transport activity suggests that these residues may interact with substrate directly or modulate translocation steps.

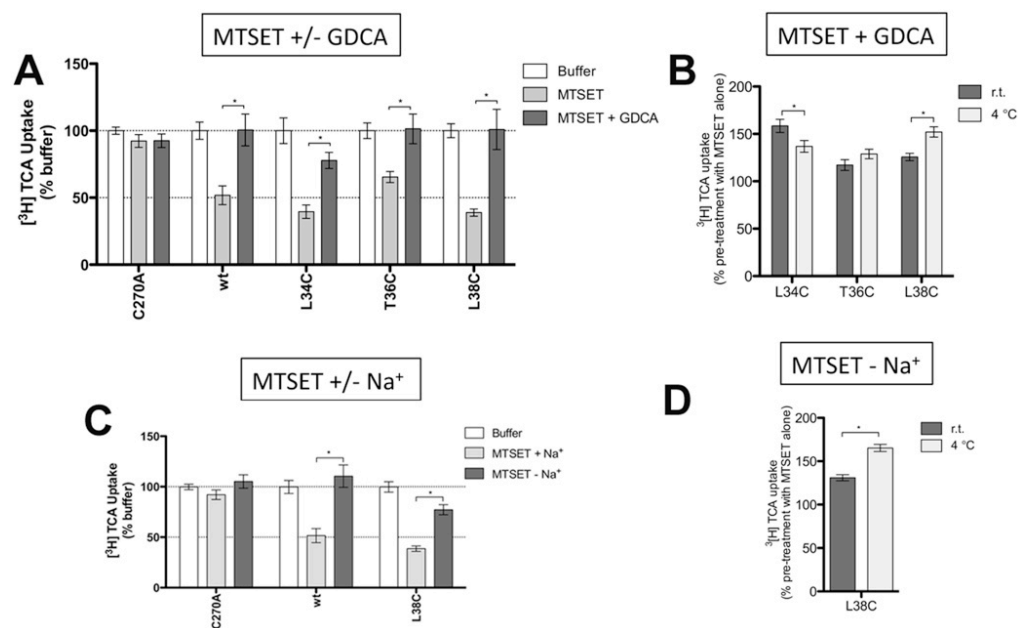


Figure 11. Effect of GDCA or sodium on uptake recovery from MTSET modification.

Transiently transfected COS-1 cells were pre-incubated with buffer alone or 1 mM MTSET +/- GDCA or +/- Na⁺, for 10 min, followed by washes, 15 min incubation in buffer alone, and [³H]-TCA uptake. A, MTSET +/- 200 μM GDCA. For each mutant, results were expressed as a percentage of the uptake in buffer alone (Initial rates of uptake). B, Effect of temperature on GDCA protection from MTSET labeling. Pre-incubation with MTSET + GDCA at r.t. vs. 4 °C for 10 min. For each mutant, results were expressed as a percentage of the uptake after pre-incubation in MTSET alone. C, MTSET +/- Na⁺. ChCl was used an equimolar replacement for NaCl. For each mutant, results were expressed as a percentage of the uptake in buffer alone (Initial rates of uptake). D, Effect of temperature on sodium protection from MTSET labeling. MTSET - Na⁺ at r.t. vs. 4 °C for 10 min. For each mutant, results were expressed as a percentage of the uptake after pre-incubation in MTSET alone. Bars represent the S.E.M. of three independent experiments, each performed in triplicates. Student's t test of significant mean differences with p < 0.05 (*) are indicated.

In addition to bile acid, binding of sodium may alter protein conformation to occlude previously accessible sites or reveal previously inaccessible residues. MTSET pretreatment in the absence of sodium significantly protected L38C against MTSET modification (Figure 11B) compared to parallel experiments in the presence of sodium. These data suggest that accessibility for this residue is altered by sodium interaction events. Combined, both bile acid and sodium binding modulate solvent accessibility for Leu³⁸.

To discriminate between direct and indirect occlusion of L34C, T36C and L38C by sodium and bile acid, we determined the temperature-dependence of substrate protection for these mutants. While MTSET access to a residue should not vary with temperature, residues located at conformationally sensitive regions will exhibit different protection patterns at 4 °C, where molecular motions are expected to be slower. GDCA prevents MTSET access to L34C and L38C, but not to T36C, in a temperature-dependent fashion (Figure 11), whereas protection increases at low temperatures for L38C. These results suggest that L34C is placed in a region sensitive to conformational changes caused by bile acid, but not sodium, translocation. GDCA protection for T36C was independent of temperature, suggesting that T36C is not governed by dynamic changes in protein conformation. Instead, it is possible that T36C is located near the bile acid binding pocket or translocation pathway. L38C may be placed in a flexible region of TM1 modulated by translocation of both sodium and bile acid. Interestingly, GDCA protection at 4 °C decreases for L34C and increases for L38C, which tempts speculation that Leu³⁴ and Leu³⁸ sense distinct, possibly opposite forces during bile acid translocation, alternating solvent accessibility.

3.3.5 Kinetic Analysis of Select TM1 Mutants

To further analyze the role of TM1 residues affected above, we performed kinetic evaluation on a subset of mutants affording their Michaelis-Menten constant (K_T). N27C, L30C, L38C, T39C and M46C exhibited significantly altered sodium affinity (K_{Na}), whereas only L30C concomitantly displayed significant changes in substrate affinity (K_T) (Table 2). Mutation at Leu³⁸ significantly increases J_{max} without affecting K_T . Despite significant solvent accessibility and substrate protection, mutants L34C and T36C had

analogous K_T and K_{Na} values compared to C270A control, consistent with placement of these residues within solvent accessible pockets that are indirectly modulated by substrate binding and translocation, *e.g.* via global changes in protein conformation.

3.3.6 Analysis of select TM1 Mutants against wt-ASBT background

The results above for C270A scaffold mutants prompted us to further investigate functional relevance of these residues in wt-hASBT. Accordingly, we generated N27A, L30A, L38A and M46A on the wt-hASBT background, and assessed mutant function by [³H]-TCA uptake (Figure 12A). T39A could not be generated. We evaluated the impact of side chain size and charge for Asn²⁷, via additional N27D and N27Q mutants. All Asn27 mutants had minimal activity compared to the wt-ASBT control, underscoring the specific need of an asparagine in this position. Approximately 25% activity was observed for L30A. L38A and M46A showed about 80% of wt-ASBT activity, and were further inspected for their sodium sensitivity. Consistent with the previous results L38C/C270A and M46C/C270A double mutants, sodium sensitivity for L38A increased while M46A was less sensitive compared to wt-ASBT control. These results support a central role for Leu³⁸ and Met⁴⁶ during sodium translocation events.

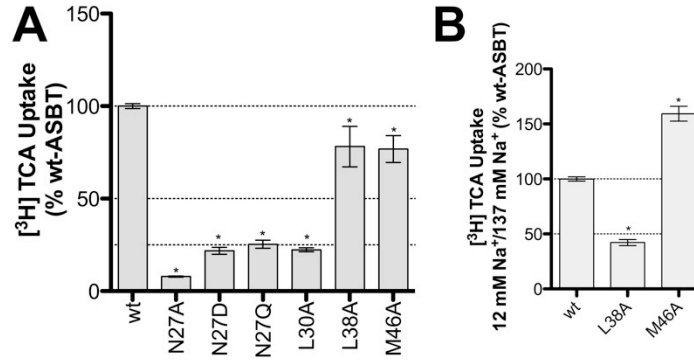


Figure 12. Effect of mutation on wt-hASBT Function and Sodium Dependence of Select Mutants.

A, [³H]-TCA uptake of COS-1 cells transfected with the wt-ASBT or mutant proteins. Rates of uptake were expressed as a percentage of the parental transporter, wt-ASBT, in pmoles [³H]-TCA internalized per minute per milligram of protein. Bars represent the S.E.M. of two independent experiments, each performed in triplicates. ANOVA with $p < 0.05$ (*) indicate significant mean differences. B, Ratios of [³H]-TCA uptake under saturating (137 mM) vs. equilibrating (12 mM) sodium concentrations. Uptake levels in COS-1 cells transfected with wt-ASBT or mutant plasmid, in pmoles [³H]-TCA internalized per minute per milligram of protein, calculated as the ratio of 12 mM/137 mM sodium concentrations, and further normalized as a percentage of the parental wt-ASBT sensitivity (12 mM/137 mM). Bars represent the S.E.M. of two independent experiments, each performed in triplicates. ANOVA with $p < 0.05$ (*) indicate significant mean differences.

3.3.7 Residue Gly⁵⁰ is critical for ASBT folding

Total protein expression of G50C is dramatically decreased (Figure 13B). Since [³H]-TCA transport could be measured, this suggests that mutation at Gly⁵⁰ produces a functional transporter. Based on these observations, we hypothesized that mutation resulted in rapid protein degradation via either proteasomal or lysosomal pathways. Treatment with increasing concentrations of proteasomal inhibitor MG132 [181] resulted in a dose-dependent increase in G50C protein levels in cell lysates (Figure 13C), confirming that proteasomal degradation constitutes a major degradation pathway for this mutant. Treatment with MG132 also resulted in increased G50C uptake compared to untreated cells (buffer only) (Figure 13D). Most notably, MG132 treatment led to increased transport function (Figure 13D) and cell surface expression (Fig. 13E) of G50C. Treatment with lysosomal pathway inhibitors NH₄Cl and leupeptin/pepstatin [181] did not significantly affect G50C protein expression, thus suggesting minimal lysosomal

degradation of mutant and control proteins (Fig. 13A, B and D). The ubiquitin-proteasome system (UPS) plays a crucial role in endoplasmic reticulum (ER) quality control by eliminating defective proteins from the cell. We hypothesized that mutations at Gly⁵⁰ caused folding abnormalities that culminate in the mutant's rapid degradation by the UPS. "Substrate-assisted folding" may rescue protein levels when substrate is present during protein folding by interacting with the active site, and stabilize its conformation, thereby aiding the mutant protein in passing ER quality control [182]. We chose the hASBT substrate cholic acid (CA); its relatively high lipophilicity would facilitate permeation through the plasma membrane to reach the ER. However, treatment with CA (Figure 13E) did not significantly restore G50C protein levels. Other common ASBT substrates, such as CDCA and LCA, rendered identical results (data not shown).

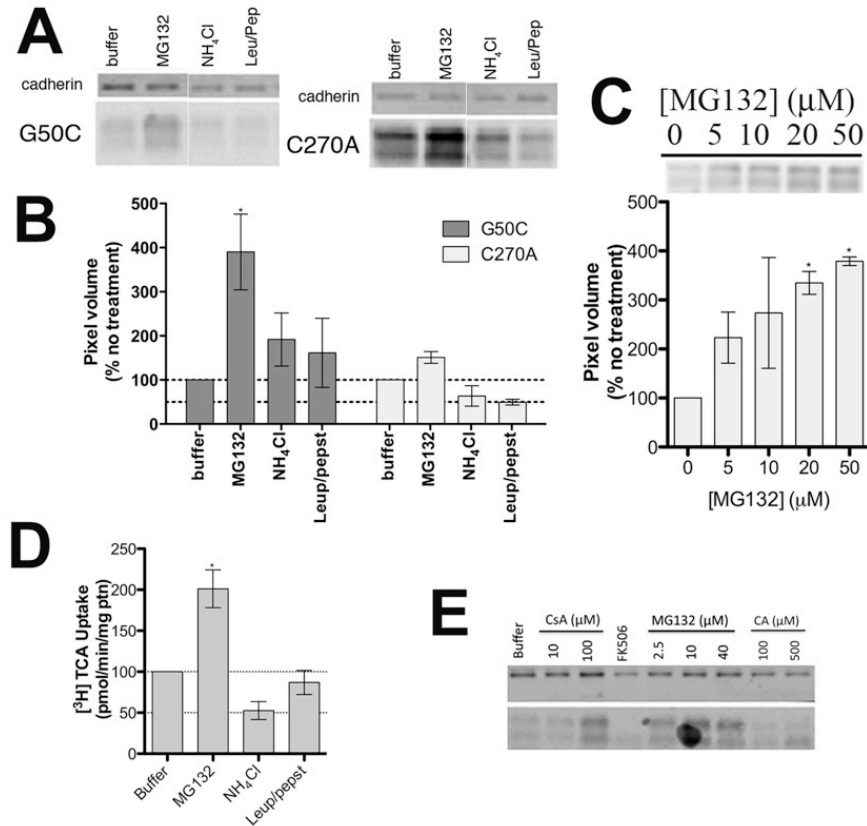


Figure 13. Mechanism of G50C Instability.

COS-1 cells transiently transfected with C270A or G50C were treated with appropriate reagents for specified amounts of time. For the protein expression experiments, equal amounts of protein were loaded on a 12.5 % Tris.HCl polyacrylamide gel (7 μg/lane for C270A and 8.5 μg/lane for G50C). Protein bands were visualized with the primary antibodies rabbit anti-hASBT (1:1,000) and mouse anti-cadherin (1:1,000), and the secondary antibodies anti-mouse IRDye 680 (1:10,000) and anti-rabbit DyLight 800 (1:10,000). Blots are representative of two independent experiments. A, Effect of degradation Inhibitors on G50C Expression. Cells were treated with 20 μM MG132, 15 mM NH₄Cl, and leupepsin/pepstatin (100 μg/mL of each). After 8h, which corresponds to the ASBT protein degradation half-life as determined after cyclohexamine treatment (data not shown), cells were harvested and submitted to Western blotting. B, Densitometric analysis of the Western blot bands, normalized to loading amounts and the loading control cadherin. Bars represent the S.E.M. of two independent experiments, relative to untreated control. C, Dose-dependent inhibition of G50C proteasomal degradation with MG132 and densitometric analysis of Western blot bands. Cells were treated with various MG132 concentrations (5 - 50 μM) for 8h, after which cells were harvested and submitted to Western blot. Densitometric analysis included normalization to loading amounts and the loading control cadherin. Bars represent the S.E.M. of two independent experiments, relative to untreated control. D, [³H]-TCA uptake of G50C treated with degradation inhibitors. Transfected COS-1 cells were treated with the appropriate reagents (20 μM MG132, 15 mM NH₄Cl, and leupepsin/pepstatin 100 μg/mL of each) for 8h, followed by TCA uptake as described in methods. Rates of uptake were expressed as a percentage of untreated control (buffer), normalized for negative control (mock), in pmoles [³H]-TCA internalized per minute per milligram of protein. Bars represent the S.E.M. of two independent experiments, each performed in triplicate. E, G50C Cell surface expression after treatment with degradation inhibitors/chaperones. Cells were treated with CsA (10 and 100 μM), FK506 (100 μM), and CA (100 and 500 μM) for 24h and MG132 (2.5, 10 and 40 μM) for 8h followed by biotinylation of cell surface proteins as described in Methods.

Cis-trans isomerization of proline-linked peptide bonds is a rate-limiting step in protein folding, catalyzed by peptidyl-prolyl isomerases (PPIs) including cyclophilin A (CyPA) and FK506-binding protein (FKBP) [183, 184]. PPI inhibition will likely affect protein levels and potentially reveal the mechanism involved in protein (mis)folding of PPI substrates. We employed the CyPA inhibitor cyclosporine A (CsA) and the FKBP inhibitor FK506, in order to evaluate the effect of PPI inhibition on G50C levels (Figure 13E). Treatment with 100 μ M CsA, but not FK506, clearly increased G50C levels at the cell surface, suggesting a specific role for CyPA on G50C stability, and a possible role for Gly⁵⁰ in ASBT folding.

To confirm that the observed effects were not specific to the G50C mutant, we constructed a wt-G50A mutant. Similarly to G50C, G50A displayed negligible protein levels, both in whole cell lysate and in biotinylated samples (Figure 14A), as well as low [³H]-TCA transport (Figure 14B). While the lysosomal inhibitors leupeptin/pepstatin and NH₄Cl failed to rescue G50A surface expression levels, MG132 increased protein surface expression in a dose-dependent fashion, thus confirming the major role of the proteasome in G50A degradation. Treatment with 100 μ M CsA, but not FK506, recovered cell-surface-resident G50A, thus corroborating the G50C data. The chemical chaperone 4-PBA did not rescue G50A expression (Figure 14C), but 4-PBA activity may be highly mutant specific [185, 186]. Taken together, our data suggest that mutation at Gly⁵⁰ produces a functionally intact transporter that undergoes accelerated degradation by the proteasome, partly due to folding defects induced by cyclophilin A.

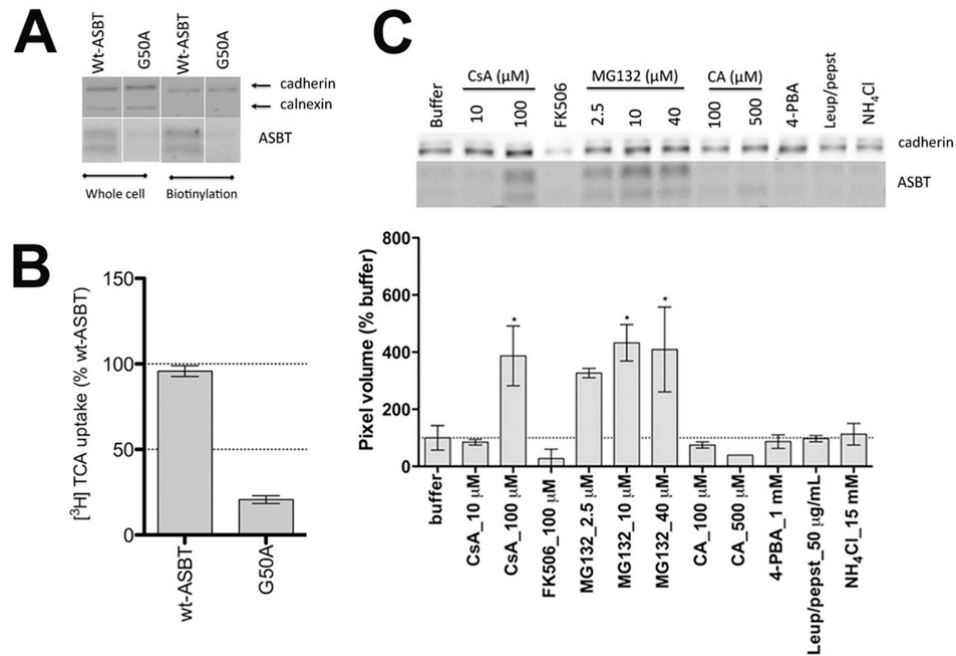


Figure 14. Mechanism of G50A Instability.

A, G50A total (whole cell) and cell surface (biotinylation) expression. COS-1 cells transfected with G50A or wt-ASBT were biotinylated 24 – 48 h post-transfection. Cells were lysed and total protein content was determined with Bradford assay, after which protein concentrations were equalized, a small aliquot was separated for total protein measurements, from which 7 $\mu\text{g/lane}$ of wt-ASBT samples and 8.5 $\mu\text{g/lane}$ of G50A were loaded onto a 12.5% denaturing polyacrylamide gel. Streptavidin beads were added to the remaining lysate, and samples prepared in reducing buffer were loaded on the gel, with G50A always loaded on the same gel as the wt-ASBT control for the corresponding experiment (whole cell or biotinylated). Blots are representative of two independent experiments. B, $[^3\text{H}]$ -TCA uptake of COS-1 cells transfected with G50A or the wt-ASBT control. Rates of uptake were expressed as a percentage of the parental transporter, wt-ASBT, in pmoles $[^3\text{H}]$ -TCA internalized per minute per milligram of protein. Bars represent the S.E.M. of at least three independent experiments, each performed in triplicates. ANOVA with $p < 0.05$ (*) indicate significant mean differences. C, G50A cell surface expression after treatment with inhibitors, substrates, or chaperones. Cells were treated with CsA (10 and 100 μM), FK506 (100 μM), CA (100 and 500 μM) and 4-PBA (1 mM) for 24h and MG132 (2.5, 10 and 40 μM), leupepsin/pepstatin (50 $\mu\text{g/mL}$) NH₄Cl (15 mM) for 8h followed by biotinylated of cell surface proteins as described above. Below the protein bands is the densitometric analysis normalized to the loading control cadherin. Bars represent the S.E.M. of two independent experiments, relative to untreated control. ANOVA with $p < 0.05$ (*) indicate significant mean differences.

3.4 Discussion

We determined the contributions of TM1 residues during substrate turnover and degradation processes of the bile acid transporter, SLC10A2. We show that the TM1 helix comprises a moderately solvent-accessible membrane-spanning domain, with accessible sites discretely spaced along one side of the exofacial half of the helix (Fig 10A). TM1 likely plays a role in both sodium and bile acid handling, as suggested by kinetic evaluation of select mutants (Table 2) and substrate protection studies in which bile acid and/or sodium influences MTSET modification rates (Figure 11). Furthermore, an intriguing role for Gly⁵⁰ is suggested during folding of the native transporter, since both G50A and G50C mutants demonstrate accelerated degradation, likely due to improper folding.

Cysteine-scanning mutagenesis of the TM1 helix and its two adjacent Asn residues demonstrates that ~70% of mutants were significantly affected by Cys mutation relative to C270A control (Fig. 2A). However, compared to our previous analysis of TM7 [119], which exhibited severe intolerance to mutation, TM1 mutants are moderately functional. Of note are residues Asn²⁷ and Gly⁵⁰, which were severely hampered ($\leq 20\%$ residual activity) by mutation. Loss of function for the G50C mutant was directly linked to a substantial increase in protein degradation, both within whole cell lysates and at the plasma membrane. In contrast, expression of the N27C mutant at the cell surface was not affected, suggesting a role for this residue in substrate interaction events.

We next examined the effects on transport of removing the electromotive force of the sodium gradient. Transport function for each mutant was evaluated at equilibrating extracellular sodium concentrations (*i.e.* $[\text{Na}^+]_{\text{out}} \sim [\text{Na}^+]_{\text{in}}$) and found that five mutants

(N27C, L30C, L38C, T39C, M46C) were affected by altered $[\text{Na}^+]$ (Figure 9). Subsequent kinetic evaluation corroborated a significant change in sodium affinity (K_{Na}) (Table 2). Bile acid affinity (K_{T}) was unaltered for these residues (except L30C), signifying their involvement during sodium binding events. In contrast, equilibrative $[\text{Na}^+]$ resulted in increased transport function for M46C (Figure 9), suggesting that loss of the sodium gradient restored M46C function. Subsequent kinetic analysis of M46C revealed a significantly higher affinity for sodium (K_{Na}) but not for bile acid, which validates the proposed role of M46C in sodium binding events. This decrease in sodium sensitivity was reproducible for the M46A mutant generated on the wt-ASBT background (Figure 12). Similar results were observed for Leu³⁸ mutants L38C and L38A. Because both Leu³⁸ and Met⁴⁶ are uncharged residues, but nonetheless appear to affect sodium transport, we posit that these residues may form part of a highly sodium sensitive region that cooperates to modulate sodium permeability.

Our next set of functional studies exploited the thiol reactivity of cysteine groups introduced along the TM1 helix, and measured transport inhibition upon pre-incubation with MTSET reagent. Significant inhibition of TCA transport was observed predominantly for residues lining the exofacial half of the TM1 helix (Figure 10), specifically Leu³⁰–Thr³⁹. The inhibition pattern of these residues forms a roughly a-helical pattern, especially Leu residues (L30, L34, L38) flanked by hydrophilic amino acids (S/T); further, discrete partitioning is observed toward one face of the TM1 helix when mapped to a helical wheel representation (Figure 15A). Kinetic analysis supports sodium and bile acid interactions for Leu³⁰ and sodium interactions for Asn²⁷, Leu³⁸, Thr³⁹, and Met⁴⁶ (Table 2). Subsequently, substrate protection studies were conducted to

Our ASBT homology model [116] predicts proximity of Asn²⁷ to the highly solvent accessible exofacial half of TM7 (Fig. 15B,C), particularly Phe²⁸⁷ and Thr²⁸⁸ which are both located in the vicinity of a structural anchor comprising residues Phe²⁸⁹, Tyr²⁹³, Asp²⁹⁷, Ala³⁰¹, Phe³⁰⁷ and Tyr³⁰⁸ [119]. Because neither conservative nor non-conservative mutations of Asn²⁷ restored activity (Figure 12A), we conclude that this residue is essential at this particular position, perhaps by forming cation- π point interactions with Phe²⁸⁷ and Na⁺ to stabilize an optimal three-dimensional conformation required for ASBT function (Figure 13C). Since cation- π interactions can accept a third electron-deficient group [187] and our model indicates that Asp²⁷ and Phe²⁸⁷ are located in the vicinity of Ile¹⁰³, Gly¹⁰⁴, Thr¹¹⁰, Leu¹¹⁵, Ala¹¹⁶, and Val¹¹⁹ in EL1 [121], and Val¹²⁷ and Ser¹²⁸ in TM3 [124], all of which are sodium sensitive, we propose an arrangement where Phe²⁸⁷ is sandwiched between the Asn²⁷ amide proton and the sodium ion (Figure 15C), which may serve to stabilize conformations that promote bile acid transport.

Finally, we report accelerated hASBT degradation rates upon mutation of highly conserved Gly⁵⁰ and conclude that this residue may be critical for hASBT folding (Figures 8, 13, 14). We demonstrate that mutations at Gly⁵⁰ produced functionally intact proteins, and that G50A and G50C expression could be rescued by the proteosomal degradation inhibitor MG132 but not by lysosomal inhibitors. Moreover, G50A (Figure 14C) and G50C (Figure 13E) proteins that escaped from the ER (due to MG132 treatment) could be properly inserted into the plasma membrane. Data with CsA and FK506 support a partial role for Gly⁵⁰ on cis-trans isomerization of hASBT prolines by CyPA, but not FKBP. The definitive mechanism involved in CsA rescue of G50A and G50C expression is presently unclear. CyPA does not require a specific recognition motif

in its substrates in order to execute its proline isomerization activity [188]. We speculate that Gly⁵⁰ resides next to a critical hASBT region for CyPA recognition, and mutation at this residue may affect the final catalysis product, potentially leading to excessive protein isomerization and improper folding.

In summary, we demonstrate that the TM1 helix is important for both sodium and bile acid transport events, with residues situated along the exofacial helix likely participating during substrate permeation. Residues Asn²⁷, Leu³⁰, Leu³⁸, Thr³⁹ and Met⁴⁶ play a crucial role in sodium affinity, while only residue Leu³⁰ appears to be essential for bile acid affinity. We also report an intriguingly and possibly regulatory role of Gly⁵⁰ on hASBT folding. Overall, these data in combination with our previous studies reveal interactions at the molecular level of ASBT that provide a deeper insight into its functional transport cycle (Figure 6).

Chapter 4 Charged Residues At The First Half Of The Intracellular Loop I Are Critical For Protein Stability Of The Apical Sodium-Dependent Bile Acid Transporter (ASBT; SLC10A2), And Respond Specifically To Cyclosporine A

4.1 *Introduction*

The human apical sodium-dependent bile acid transporter (hASBT, SLC10A2) is the chief intestinal bile acid transporter and is key to the enterohepatic circulation of bile acids (EHC). Topologically, hASBT is a glycoprotein that spans the membrane bilayer seven times, oriented with an extracellular N-terminus and cytoplasmic C-terminus ($N_{\text{exo}}/C_{\text{cyt}}$) [75, 89, 90, 145]. It utilizes cellular sodium gradient to actively concentrate bile acids in the enterocytes. We and others [189] have indicated transmembrane domain (TM) 1, 3, 4, 6 and 7; extracellular loop (EL) 1 and 3 [119-124, 127]; and the C-terminus [189] as participants on this concerted translocation process. Yet, the relevance of intracellular regions on hASBT function or stability is unclear. In NTCP, Asp¹¹⁵, located in the intracellular loop (IL) III, was shown to be essential for taurocholic acid (TCA) transport [190]. Charged residues in the IL connecting the TM6 and TM7 of the human intestinal di-/tripeptide transporter (hPEPT1), are critical for glycylsarcosine uptake [191]. In the multidrug resistance protein 1 (MRP1/ ABCC1), mutation at the cytoplasmic loops (CL) 3 and 7 affect MRP1 surface expression or function [192]. Here, we report our investigations on the highly conserved (Figure 16) hASBT IL1, and its

contribution to hASBT function and protein expression. Alanine replacement of individual amino acids along IL1 (Cys⁵¹-Phe⁷²) was detrimental for function in approximately 70% of mutants, as measured by [³H]-taurocholate uptake. For a cluster of amino acids in the first half of the loop, namely, Cys⁵¹ – Lys⁵⁷, Ala mutation resulted in hampered activity, with corresponding deficient protein expression (except N52A, I55A and K56A) (Figure 17). In contrast, for the majority of residues following Lys⁵⁷, reduced activity was unrelated to protein levels. As reported for hPEPT1 [191], charged residues may play an important role in substrate transport events. Moreover, positively charged amino acids located in cytoplasmic regions of membrane proteins may function as topogenic signals [193], and influence protein orientation and stability. There are six highly (Glu⁵⁴, Lys⁵⁷, His⁶¹ and Arg⁶⁴) or moderately (Lys⁵⁶ and Lys⁶³) conserved charged residues in IL1. Along the entire loop, only one of these residues is acidic (Glu⁵⁴), while the vast majority of charged residues is basic. To gain insight on the role of charged residues in IL1, we further examined them with conservative and non-conservative mutations. We included Cys⁵¹ in our investigations due to their high levels of inter-species conservation and their proximity to Gly⁵⁰, previously shown to be critical for hASBT stability [127]. Recovery of cell surface expression upon MG132 and cyclosporine A (CsA) treatment for C51A, C51S, E54A, E54L, K57A and K57E, support a role for Gly⁵¹, Glu⁵⁴ and Lys⁵⁷ in hASBT stability and possibly folding. CsA is employed in protein folding studies primarily due to its ability to inhibit proline isomerization catalyzed by cyclophilin A (CyPA), a rate-limiting step in protein folding. Intriguingly, we observed a striking increase in cell surface expression for the tested mutants, as well as for the wt-hASBT, compared to non-treated control (Figures 19 and

22) suggesting that the mechanism of augmented protein expression observed may or may not involve CyPA inhibition. Instead, because CsA is an inhibitor of ASBT transport, we hypothesize that this effect may be due to ligand-induced folding of poorly expressed mutants, or improved wt-hASBT folding. Further investigations in this regard are underway. Conservative and non-conservative mutations at His⁶¹, Lys⁶³ and Pro⁶⁵ also suggest that these residues are important for hASBT function. Overall, our results support a role for the first half of IL1 in hASBT stability, and for the remaining IL1 amino acids in transport function.

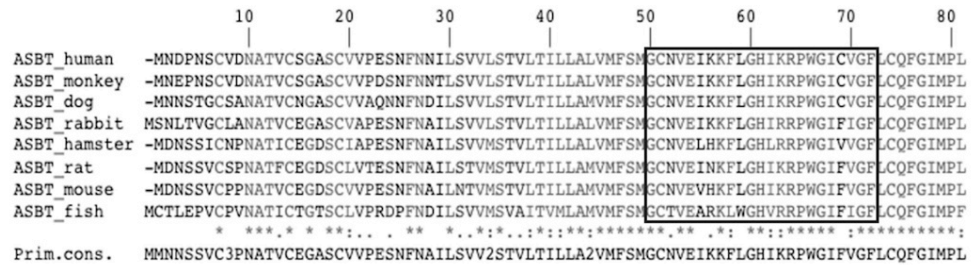


Figure 16. ASBT (SLC10A2) protein sequence conservation across species. Amino acids comprising IL1 (Gly⁵⁰-Phe⁷²) are indicated by a box. Sequences were aligned with ClustalW [179], and the levels of conservation are highlighted, with asterisks (*) representing identical residues, colons (:) demonstrating strongly similar residues, and a period (.) denoting weakly similar residues.

4.2 *Materials and Methods*

4.2.1 Materials

[³H]-Taurocholic acid (0.2 Ci/mmol) was purchased from American Radiolabeled Chemicals, Inc, (St. Louis, MO); taurocholic acid (TCA) from Sigma (St. Louis, MO); immobilized streptavidin from Pierce Biotechnology, Inc. (Rockford, IL); MG132 from Cayman Chemical (Ann Harbor, MI); cell culture media and supplies were obtained from Invitrogen (Rockville, MD). All other chemicals were of the highest purity available commercially.

4.2.2 Site-directed mutagenesis, transfection, cell culture and protein expression

Mutations were introduced at the pCMV5-hASBT vector (a kind gift from Dr. Paul Dawson), by site-directed mutagenesis using a QuickChange kit from Stratagene (La Jolla, CA). After sequencing confirmation, mutants were transiently transfected in COS-1 cells as described [177]. Protein total and cell surface expression was measured by biotinylation with the membrane impermeable EZ Link NHS-SS-Biotin (Pierce, Rockford, IL), followed by Western blot of the whole cell lysate (total) or streptavidin-pulled biotinylated samples (cell surface). Before streptavidin addition, concentrations were determined by the Bradford assay, and equalized with PBS. A small aliquot (30 μ L) was removed for total protein measurements, from which equal amounts (8.5 μ g/lane for low expression mutants, or 7 μ g/lane for the wt-hASBT), were loaded in a 12.5% Tris-HCl acrylamide gel. Protein bands were identified with a custom-designed rabbit polyclonal anti-hASBT antibody (1:1,000) [116] and visualized on an Odyssey imaging system (Licor, NE). Selectivity of cell surface labeling was confirmed by the absence of a 90 KDa band for the ER protein calnexin (mouse anti-calnexin; Sigma;1:1,000), and presence of a 140 KDa band for the cell surface marker pan-cadherin (mouse anti-cadherin; 1:1000; Abcam). Protein bands were normalized to the amount loaded per well, and to the loading control cadherin. Blots are representative of two independent experiments.

4.2.3 Substrate transport of IL1 mutants

COS-1 cells transiently transfected with pCMV5-hASBT or mutants were incubated with 5.0 μ M cold TCA spiked with 1 μ Ci/mL [3 H]-TCA in modified Hanks'

balanced salt solution (MHBSS), pH 7.4, at 37 °C for 12 min. To halt uptake, cells were washed with ice-cold DPBS containing 0.2% fatty acid-free BSA and 0.5 mM TCA, lysed in 350 μ L 1N NaOH, and substrate incorporation was measured by liquid scintillation counting, using a LS6500 liquid scintillation counter. Rates of uptake were calculated as pmols of [3 H]-TCA internalized per min per mg of protein, using the Bradford assay for total protein quantification.

4.2.4 Bile acid kinetics of IL1 charged mutants

Charged residues in IL1 that exhibited impaired uptake despite normal protein levels, were selected and their TCA kinetics measured with a variety of TCA concentrations. Transiently transfected COS-1 cells were incubated with a wide range of cold TCA (0 – 200 μ M TCA) concentrations, spiked with 2 μ Ci/mL [3 H]-TCA, in modified Hanks' balanced salt solution (MHBSS), pH 7.4, at 37 °C for 12 min. The amount of radiolabeled TCA employed guaranteed measurements above background levels for all concentrations used. Kinetic parameters were derived by nonlinear regression using GraphPad 5.0 software (San Diego, CA) as described [121].

4.2.5 Assessment of proteasomal degradation and hASBT folding

COS-1 cells transiently transfected with the wt-hASBT or mutant proteins were treated with MG132, cyclosporine A (CsA), FK506, cholic acid (CA), 4-PBA and leupepsin/pepstatin at the concentrations described at the figure legends. Twenty-four hours post-transfection, cells were washed with Dulbecco's Modified Eagle Medium, and incubated in antibiotic-free, 10% FBS DMEM, *i.e.*, AB-free DMEM with or without Cyclosporine A, FK506 and CA. The next day (9 h prior to experiment), MG132, 4-PBA

and leupepsin/pepstatin in AB-free DMEM were added to the appropriate wells. Media in all wells was replaced with AB-free DMEM 45 min - 1 hour prior to experiment, to allow for recovery of monolayers before biotinylation, thereby preventing labeling of internal lysines. Finally, cells were washed twice in ice-cold PBS, lysed or biotinylated as described above.

4.2.6 Data Analysis

When appropriate, One-way analysis of variance (ANOVA) with Dunnett's post-hoc test was employed, using GraphPad 5.0 or Kaleidagraph 4.0. Statistically significant differences ($p \leq 0.05$) are indicated by (*). Bars represent the standard error of the mean (SEM) for $n \geq 2$.

4.3 *Results*

4.3.1 Taurocholate uptake and protein expression of IL1 mutants

To investigate the role of the intracellular loop 1 (IL1), we have replaced individual amino acids along this loop region (Cys⁵¹-Phe⁷²) with alanine, and assessed the functional consequences of mutation with taurocholate (TCA) uptake. Approximately 70% of mutants had impaired activity, which did not correlate with their protein expression, except for mutants of a group of residues (Cys⁵¹ – Lys⁵⁷) located in the first half of IL1 (Figure 17).

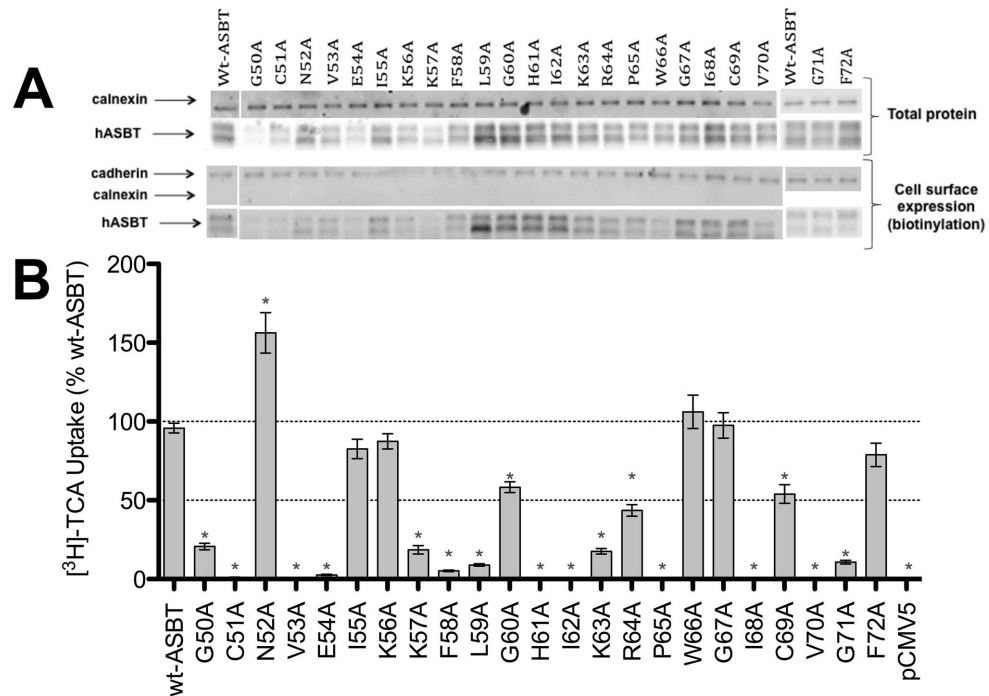


Figure 17. ^3H -TCA uptake and protein expression of IL1 cysteine mutants.

A, Total (whole cell) and cell surface (biotinylation) protein expression of Cys mutants. Equal amounts of protein (7 $\mu\text{g}/\text{lane}$) were loaded on a 12.5% denaturing polyacrylamide gel, and hASBT protein was identified using a custom anti-hASBT antibody (1:1,000). Labeling selectivity to cell surface proteins was confirmed by the absence of a 90 KDa band for the ER protein calnexin (mouse anti-calnexin; 1:1,000), and presence of a 140 KDa band for the cell surface marker pan-cadherin (mouse anti-cadherin; 1:1,000). Mature glycosylated hASBT visualizes as the 41kDa band while the lower, 38kDa band (not indicated) represents the unglycosylated species. Blots are representative of two independent experiments. B, COS-1 cells were transfected with wt-hASBT or mutant plasmids as described in Methods. Rates of uptake were expressed as a percentage of the parental transporter, wt-hASBT, in pmoles ^3H -TCA internalized per minute per milligram of protein. Bars represent the S.E.M. of three independent experiments, each performed in triplicate. ANOVA with $p < 0.05$ (*) indicates significant mean differences.

As shown for MRP1 [192], charged amino acids in intracellular loops may play an important role in transporter function or expression. To further examine the impact of charged residues in IL1, we generated their conservative and non-conservative mutants, and assessed their TCA uptake and total protein expression (Figure 188). Additionally, poorly expressed Ala mutants were treated with the prolyl-peptidyl isomerase inhibitors cyclosporine A (inhibits cyclophilin A or CyPA) and tacrolimus (FK506; inhibits the FK506-binding protein or FKBP), the proteasomal inhibitor MG132, and the chemical chaperones Trimethylamine n-oxide (TMAO) and sodium 4-phenylbutyrate (4-PBA).

Only CsA and MG132 recovered cell surface levels for the tested mutants, suggesting that the low expression observed for these mutants was likely due to proteasomal degradation, possibly as a consequence of folding defects (Figure 19).

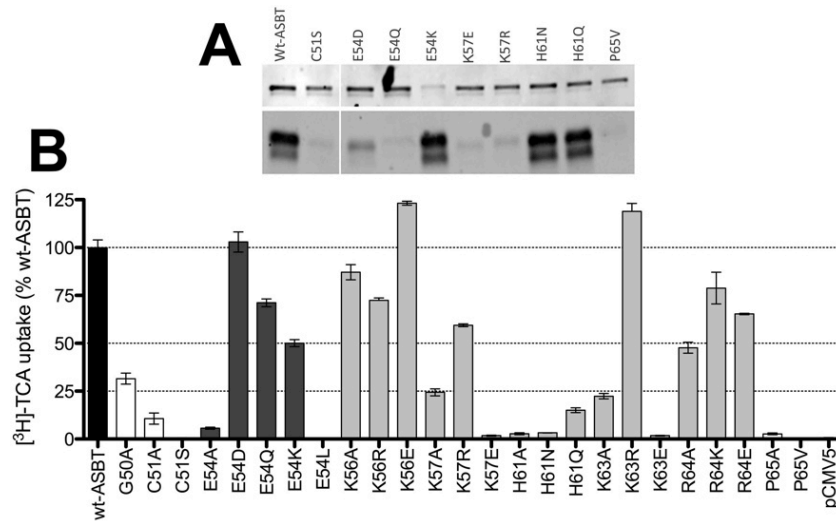


Figure 18. Effect of conservative and non-conservative mutation on wt-hASBT Function and Protein Expression of Select Mutants.

A, Protein expression in whole cell lysates of COS-1 cells transfected with the wt-hASBT or mutant proteins. COS-1 cells transfected with mutants or wt-hASBT were lysed 24h – 48h post-transfection, and the total protein content was determined with Bradford assay. Protein concentrations were equalized, and 7 $\mu\text{g}/\text{lane}$ of wt-ASBT samples and 8.5 $\mu\text{g}/\text{lane}$ of mutants were loaded onto a 12.5% denaturing polyacrylamide gel. Samples were prepared in reducing buffer and loaded on the gel, with mutants always loaded on the same gel as the wt-hASBT control for the corresponding experiment. B, ^3H -TCA uptake of COS-1 cells transfected with the wt-hASBT or mutant proteins. Rates of uptake were expressed as a percentage of the parental transporter, wt-hASBT, in pmoles ^3H -TCA internalized per minute per milligram of protein. Bars represent the S.E.M. of two independent experiments, each performed in triplicates.

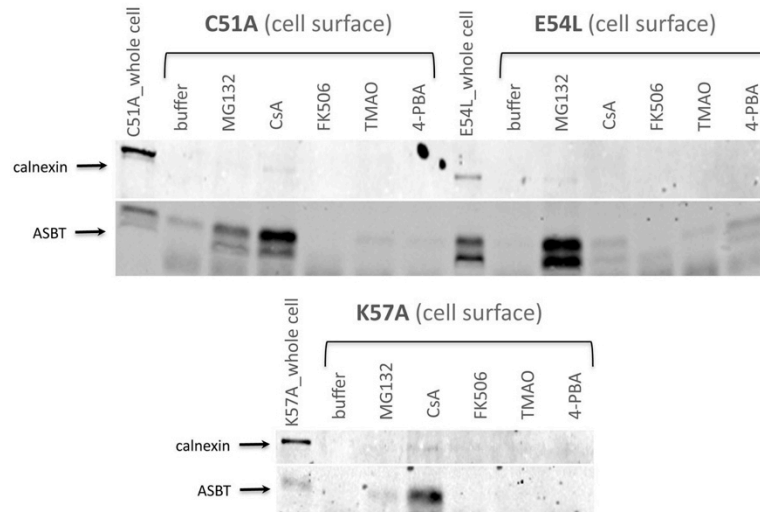


Figure 19. Mechanism of Instability of Select Mutants.

COS-1 cells transfected with mutants or wt-hASBT were treated, 24 – 48 h post-transfection, with CsA (10 and 100 μ M), FK506 (100 μ M), TMAO (500 μ M) and 4-PBA (1 mM) for 24h and MG132 (2.5, 10 and 40 μ M), leupepsin/pepstatin (50 μ g/mL) NH_4Cl (15 mM) for 8h before biotinylation of cell surface proteins. Cells were lysed and total protein content was determined with Bradford assay. Protein concentrations were equalized, a small aliquot was separated for total protein measurements, from which 7 μ g/lane of wt-ASBT samples and 8.5 μ g/lane of mutants were loaded onto a 12.5% denaturing polyacrylamide gel. Streptavidin beads were added to the remaining lysate, and samples were prepared in reducing buffer and loaded on the gel, with mutants always loaded on the same gel as the wt-hASBT control for the corresponding experiment (whole cell or biotinylation).

For the single acidic residue in IL1, namely, Glu⁵⁴, alanine replacement (E54A) obliterated function and protein expression both in whole cell lysates as well as in the cell surface, whereas leucine (E54L) only reduced levels in the cell surface. In contrast, presence of Asp (E54D), Lys (E54K) and Gln (E54Q) at this position, rescued both uptake and total protein expression, suggesting that a combination of size chain size with electronegative groups (regardless of being donors or acceptors of hydrogen bond) is necessary at position 54.

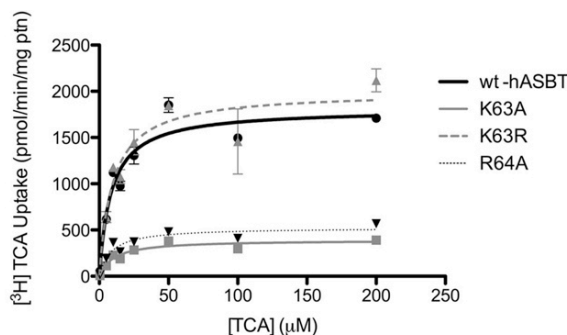
The moderately conserved Lys⁵⁶ was minimally affected by mutation, and does not appear to play an essential role in hASBT function or stability. On the contrary, the Lys⁵⁷ mutants K57A and K57E affected both protein expression and function, while the conservative K57R restored function to wt-hASBT levels. The K63A and K63E mutants

exhibited impaired function, which was fully restored with re-introduction of a basic amino acid (K63R). It is noteworthy that Lys⁵⁷ and Lys⁵⁶ as well as Lys⁶³ and Arg⁶⁴ form pairs of basic residues with, respectively, high and low levels of tolerance to mutation. Both Lys⁵⁷ and Lys⁶³ are highly conserved among different species, and exhibited a strict requirement for a basic group in their locations. It is tempting to speculate that Lys⁵⁶ and Arg⁶⁴ evolved to provide an alternative basic environment in that region. Differently from mutation at Lys⁵⁷, the Lys⁶³ mutants exhibited measurable protein levels, suggesting that their hampered activity was due to alterations in protein function. TCA affinity was unaltered for K63A, K63R, and R64A (Figure 20), suggesting that Lys⁶³ and Arg⁶⁴ do not interact with bile acids directly.

To examine His⁶¹, we generated Ala as well as the allegedly conservative Gln and Asn mutations. According to Leatherbarrow and Fersht [194], “*The amide-NH₂ of Gln may be considered stereochemically equivalent to the epsilon-NH of His whereas the amide-NH₂ of Asn is comparable to the delta-NH of histidine*”. In their work, Gln functioned as a semiconservative His⁴⁵ replacement in stabilizing the transition-state during amino acid esterification by the tyrosyl-tRNA synthetase of *Bacillus stearothermophilus*. In contrast to their observation, Gln replacement was not conservative at position 61, and H61Q, in addition to H61N and H61A, exhibited impaired activity, without affecting protein levels, suggesting that His⁶¹ is essential for hASBT function.

Proline residues are renowned for their relevance in forming protein loops and turns [195]. P65A exhibited impaired function, which prompted us to further examine Pro⁶⁵ with the P65V mutant. We chose this mutation, because despite proline’s unique

structure, it has been shown that a valine functioned as a conservative replacement at retinoic acid binding protein II and cellular retinol binding protein I [196]. Interestingly, while only function was affected by alanine replacement, presence of a valine at position 65 disrupted both function and protein expression. These observations indicate that Pro⁶⁵ is important for hASBT function, although the reason for this Ala vs. Val difference is unclear.



	Wt-hASBT	K63A	K63R	R64A
J_{\max} (pmol.min ⁻¹ .mg protein ⁻¹)	1809 ± 94.34	392.8 ± 23.56	1996 ± 141.0	525.9 ± 34.68
K_m (μM)	8.589 ± 1.836	10.44 ± 2.406	9.595 ± 2.677	8.543 ± 2.314

Figure 20. Kinetic Parameters of Select IL1 Mutants.

COS-1 cells transiently transfected as described in "Materials and Methods", and uptake was measured with TCA concentrations ranging from 0 - 200 μM (measured in triplicate). Kinetic data analyzed using Graphpad Prism software, with constants determined via nonlinear regression, and one-way ANOVA for significance. Parameters significantly different from the wt-hASBT control are indicated, *p ≤ 0.05.

4.3.2 Residues Cys⁵¹, Glu⁵⁴ and Lys⁵⁷ are critical for ASBT stability

We have recently shown that Gly⁵⁰, a residue located at the interface of TM1 with IL1, is critical for hASBT protein stability [127]. Cell surface expression of the unstable G50A and G50C mutants was recuperated upon MG132 and CsA treatment, suggesting a role for Gly⁵⁰ during hASBT stability and possibly folding. These observations prompted us to hypothesize that Gly⁵⁰ forms part of a region involved with hASBT stability, with potential participation of vicinal amino acids. Alanine replacement of IL1 amino acids revealed a cluster of residues Cys⁵¹ – Lys⁵⁷ with obliterated protein levels (except N52A,

I55A and K56A). We further examined charged amino acids potentially involved in hASBT stability, and included Cys⁵¹ in our investigations, due to its proximity with Gly⁵⁰, and the low protein levels observed for C51A and C51S. Treatment with MG132 and CsA recovered protein levels in the cell surface for C51A, E54L and K57A (Figure 19), suggesting that these mutants are rapidly degraded by the proteasome, possibly as a consequence of folding abnormalities. This data supports participation of the first half of IL1, specifically, Cys⁵¹, Glu⁵⁴ and Lys⁵⁷, in ensuring hASBT stability and possibly folding, and the second half in hASBT function (Figure 21).

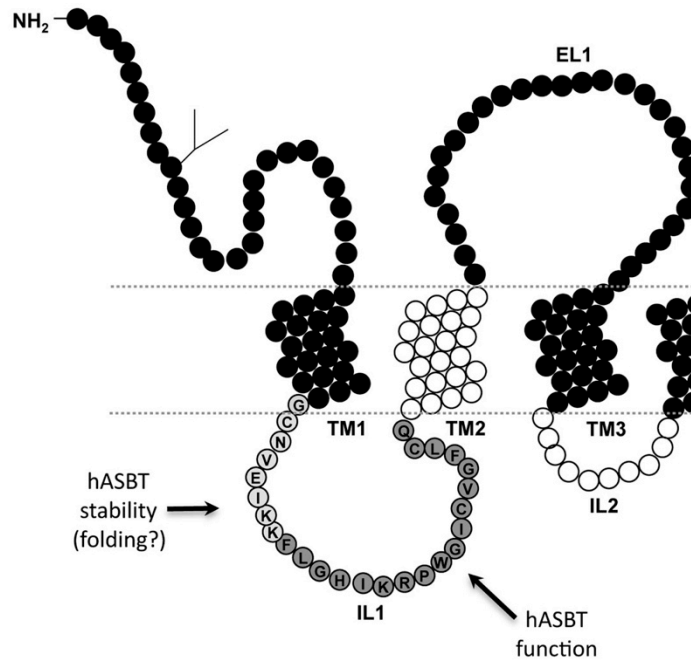


Figure 21. Graphic representation of IL1 amino acids relevant for hASBT function and stability.

Secondary structure of ASBT based on our validated topology model [126]. Circles represent single amino acid residues; dotted lines indicate the lipid-aqueous interface, with large-scale protein features (*i.e.*, N-terminus, extracellular loop (EL), intracellular loop (IL) and transmembrane (TM) regions); black circles indicate residues studied previously. Residues comprising IL1 contain their single-letter amino acid designation in black, with the IL1 region putatively relevant for hASBT stability highlighted in light-shaded gray, and the IL1 region putatively relevant for hASBT function in dark-shaded gray.

4.3.3 Cyclosporine A increases wt-ASBT Expression

Peptidyl-prolyl-cis/trans isomerases (PPIases) are “folding helper” enzymes that catalyze *cis-trans* proline isomerization; a rate-limiting step in protein folding. Three structurally unrelated families constitute the PPIases: the cyclophilins (CyP), the FK506 binding proteins (FKBPs) and the parvulins [197]. Cyclosporine A (CsA) and tacrolimus (FK506) are strong inhibitors of, respectively, cyclophilin A (CyPA) [198] and FKBP, which imparts them useful in protein folding studies. These inhibitors widely employed in the clinic as immunosuppressants, to prevent and treat rejection of transplanted organs [199], but the mechanism of immunosuppression is distinct from their PPIase inhibition. Namely, the CsA-CyPA or FK506-FKBP complex inhibits phosphatase 2B (calcineurin), leading to over-phosphorylation of the nuclear factor of activated T cells (NF-AT) and finally, silencing of T-lymphocyte transcription [199, 200], thereby suppressing the immune system. Remarkably, CsA is also a non-competitive inhibitor of hASBT expressed in COS-1 [64], and in rat ileum *in vivo* as well as everted gut sacs, whereby it exhibited time- and dose-dependent inhibition of bile acid transport [201]. Moreover, Hulzebos *et al* [202] reported that chronic CsA administration *in vivo* increased rat Asbt expression by 2-fold, while both FXR and ASBT mRNA levels remained unchanged. Consistent with Hulzebos’ findings, wt-hASBT treatment with CsA increased wt-hASBT protein expression in the cell surface (Figure 222) in transiently transfected COS-1 cells. One may argue that PPIase inhibition would expectedly decline protein levels due to improper folding, rather than increase it. In fact, FK506 had the predictable effect of reducing wt-hASBT protein levels, as shown in Figure 222. While these results indicate FKBP as a likely participant in wt-hASBT folding, the role of CyPA remains unclear.

Furthermore, it is possible that the mechanism of CsA effect on the wt-hASBT (and possibly its mutants) is more complex than simply CyPA inhibition. We are tempted to speculate that the aforementioned *in vitro* [64] and *in vivo* [201] inhibition of ASBT by CsA, may impart CsA with the ability to interact with ASBT (and mutants) and act as a chaperone with “ligand-induced folding”, similarly to what occurs when P-glycoprotein (Pgp) misfolded mutants were treated with CsA [203], which is a Pgp substrate.

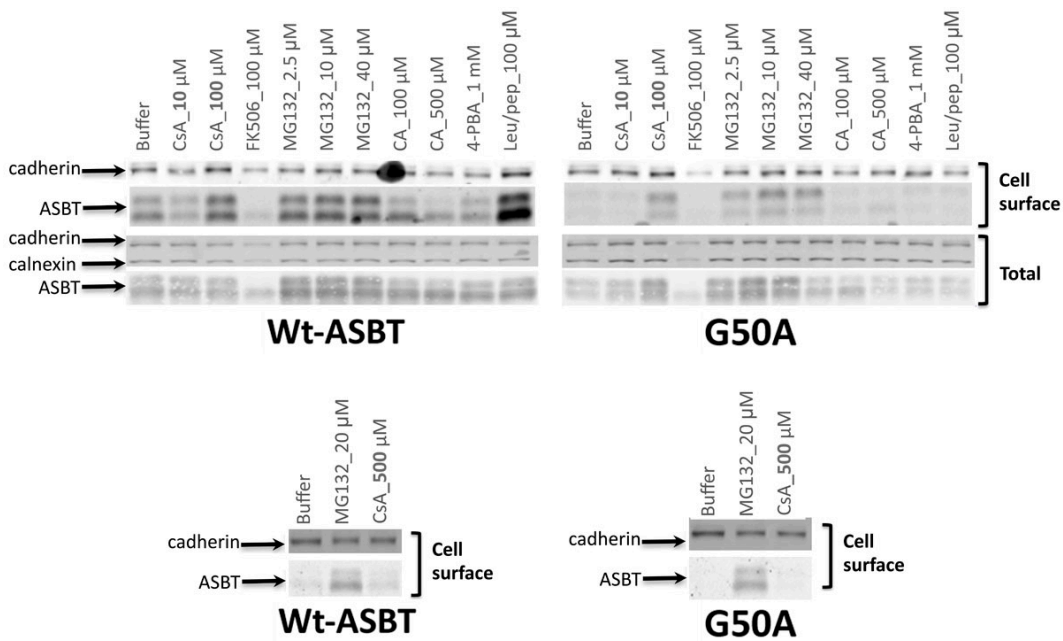


Figure 22. Effect of Degradation Inhibitors/Chaperones on wt-hASBT and G50A Cell Surface Expression

COS-1 cells transfected with G50A or wt-hASBT were treated with CsA (10 and 100 μ M), FK506 (100 μ M), CA (100 and 500 μ M), 4-PBA (1 mM) for 24h and MG132 (2.5, 10 and 40 μ M), leupepsin/pepstatin (50 μ g/mL) NH_4Cl (15 mM) for 8h followed by biotinylation of cell surface proteins 24 – 48 h post-transfection. Cells were lysed and total protein content was determined with Bradford assay. Protein concentrations were equalized, a small aliquot was separated for total protein measurements, from which 7 μ g/lane of wt-ASBT samples and 8.5 μ g/lane of mutants were loaded onto a 12.5% denaturing polyacrylamide gel. Streptavidin beads were added to the remaining lysate, and samples prepared in reducing buffer were loaded on the gel, with mutants always loaded on the same gel as the wt-hASBT control for the corresponding experiment (whole cell or biotinylation).

4.3.4 Integrated data on residues important for hASBT stability

It is well known that replacement or deletion of critical amino acids may potentially obliterate transporter activity or protein expression, likely by disruption of key interactions between the residue and the substrate, or between other amino acids necessary to maintain protein structure. Alternatively, mutation may perturb key steps during protein processing - synthesis, maturation, cell surface expression, turnover rates – and cause protein instability, thereby reducing transporter residence in the cell surface, and finally impairing function. Understanding the mechanism that underlies this effect is vital, not only to gain insight on transporter physiology, but also to properly address diseases caused by transporter malfunction.

Misfolding is one of possible consequences of mutation that will disturb protein stability. Incorrectly folded proteins are rapidly degraded by the strict quality control in the endoplasmic reticulum (ER), the ER-associated degradation (ERAD) pathway, which ensures that defective proteins are cleared from the cell before they reach downstream compartments, such as the Golgi apparatus or the plasma membrane [204]. The ubiquitin-proteasome system (UPS) is the major route of degradation in the ERAD, as well as in the nucleus and the cytosol [205], whereby it recognizes defective proteins, labels them with ubiquitin, and directs them to the proteasome for degradation. Experimentally, unstable mutants can be identified in protein measurements, such as immunoblotting, by poor or absent protein expression in the blots, compared to the non-mutated control. Hampered protein expression in whole cell lysates exhibited by G50A, G50C, C51A, C51S, E54A, E54L, K57A, K57E, C74A, C74T, S112C, S126C, P234C, P234G, E282C (see Appendix A) is an initial indication that Gly⁵⁰, Cys⁵¹, Glu⁵⁴, Lys⁵⁷, Cys⁷⁴, Ser¹¹²,

Ser¹²⁶, Pro²³⁴, and Glu²⁸² may be relevant for hASBT stability. It is important, however, to verify that the protein stability is not mutant-specific. For example, Phe²⁷⁸ replacement with tryptophan (F278W) hampered protein expression, whereas for F278Y both total and surface levels were unaffected. Thus, to reveal the mechanism underlying protein stability unambiguously, it is recommended to perform a variety of mutations and treatments. In fact, additional inspection of Gly⁵⁰, Cys⁵¹, Glu⁵⁴, Lys⁵⁷ corroborated these residues' alleged importance for hASBT stability. Recovery of cell surface expression of G50A, G50C, C51A, C51S, E54A, E54L, K57A and K57E with the proteasomal inhibitor MG132, indicated that these mutants are rapidly degraded by the UPS. Moreover, CsA treatment (discussed below) increased their protein levels at the plasma membrane, suggesting that misfolding may be the basis of their instability, and supporting a role for Gly⁵⁰, Cys⁵¹, Glu⁵⁴, Lys⁵⁷ in hASBT folding.

Another possible consequence of mutation is impaired transporter availability in the cell surface, which is likely due to disruption of key steps during protein trafficking or insertion into the plasma membrane, or protein turnover. Because synthesis or stability is not affected, the mutant protein is retained in the cytoplasm, and can be visualized in whole cell lysates, but not in cell surface measurements. For instance, P234C and I165C (Appendix A) had deficient cell surface expression with virtually unaltered whole cell lysates, suggesting that Pro²³⁴ and Ile¹⁶⁵ may play an important role in hASBT sorting to the plasma membrane or downstream events.

4.4 *Discussion*

We hereby showed that Ala replacement of residues comprising the hASBT IL1 (Cys⁵¹ – Phe⁷²) negatively affected function for 70 % of the mutants, and that hampered function for mutants of a number of residues in the region Cys⁵¹ – Lys⁵⁷ correlated with low or absent protein levels (Figure 17). Treatment of the poorly expressed mutants with MG132 and CsA recuperated protein expression in the cell surface (Figure 19), suggesting that proteasomal degradation accounted for their low protein levels, and was possibly a consequence of folding defects. Further examination of IL1 charged residues by conservative and non-conservative mutations further corroborate the alleged role of Cys⁵¹, Glu⁵⁴ and Lys⁵⁷ in hASBT stability, and of His⁶¹, Lys⁶³ and Pro⁶⁵ in function (Figure 18). Combined, our observations highlight the importance of the first half of IL1 for hASBT stability, and the remaining IL1 residues for transporter function, as suggested in Figure 21.

Notably, CsA increased cell surface expression of the unstable G50A, G50C, C51A, C51S, E54A, E54L, K57A and K57E mutants, suggesting that misfolding would possibly be the basis of their rapid degradation. While this conjecture remains feasible, the observation that CsA also increases wt-hASBT expression was confounding (Figure 22), as one would anticipate the wt-hASBT would not exhibit folding defects. From the PPIase perspective, this increase in wt-hASBT expression is unexpected, as one would predict decreased protein expression, as occurs upon incubation with FK506. Moreover, if the CsA effect observed is due to ligand-induced folding, the effect on wt-hASBT would also be surprising, as one would not anticipate folding defects for the wt transporter, or any need for externally applied chaperone. For the mutants examined, it is

clear that the CsA effect on G50A (Figure 22), C51A, E54A and K57A (Figure 19) is specific, as other treatments did not alter protein levels. In contrast, wt-hASBT levels also increase upon inhibition of lysosomal (leupeptin with pepstatin) as well as proteasomal degradation, suggesting that both these compartments participate in hASBT degradation. Typically, approximately 30 % of newly synthesized proteins exhibit folding defect, and are thus discarded from the cell [212]. It would be interesting to exploit the hypothesis that CsA rescues newly synthesized wt-hASBT, that would otherwise have been rejected by the cell machinery. Similarly, CsA would assist in the folding of the putatively misfolded mutants G50A, C51A, E54A and K57A. Interference with protein turnover, possibly by decreasing the rates of degradation and thereby increasing residence time in the plasma membrane would be an alternative theory for the observed effect in the wt-hASBT. However, this conjecture would not apply for the aforementioned mutants, as they are supposedly short-lived and may not have time to reach the membrane. It is possible that the mechanism underlying the CsA effect is distinct for the wt-hASBT and the mutants. Nonetheless, CsA effect is clearly specific for G50A, C51A, E54A and K57A, since other treatments failed to change the poor protein expression for these mutants. Also noteworthy is the dose-dependent nature of CsA effect on G50A and the wt-hASBT (Figure 22), which exhibits a proportional increase at 10 and 100 μ M, but no effect at 500 μ M CsA. Presently, we are unable to explain these results, but further studies are underway to elucidate this conundrum.

Chapter 5 Discussion and Future Directions

The apical sodium-dependent bile acid transporter (ASBT, SLC10A2) is the chief bile acid transporter in the intestine, and plays a key role in the enterohepatic circulation of bile acids (EHC). Understanding ASBT at the molecular level is essential to gain insight on ASBT physiology and to fully benefit from its potential as a pharmacological target. In the first and second chapters of this dissertation, we describe advances made by our group and others in the quest to understand ASBT structure-function relationships and its complex mechanism of bile acid transport.

5.1 *ASBT Topology*

In chapters 3 and 4, we report contributions of TM1 and IL1 for hASBT function and stability, revealed by a combination of site-directed mutagenesis, bile acid uptake and kinetics, sodium-activation assays, the substituted-cysteine accessibility method, and inhibition of enzymes involved in various stages of protein processing and regulation, such as proline isomerization, and proteasomal and lysosomal degradation. Specifically, the residues located along TM1 putatively participate in sodium transport, whereas a residue placed at the interface of TM1 with IL1, namely, Gly⁵⁰, was shown to be critical for hASBT stability. Expanding our studies to IL1, we identified a cluster of amino acids in the Cys⁵¹ – Lys⁵⁷ region, likely implicated in hASBT protein stability, while residues downstream Lys⁵⁷ appear to be relevant for transport, albeit not by direct interaction with bile acids. Additional studies on sodium kinetics may reveal the role of these residues on ASBT function. We have revealed the role of TM1, TM3, TM4, TM6, TM7, IL1, EL1

and EL3 in hASBT function and stability, and studies on TM2 and TM5 are underway at the time of this writing. Finally, we integrate our data to propose an overall schematic of hASBT transport (Figure 6).

5.2 *ASBT Stability*

Concerning the ASBT stability studies hereby presented, it would be advantageous to provide a definitive explanation to the mechanism of increased protein levels of wt-hASBT and mutants, upon CsA treatment. Cyclosporine A interferes with several transporters in the EHC, including inhibition of NTCP uptake [206], BSEP efflux [207] and bile acid synthesis [202], which may possibly underlie the cholestasis, *i.e.*, obstruction of bile flow, in patients chronically exposed CsA [202, 208]. In contrast to what happens with ASBT, CsA effect on BSEP is not related to transporter protein expression [209]. Considering the physiological and pharmacological relevance of both ASBT and CsA, this question merits further consideration. It would, therefore, be informative to explore the following hypotheses:

5.2.1 Misfolding

Mutation at Gly⁵⁰ may have caused conformational changes that prevented CyPA access to a prolyl bond, resulting in folding defects. While the wt-hASBT is not expected to exhibit folding defects, approximately 30 % of newly synthesized proteins are rejected due folding defects [212]. It would be interesting to exploit the possibility that CsA recovered a proportion of the wt-hASBT that would otherwise have been discarded, and by a similar mechanism (ligand-induced folding), recuperated protein levels for the putatively misfolded G50A, C51A, E54A and K57A.

5.2.2 Increased wt-hASBT exocytosis.

One way to store membrane proteins intracellularly, for subsequent recycling or lysosomal or proteasomal degradation, is by endocytic internalization. For apically-expressed seven-transmembrane G-protein coupled receptors (GPCR), endocytosis participate in receptor downregulation [210]. Xia *et al* [33, 211] proposed a model for ASBT turnover in the cholangiocytes, whereby ASBT resides in the cytoplasm and translocate to the apical membrane by exocytosis upon demand for bile acid uptake. Hulzebos *et al* [202] have shown that the 2-fold increase in rat Asbt expression occurs post-transcriptionally, consistent with our observation that CsA increases wt-hASBT surface levels, it would be feasible to theorize that CsA may act by stimulation of ASBT exocytosis from intracellular vesicles. However, in order to pursue this conjecture, we need to confirm that wt-hASBT cytoplasmic levels, currently inconclusive from whole cell lysate measurements, do not change in presence of CsA.

5.2.3 Altered protein turnover rates or degradation.

Whether a membrane protein resides in the cell surface or temporarily in the cytoplasm (due to synthesis or folding mishaps, or simply awaiting membrane shuttling and recycling), these proteins are eventually degraded in lysosomes or the proteasome. Ubiquitin tagging of intracellular domains can function as a signal for internalization and proteasomal degradation of polytopic proteins [210]. It is possible that CsA inhibited either protein tagging by ubiquitin or downstream events, thereby increasing residence time in the cell surface.

5.2.4 CsA effect is indirect

5.2.4.1 inhibition of ERAD enzymes.

The ERAD may not permit several protein conformers with minor defects to pass its strict quality control. It is possible that CsA inhibited one of the enzymes implicated in this process, and thereby allowed proteins with suboptimal conformations, to escape the ERAD.

5.2.4.2 Recruitment of alternative PPIases or folding pathways.

PPIases are not the sole players during protein folding, and can act together with chaperones, disulfide isomerases, and other folding enzymes [199]. It would be reasonable to think that CyPA inactivation by CsA may have activated other pathways that ensured proper hASBT and mutants's folding. Moreover, our results support FKBP participation in wt-hASBT folding, as inhibition of this enzyme clearly lowers wt-hASBT levels in both whole cell lysates and biotinylated samples (Figure 22). For mutants of Gly⁵⁰, Cys⁵¹, Glu⁵⁴ and Lys⁵⁷, FK506 treatment was inconclusive due to the mutants' originally reduced protein levels. Because both CyPA and FKBP activities are conformation (and not sequence) specific [188], both enzymes are potentially capable of recognizing and binding one or several of the 18 prolyl bonds in hASBT. It would be enlightening to examine a possible competition for hASBT catalysis between these two enzymes.

5.3 Conclusions

As highlighted in the previous chapters of this dissertation, great progress was made in several fronts to understand ASBT's clinical, pharmacological, physiological,

and protein structure-activity features. Nonetheless, in order to obtain a big picture of ASBT transport, several pieces of the puzzle still need to be revealed, including the role of TM2, TM5, IL2, IL3, EL2, and the N-terminus in hASBT function and/or stability. Additionally, a final definition on the relevance of the C-terminus as well as of the single glycosyl moiety in the transporter, in addition to an ASBT crystal structure are yet to be attained. Finally, the development of a mechanistic model that may potentially serve as a general paradigm for proteins in the SLC10 family is highly desirable.

Appendix A: Residues Pertinent To ASBT Function Or Stability, As Reported By The Swaan Laboratory

REF.	Protein/ Mutant	Surface	TCA uptake (% control)	TCA uptake, 12 mM Na ⁺ (% control)	K _m (μM)	J _{max} (pmol.min ⁻¹ .mg protein ⁻¹)
[126]	Wt-hASBT				11.2 ± 0.4	300.2 ± 8.3
[116]	N10D [Ⓢ]	+	48			
	E281A [Ⓢ]	+	≈ 40			
	E282A [Ⓢ]	+	☠			
	E282D [Ⓢ]	+	≈ 50			
	E282K [Ⓢ]	+	☠			
	N328D [Ⓢ]	+	≈ 100			
[86]	Wt-hASBT	+	100		11.1 ± 0.4	300.23 ± 8.3
	C7A [Ⓢ]		85.5		21.8 ± 1.7	83.84 ± 2.5
	C7T [Ⓢ]		131.9			
	C14A [Ⓢ]		101.3		13.5 ± 1.6	419.5 ± 1.0
	C14T [Ⓢ]		76.5			
	C19A [Ⓢ]		66.1		14.3 ± 1.0	291.6 ± 1.7
	C19T [Ⓢ]		149.8			
	C51A [Ⓢ]	+	10.6			
	C51T [Ⓢ]	+	2.7			
	C69A [Ⓢ]		40.4			
	C69T [Ⓢ]		44.2			
	C74A ^{Ⓢ§}	☠	2.5			
	C74T ^{Ⓢ§}	☠	2.6			
	C105A [Ⓢ]	+	2.3			
	C105T [Ⓢ]	+	3.6			
	C106A [Ⓢ]		68.0		7.3 ± 1.1	84.34 ± 5.9
	C106T [Ⓢ]		10.6			
	C132A [Ⓢ]		23.4			
	C132T [Ⓢ]		15.5			

[Ⓢ] On wt-ASBT background

☠ Total loss of function or cell surface expression

	C144A ^④	+	2.3			
	C144T ^①	+	84.0			
	C255A ^①	+	24.1			
	C255T ^①	+	9.6			
	C270A ^①	+	110.3		17.1 ± 3.5	254.3 ± 12.3
	C270T ^①		6.2			
	C314A ^①		60.1			
	C314T ^①		73.0			
[127]; TM1	C270A	+	100		8.9 ± 1.6 (Na ⁺) 9.7 ± 2.4 (TCA)	380.3 ± 16.8 (Na ⁺) 892.8 ± 57.7 (TCA)
	N27A ^①		< 10			
	N27C [●]	+	≈ 25	↓	34.0 ± 8.3 (Na ⁺) 21.5 ± 6.2 (TCA)	934 ± 8.2 (Na ⁺) 312.5 ± 28.7 (TCA)
	N27D ^①		≈ 25			
	N27Q ^①		≈ 25			
	N28C [●]	+	≈ 100		5.5 ± 2.0 (Na ⁺) 17.7 ± 2.2 (TCA)	347.7 ± 25.1 (Na ⁺) 1469.0 ± 55.6 (TCA)
	L30A ^①		≈ 25			
	L30C [●]	+	50	↓	19.5 ± 2.6 (Na ⁺) 59.8 ± 25.0 (TCA)	198.1 ± 8.2 (Na ⁺) 1047.0 ± 183.5 (TCA)
	V33C [●]	+	≈ 100			
	L34C [●]	+	≈ 70		7.5 ± 1.2 (Na ⁺) 11.6 ± 1.7 (TCA)	178.4 ± 6.9 (Na ⁺) 592.7 ± 23.3 (TCA)
	S35C [●]	+	≈ 50		11.3 ± 1.5 (Na ⁺) 5.7 ± 2.6 (TCA)	270.3 ± 9.4 (Na ⁺) 389.5 ± 35.6 (TCA)
	T36C [●]	+	≈ 70		9.9 ± 1.9 (Na ⁺) 8.6 ± 1.6 (TCA)	336.5 ± 16.7 (Na ⁺) 801.8 ± 37.1 (TCA)
	L38A ^①		≈ 70	↓		
	L38C [●]	+	≈ 150	↓	24.1 ± 5.6 (Na ⁺) 10.6 ± 0.9 (TCA)	716.6 ± 54.7 (Na ⁺) 1507.0 ± 32.2 (TCA)
	T39C [●]	+	≈ 100	↓	16.4 ± 2.4 (Na ⁺) 6.3 ± 3.6 (TCA)	406.9 ± 17.5 (Na ⁺) 553.5 ± 70.0 (TCA)
	M46A ^①		≈ 70	↑		

⁴ C144A is a loss of function mutant, associated with BA malabsorption [144]

⁺ Present; measurable levels.

	M46C ^⓪	+	≈ 30	↑	1.3 ± 0.8 (Na ⁺) 8.4 ± 3.3 (TCA)	164.2 ± 8.4 (Na ⁺) 239.2 ± 25.2 (TCA)
	F47C ^⓪	+	100		12.8 ± 2.0 (Na ⁺) 6.5 ± 4.0 (TCA)	297.6 ± 13.0 (Na ⁺) 453.8 ± 64.6 (TCA)
	G50A ^{⓪§}	☒	< 5			
	G50C ^{⓪§}	☒	< 5			
[121];	Wt-hASBT ⁵				11.3 ± 1.9	312.5 ± 12.8
EL1	I103C ^⓪		≈ 500	↓		
	G104C ^⓪		≈ 100	↓		
	T110C ^{⓪⁶}		≈ 150	↓		
	S112C ^{⓪§}	☒	☒			
	L115C ^{⓪⁷}	☒	≈ 200	↓		
	A116C ^⓪		≈ 100	↓		
	Y117C ^⓪	☒	☒			
	V119C ^⓪		≈ 100	↓		
	D120A ^⓪	+	☒			
	D120C ^⓪	+	☒			
	D122A ^⓪	+	↓↓			
	D122C ^⓪	+	☒			
	D124A ^⓪	+	≈ 80		48.5 ± 6.2	1004.4 ± 50.9
	D124N ^⓪				30.1 ± 6.0	361.8 ± 24.2
	S126C ^{⓪§}	☒	☒			
	R254A ^{⓪⁸}		similar to wt		similar to wt	similar to wt
	E281A ^{⓪⁹}				19.6 ± 4.5	131.6 ± 9.0
	E282D ^⓪				12.3 ± 3.4	104.4 ± 7.5
[124];	Wt-hASBT	+	100		11.6 ± 2.39	176.3 ± 7.08
TM3	C270A	+	100		7.9 ± 1.95	655.6 ± 32.46
	S128C ^⓪				17.24 ± 4.74	309.9 ± 20.7
	M129C ^⓪	+				
	T130C ^⓪	+	< 10			
	C132	Endogenous				

⁵ K_{Na+} = 10.4 ± 0.8; Hill coeff = 2.1 ± 0.3

⁶ Only MTSET sensitive mutant in this region

⁷ High uptake despite undetectable cell surface expression. Not detected by NHS-SS-biotin but detected by MTSEA-biotin only in presence of Na⁺.

⁸ K_{Na+} = 22.4 ± 1.3; Hill coeff = 3.0 ± 0.5

⁹ K_{Na+} = 12.3 ± 1.7; Hill coeff = 2.2 ± 0.5

	S133C [○]	+	< 10			
	M141C [○]	+	< 10			
	P142A [○]	↓	< 5			
	P142C [○]	+	⊗			
	P142C [○]	↓	< 5			
	P142G [○]	↓	< 5			
	L143C ^{○10}	+				
	C144 ¹¹	Endogenous				
	L145C [○]	+			16.51 ± 3.77	281.2±15.47
	L146C [○]	+	≤ 50		15.56 ± 3.52	1223 ±65.60
	I147C [○]	+			22.72 ± 4.93	1454±82.81
	Y148C [○]	+				
	T149C [○]					
	F287C [○]				61.52 ± 5.86	1016±32.77
	F289C [○]				34.44 ± 7.37	302.3±18.49
	L291C [○]				35.44 ± 6.32	1047±53.77
	Y293C [○]				72.03 ± 20.83	1364±72.00
[123];	I160C [○]	+	≤ 20			
TM4	P161C [○]	⊗	⊗			
	Y162C [○]	+	≤ 20			
	D163C [○]	+	≈ 100	↓		
	N164C [○]	+	≤ 80			
	I165C ^{○†}	+	≤ 20			
	L169C [○]	+	≤ 80			
	A171C ^{○12}	+	≈ 100	↓		
	L172C ^{○13}	+	≤ 80	↓		
	P175C [○]	+	≈ 100	↓		
	V176C [○]	+	≤ 80			
	S177C [○]	+	≈ 100	↓		
	G179C [○]	+	≤ 20			
	M180C [○]	+	≤ 80			
[120];	C255	endogenous				

¹⁰ 429G>C is a synonymous polymorphism (L143L) in Chinese-American population [144]

¹¹ C144T is a common polymorphism in European-American population [144]

¹² A171S is a functionally silent polymorphism [144]

¹³ 516C>T is a synonymous polymorphism (L172L) [144]

EL3	R256A ^⓪	+	⊗		
	R256C ^⓪	+	⊗		
	T257C ^⓪	+	⊗		
	V258C ^⓪	+	⊗		
	E261A ^⓪	+	< 10%		
	E261C ^⓪	+	⊗		
	T262C ^{⓪14}	+	≈ 100		
	M264C ^{⓪15}	+	≈ 80		
	Q265C ^⓪	+	⊗		
	N266C ^⓪	+	⊗		
	T267C ^⓪	↓	≈ 70		
	T268C ^⓪	+	≈ 40		
	L269C ^⓪	+	< 10		
	C270	endogenous			
	S271C ^⓪	+	< 10		
	T272C ^⓪	+	< 10		
	I273C ^⓪	+	< 10		
	V274C ^⓪	+	≈ 100		
	Q275C ^⓪	+	≈ 30		
	L276C ^⓪	+	≈ 80		
	S277C ^⓪	+	≈ 20–30		
	F278C ^⓪	+	< 10%		
	F278Y ^⓪	+	⊗		
	F278W ^{⓪§}	⊗	⊗		
	T279C ^⓪	↓	≈ 50%		
	P280C ^⓪	+	≈ 20–30%		
	E281C ^⓪	+			
	E282C ^{⓪§}	⊗	---		
	L283C ^⓪	+	≈ 20–30%		
	V285C ^⓪	+			
	V286C ^⓪	+			
[122];	I229C ^⓪	+	↓↓		
TM6	P234A ^{⓪†}	↓	↓		

¹⁴ T262M is a loss of function mutant associated with PBAM, it has normal cell surface expression [144]

¹⁵ M264V is a rare polymorphism [144]

[†] Only surface expression is decreased; levels in the whole cell lysate are normal.

	P234C ^{Ⓣ§}	⊗	⊗			
	P234C ^{Ⓣ§}	⊗	⊗			
	P234G ^{Ⓣ§}	⊗	⊗			
	G237C [Ⓣ]	+	⊗			
	G241C [Ⓣ]	+	⊗			
	L243C ^{Ⓣ16}	+	≈ 150			
	G249C [Ⓣ]	+	↓↓			
	Y253C [Ⓣ]	+	≈ 80			
[119];	C270A	+	100	≈ 80		104.99 ± 3.83
TM7	F287C [Ⓣ]	+	≈ 60	↑		
	F289C [Ⓣ]	+	< 20			
	P290C ^{Ⓣ17}	+	≈ 70			
	L291C [Ⓣ]	+	≈ 60			
	Y293C [Ⓣ]	+	< 20			
	S294C [Ⓣ]	+	≈ 200	↓		
	I295C [Ⓣ]	+	≈ 200	↓		
	F296C [Ⓣ]	↓	≈ 200	↓		
	Q297C [Ⓣ]	+	⊗			
	A301C [Ⓣ]	↓	< 20			
	A302C [Ⓣ]	↓	≈ 80			
	I303C [Ⓣ]	+	≈ 100	↓		
	F304C [Ⓣ]	+	≈ 100	↓		
	G306C [Ⓣ]	↓	> 100	↓		
	F307C ^{Ⓣ§}	↓	⊗			
	Y308C [Ⓣ]	↓	⊗			

¹⁶ L243P is a loss of function mutant associated with PBAM; it has normal cell surface expression [144]

↑ Increased

¹⁷ P290S is a loss of function mutant associated with PBAM [141]. It has normal cell surface expression [189]. In our experiments, P290C was highly solvent accessible.

Ⓣ On C270A background

§ Hampered total protein levels

↓ Decreased

Bibliography

1. Zheng X, Polli JE: Synthesis and *in vitro* evaluation of potential sustained release prodrugs via targeting ASBT. *Int J Pharm*, 396(1-2):111-118.
2. Rais R, Fletcher S, Polli JE: Synthesis and *in vitro* evaluation of gabapentin prodrugs that target the human apical sodium-dependent bile acid transporter (hASBT). *J Pharm Sci*, 100(3):1184-1195.
3. Kramer W, Wess G, Enhsen A, Bock K, Falk E, Hoffmann A, Neckermann G, Gantz D, Schulz S, Nickau L *et al*: Bile acid derived HMG-CoA reductase inhibitors. *Biochim Biophys Acta* 1994, 1227(3):137-154.
4. Konishi T: [Basic studies on the utility of ursodeoxycholic acid derivatives for clinical medicine]. *Yakugaku Zasshi* 2000, 120(1):1-15.
5. Tolle-Sander S, Lentz KA, Maeda DY, Coop A, Polli JE: Increased acyclovir oral bioavailability via a bile acid conjugate. *Mol Pharm* 2004, 1(1):40-48.
6. Balakrishnan A, Polli JE: Apical sodium dependent bile acid transporter (ASBT, SLC10A2): a potential prodrug target. *Mol Pharm* 2006, 3(3):223-230.
7. Kim SK, Lee DY, Lee E, Lee YK, Kim CY, Moon HT, Byun Y: Absorption study of deoxycholic acid-heparin conjugate as a new form of oral anti-coagulant. *J Control Release* 2007, 120(1-2):4-10.
8. Dawson PA: Role of the intestinal bile acid transporters in bile acid and drug disposition. *Handb Exp Pharmacol* (201):169-203.
9. Zheng X, Diao L, Ekins S, Polli JE: Why we should be vigilant: drug cytotoxicity observed with *in vitro* transporter inhibition studies. *Biochem Pharmacol*, 80(7):1087-1092.
10. Zheng X, Ekins S, Raufman JP, Polli JE: Computational models for drug inhibition of the human apical sodium-dependent bile acid transporter. *Mol Pharm* 2009, 6(5):1591-1603.
11. Zheng X, Polli J: Identification of inhibitor concentrations to efficiently screen and measure inhibition K_i values against solute carrier transporters. *Eur J Pharm Sci*, 41(1):43-52.
12. Petzinger E, Geyer J: Drug transporters in pharmacokinetics. *Naunyn Schmiedebergs Arch Pharmacol* 2006, 372(6):465-475.
13. Ghibellini G, Leslie EM, Brouwer KL: Methods to evaluate biliary excretion of drugs in humans: an updated review. *Mol Pharm* 2006, 3(3):198-211.
14. Hofmann AF, Molino G, Milanese M, Belforte G: Description and simulation of a physiological pharmacokinetic model for the metabolism and enterohepatic circulation of bile acids in man. Cholic acid in healthy man. *J Clin Invest* 1983, 71(4):1003-1022.
15. Hagenbuch B, Dawson P: The sodium bile salt cotransport family SLC10. *Pflugers Arch* 2004, 447(5):566-570.

16. Zhang EY, Knipp GT, Ekins S, Swaan PW: Structural biology and function of solute transporters: implications for identifying and designing substrates. *Drug Metab Rev* 2002, 34(4):709-750.
17. Dowling RH, Mack E, Small DM: Effects of controlled interruption of the enterohepatic circulation of bile salts by biliary diversion and by ileal resection on bile salt secretion, synthesis, and pool size in the rhesus monkey. *J Clin Invest* 1970, 49(2):232-242.
18. Grundy SM: Treatment of hypercholesterolemia by interference with bile acid metabolism. *Arch Intern Med* 1972, 130(4):638-648.
19. Hofmann AF: Consequences of bile acid malabsorption. *Mayo Clin Proc* 1973, 48(9):656-659.
20. Lack L: Properties and biological significance of the ileal bile salt transport system. *Environ Health Perspect* 1979, 33:79-89.
21. Packard CJ, Shepherd J: The hepatobiliary axis and lipoprotein metabolism: effects of bile acid sequestrants and ileal bypass surgery. *J Lipid Res* 1982, 23(8):1081-1098.
22. Kulneff-Herlin AE, Herlin PM, Gimmon Z, Kelley RE, Simko V, Fischer JE, Joffe SN: Increased lithogenicity of the bile after jejunoileal bypass in the rat. *Digestion* 1983, 27(1):16-20.
23. Turley SD, West CE: Effect of cholesterol and cholestyramine feeding and of fasting on sterol synthesis in the liver, ileum, and lung of the guinea pig. *Lipids* 1976, 11(7):571-577.
24. Ukai M, Tomura A, Ito M: Cholesterol synthesis in germfree and conventional rats. *J Nutr* 1976, 106(8):1175-1183.
25. Kosters A, Karpen SJ: Bile acid transporters in health and disease. *Xenobiotica* 2008, 38(7-8):1043-1071.
26. Dawson PA, Lan T, Rao A: Bile acid transporters. *J Lipid Res* 2009, 50(12):2340-2357.
27. Dietschy JM: Mechanisms for the intestinal absorption of bile acids. *J Lipid Res* 1968, 9(3):297-309.
28. Lewis MC, Root C: *In vivo* transport kinetics and distribution of taurocholate by rat ileum and jejunum. *Am J Physiol* 1990, 259(2 Pt 1):G233-238.
29. Aldini R, Montagnani M, Roda A, Hrelia S, Biagi PL, Roda E: Intestinal absorption of bile acids in the rabbit: different transport rates in jejunum and ileum. *Gastroenterology* 1996, 110(2):459-468.
30. Hofmann AF, Hagey LR: Bile acids: chemistry, pathochemistry, biology, pathobiology, and therapeutics. *Cell Mol Life Sci* 2008, 65(16):2461-2483.
31. Thomas C, Pellicciari R, Pruzanski M, Auwerx J, Schoonjans K: Targeting bile-acid signalling for metabolic diseases. *Nat Rev Drug Discov* 2008, 7(8):678-693.

32. Kip NS, Lazaridis KN, Masyuk AI, Splinter PL, Huebert RC, LaRusso NF: Differential expression of cholangiocyte and ileal bile acid transporters following bile acid supplementation and depletion. *World J Gastroenterol* 2004, 10(10):1440-1446.
33. Xia X, Francis H, Glaser S, Alpini G, LeSage G: Bile acid interactions with cholangiocytes. *World J Gastroenterol* 2006, 12(22):3553-3563.
34. Bergheim I, Harsch S, Mueller O, Schimmel S, Fritz P, Stange EF: Apical sodium bile acid transporter and ileal lipid binding protein in gallstone carriers. *J Lipid Res* 2006, 47(1):42-50.
35. Hofmann AF: Bile Acids: The Good, the Bad, and the Ugly. *News Physiol Sci* 1999, 14:24-29.
36. Bernstein C, Holubec H, Bhattacharyya AK, Nguyen H, Payne CM, Zaitlin B, Bernstein H: Carcinogenicity of deoxycholate, a secondary bile acid. *Arch Toxicol*, 85(8):863-871.
37. Huff MW, Telford DE, Edwards JY, Burnett JR, Barrett PH, Rapp SR, Napawan N, Keller BT: Inhibition of the apical sodium-dependent bile acid transporter reduces LDL cholesterol and apoB by enhanced plasma clearance of LDL apoB. *Arterioscler Thromb Vasc Biol* 2002, 22(11):1884-1891.
38. Kitayama K, Nakai D, Kono K, van der Hoop AG, Kurata H, de Wit EC, Cohen LH, Inaba T, Kohama T: Novel non-systemic inhibitor of ileal apical Na⁺-dependent bile acid transporter reduces serum cholesterol levels in hamsters and monkeys. *Eur J Pharmacol* 2006, 539(1-2):89-98.
39. Chey WD, Camilleri M, Chang L, Rikner L, Graffner H: A Randomized Placebo-Controlled Phase IIb Trial of A3309, A Bile Acid Transporter Inhibitor, for Chronic Idiopathic Constipation. *Am J Gastroenterol*.
40. Swaan PW, Hillgren KM, Szoka FC, Jr., Oie S: Enhanced transepithelial transport of peptides by conjugation to cholic acid. *Bioconjug Chem* 1997, 8(4):520-525.
41. Li T, Chiang JY: Regulation of Bile Acid and Cholesterol Metabolism by PPARs. *PPAR Res* 2009, 2009:501739.
42. Alrefai WA, Gill RK: Bile acid transporters: structure, function, regulation and pathophysiological implications. *Pharm Res* 2007, 24(10):1803-1823.
43. Xia X, Roundtree M, Merikhi A, Lu X, Shentu S, Lesage G: Degradation of the apical sodium-dependent bile acid transporter by the ubiquitin-proteasome pathway in cholangiocytes. *J Biol Chem* 2004, 279(43):44931-44937.
44. Irvin JL: The secretion and enterohepatic circulation of bile acids; replacement of bile acids in biliary insufficiency. *N C Med J* 1952, 13(4):206-212.
45. Siperstein MD, Hernandez HH, Chaikoff IL: Enterohepatic circulation of carbon 4 of cholesterol. *Am J Physiol* 1952, 171(2):297-301.
46. Baker RD, Searle GW: Bile salt absorption at various levels of rat small intestine. *Proc Soc Exp Biol Med* 1960, 105:521-523.

47. Lack L, Weiner IM: *In vitro* absorption of bile salts by small intestine of rats and guinea pigs. *Am J Physiol* 1961, 200:313-317.
48. Colabufo NA, Berardi F, Perrone MG, Capparelli E, Cantore M, Inglese C, Perrone R: Substrates, inhibitors and activators of P-glycoprotein: candidates for radiolabeling and imaging perspectives. *Curr Top Med Chem*, 10(17):1703-1714.
49. Inglese C, Perrone MG, Berardi F, Perrone R, Colabufo NA: Modulation and Absorption of Xenobiotics: the Synergistic Role of CYP450 AND P-gp Activities in Cancer and Neurodegenerative Disorders. *Curr Drug Metab*.
50. Weiner IM, Lack L: Absorption of bile salts from the small intestine *in vivo*. *Am J Physiol* 1962, 202:155-157.
51. Glasser JE, Weiner IM, Lack L: Comparative Physiology of Intestinal Taurocholate Transport. *Am J Physiol* 1965, 208:359-362.
52. Playoust MR, Lack L, Weiner IM: Effect of Intestinal Resection on Bile Salt Absorption in Dogs. *Am J Physiol* 1965, 208:363-369.
53. Lack L, Weiner IM: The intestinal action of benzmalecene: the relationship of its hypocholesterolemic effect to active transport of bile salts and other substances. *J Pharmacol Exp Ther* 1963, 139:248-258.
54. Tidball CS: Intestinal and Hepatic Transport of Cholate and Organic Dyes. *Am J Physiol* 1964, 206:239-242.
55. Buchwald H: Lowering of Cholesterol Absorption and Blood Levels by Ileal Exclusion. Experimental Basis and Preliminary Clinical Report. *Circulation* 1964, 29:713-720.
56. Holt PR: Intestinal Absorption of Bile Salts in the Rat. *Am J Physiol* 1964, 207:1-7.
57. Holt PR: Competitive inhibition of intestinal bile salt absorption in the rat. *Am J Physiol* 1966, 210(3):635-639.
58. Schiff ER, Small NC, Dietschy JM: Characterization of the kinetics of the passive and active transport mechanisms for bile acid absorption in the small intestine and colon of the rat. *J Clin Invest* 1972, 51(6):1351-1362.
59. Lucke H, Stange G, Kinne R, Murer H: Taurocholate--sodium co-transport by brush-border membrane vesicles isolated from rat ileum. *Biochem J* 1978, 174(3):951-958.
60. Barnard JA, Ghishan FK, Wilson FA: Ontogenesis of taurocholate transport by rat ileal brush border membrane vesicles. *J Clin Invest* 1985, 75(3):869-873.
61. Wilson FA, Burckhardt G, Murer H, Rumrich G, Ullrich KJ: Sodium-coupled taurocholate transport in the proximal convolution of the rat kidney *in vivo* and *in vitro*. *J Clin Invest* 1981, 67(4):1141-1150.
62. Wilson FA, Treanor LL: Glycodeoxycholate transport in brush border membrane vesicles isolated from rat jejunum and ileum. *Biochim Biophys Acta* 1979, 554(2):430-440.

63. Weinman SA: Electrogenicity of Na(+)-coupled bile acid transporters. *Yale J Biol Med* 1997, 70(4):331-340.
64. Craddock AL, Love MW, Daniel RW, Kirby LC, Walters HC, Wong MH, Dawson PA: Expression and transport properties of the human ileal and renal sodium-dependent bile acid transporter. *Am J Physiol* 1998, 274(1 Pt 1):G157-169.
65. Weinman SA, Carruth MW, Dawson PA: Bile acid uptake via the human apical sodium-bile acid cotransporter is electrogenic. *J Biol Chem* 1998, 273(52):34691-34695.
66. Lidofsky SD, Fitz JG, Weisiger RA, Scharschmidt BF: Hepatic taurocholate uptake is electrogenic and influenced by transmembrane potential difference. *Am J Physiol* 1993, 264(3 Pt 1):G478-485.
67. Hagenbuch B, Stieger B, Foguet M, Lubbert H, Meier PJ: Functional expression cloning and characterization of the hepatocyte Na⁺/bile acid cotransport system. *Proc Natl Acad Sci U S A* 1991, 88(23):10629-10633.
68. Geyer J, Doring B, Meerkamp K, Ugele B, Bakhiya N, Fernandes CF, Godoy JR, Glatt H, Petzinger E: Cloning and functional characterization of human sodium-dependent organic anion transporter (SLC10A6). *J Biol Chem* 2007, 282(27):19728-19741.
69. Wilson FA, Treanor LL: Studies of relationship among bile-acid uptake, Na⁺, K⁺-ATPase, and Na⁺ gradient in isolated cells from rat ileum. *Gastroenterology* 1981, 81(1):54-60.
70. Simon FR, Sutherland E, Sutherland J: Selective modulation of hepatic and ileal Na⁺-K⁺-ATPase by bile salts in the rat. *Am J Physiol* 1988, 254(5 Pt 1):G761-767.
71. Lin MC, Kramer W, Wilson FA: Identification of cytosolic and microsomal bile acid-binding proteins in rat ileal enterocytes. *J Biol Chem* 1990, 265(25):14986-14995.
72. Ruoho AE, Kiefer H, Roeder PE, Singer SJ: The mechanism of photoaffinity labeling. *Proc Natl Acad Sci U S A* 1973, 70(9):2567-2571.
73. Oelkers P, Dawson PA: Cloning and chromosomal localization of the human ileal lipid-binding protein. *Biochim Biophys Acta* 1995, 1257(2):199-202.
74. Lin MC, Gong YZ, Geoghegan KF, Wilson FA: Characterization of a novel 14 kDa bile acid-binding protein from rat ileal cytosol. *Biochim Biophys Acta* 1991, 1078(3):329-335.
75. Wong MH, Oelkers P, Craddock AL, Dawson PA: Expression cloning and characterization of the hamster ileal sodium-dependent bile acid transporter. *J Biol Chem* 1994, 269(2):1340-1347.
76. Kramer W, Girbig F, Gutjahr U, Kowalewski S: Radiation-inactivation analysis of the Na⁺/bile acid co-transport system from rabbit ileum. *Biochem J* 1995, 306 (Pt 1):241-246.
77. Mullins JG, Beechey RB, Gould GW, Campbell FC, Shirazi-Beechey SP: Characterization of the ileal Na⁺/bile salt co-transporter in brush border membrane

- vesicles and functional expression in *Xenopus laevis* oocytes. *Biochem J* 1992, 285 (Pt 3):785-790.
78. Chandler CE, Zaccaro LM, Moberly JB: Transepithelial transport of cholyltaurine by Caco-2 cell monolayers is sodium dependent. *Am J Physiol* 1993, 264(6 Pt 1):G1118-1125.
79. Gong YZ, Everett ET, Schwartz DA, Norris JS, Wilson FA: Molecular cloning, tissue distribution, and expression of a 14-kDa bile acid-binding protein from rat ileal cytosol. *Proc Natl Acad Sci U S A* 1994, 91(11):4741-4745.
80. Luxon BA, King PD, Forker EL: Only free bile acid drives ileal absorption of taurocholate. *Am J Physiol* 1986, 250(5 Pt 1):G648-652.
81. Balakrishnan A, Hussainzada N, Gonzalez P, Bermejo M, Swaan PW, Polli JE: Bias in estimation of transporter kinetic parameters from overexpression systems: Interplay of transporter expression level and substrate affinity. *J Pharmacol Exp Ther* 2007, 320(1):133-144.
82. Hidalgo IJ, Borchardt RT: Transport of bile acids in a human intestinal epithelial cell line, Caco-2. *Biochim Biophys Acta* 1990, 1035(1):97-103.
83. Woodcock S, Williamson I, Hassan I, Mackay M: Isolation and characterisation of clones from the Caco-2 cell line displaying increased taurocholic acid transport. *J Cell Sci* 1991, 98 (Pt 3):323-332.
84. Kramer W, Nicol SB, Girbig F, Gutjahr U, Kowalewski S, Fasold H: Characterization and chemical modification of the Na(+)-dependent bile-acid transport system in brush-border membrane vesicles from rabbit ileum. *Biochim Biophys Acta* 1992, 1111(1):93-102.
85. Barnard JA, Ghishan FK: Taurocholate transport by human ileal brush border membrane vesicles. *Gastroenterology* 1987, 93(5):925-933.
86. Banerjee A, Ray A, Chang C, Swaan PW: Site-directed mutagenesis and use of bile acid-MTS conjugates to probe the role of cysteines in the human apical sodium-dependent bile acid transporter (SLC10A2). *Biochemistry* 2005, 44(24):8908-8917.
87. Saeki T, Kuroda T, Matsumoto M, Kanamoto R, Iwami K: Effects of Cys mutation on taurocholic acid transport by mouse ileal and hepatic sodium-dependent bile acid transporters. *Biosci Biotechnol Biochem* 2002, 66(2):467-470.
88. Balakrishnan A, Wring SA, Polli JE: Interaction of native bile acids with human apical sodium-dependent bile acid transporter (hASBT): influence of steroidal hydroxylation pattern and C-24 conjugation. *Pharm Res* 2006, 23(7):1451-1459.
89. Hallen S, Fryklund J, Sachs G: Inhibition of the human sodium/bile acid cotransporters by site-specific methanethiosulfonate sulfhydryl reagents: substrate-controlled accessibility of site of inactivation. *Biochemistry* 2000, 39(22):6743-6750.
90. Hallen S, Bjorquist A, Ostlund-Lindqvist AM, Sachs G: Identification of a region of the ileal-type sodium/bile acid cotransporter interacting with a competitive bile acid transport inhibitor. *Biochemistry* 2002, 41(50):14916-14924.

91. Lack L, Weiner IM: Intestinal bile salt transport: structure-activity relationships and other properties. *Am J Physiol* 1966, 210(5):1142-1152.
92. Heaton KW, Lack L: Ileal bile salt transport: mutual inhibition in an *in vivo* system. *Am J Physiol* 1968, 214(3):585-590.
93. Firpi A, Walker JT, Lack L: Interactions of cationic bile salt derivatives with the ileal bile salt transport system. *J Lipid Res* 1975, 16(5):379-385.
94. Lack L, Tantawi A, Halevy C, Rockett D: Positional requirements for anionic charge for ileal absorption of bile salt analogues. *Am J Physiol* 1984, 246(6 Pt 1):G745-749.
95. Kihira K, Okamoto A, Ikawa S, Mikami T, Yoshii M, Mosbach EH, Hoshita T: Metabolism of sodium 3 alpha,7 alpha-dihydroxy-5 beta-cholane-24-sulfonate in hamsters. *J Biochem* 1991, 109(6):879-881.
96. Miki S, Mosbach EH, Cohen BI, Yoshii M, Ayyad N, McSherry CK: Sulfonate analogues of chenodeoxycholic acid: metabolism of sodium 3 alpha, 7 alpha-dihydroxy-25-homo-5 beta-cholane-25-sulfonate and sodium 3 alpha, 7 alpha-dihydroxy-24-nor-5 beta-cholane-23-sulfonate in the hamster. *J Lipid Res* 1992, 33(11):1629-1637.
97. Lillienau J, Hagey LR, Borgstrom B: Hepatic and ileal transport and effect on biliary secretion of norursocholic acid and its conjugates in rats. *Am J Physiol* 1991, 261(6 Pt 1):G1057-1064.
98. Mills CO, Iqbal S, Elias E: Ileal absorption of tyrosine-conjugated bile acids in Wistar rats. *Biochim Biophys Acta* 1987, 926(2):154-159.
99. Walker S, Stiehl A, Raedsch R, Kloters P, Kommerell B: Absorption of 7-ketolithocholic acid in rat jejunum, ileum and colon. *Z Gastroenterol* 1985, 23(12):681-683.
100. Schmassmann A, Angellotti MA, Ton-Nu HT, Scheingart CD, Marcus SN, Rossi SS, Hofmann AF: Transport, metabolism, and effect of chronic feeding of cholylsarcosine, a conjugated bile acid resistant to deconjugation and dehydroxylation. *Gastroenterology* 1990, 98(1):163-174.
101. Lillienau J, Scheingart CD, Hofmann AF: Physicochemical and physiological properties of cholylsarcosine. A potential replacement detergent for bile acid deficiency states in the small intestine. *J Clin Invest* 1992, 89(2):420-431.
102. Baringhaus KH, Matter H, Stengelin S, Kramer W: Substrate specificity of the ileal and the hepatic Na(+)/bile acid cotransporters of the rabbit. II. A reliable 3D QSAR pharmacophore model for the ileal Na(+)/bile acid cotransporter. *J Lipid Res* 1999, 40(12):2158-2168.
103. Kramer W, Stengelin S, Baringhaus KH, Enhsen A, Heuer H, Becker W, Corsiero D, Girbig F, Noll R, Weyland C: Substrate specificity of the ileal and the hepatic Na(+)/bile acid cotransporters of the rabbit. I. Transport studies with membrane vesicles and cell lines expressing the cloned transporters. *J Lipid Res* 1999, 40(9):1604-1617.

104. Kramer W, Wess G, Schubert G, Bickel M, Girbig F, Gutjahr U, Kowalewski S, Baringhaus KH, Enhsen A, Glombik H *et al*: Liver-specific drug targeting by coupling to bile acids. *J Biol Chem* 1992, 267(26):18598-18604.
105. Kramer W, Wess G, Neckermann G, Schubert G, Fink J, Girbig F, Gutjahr U, Kowalewski S, Baringhaus KH, Boger G *et al*: Intestinal absorption of peptides by coupling to bile acids. *J Biol Chem* 1994, 269(14):10621-10627.
106. Kim DC, Harrison AW, Ruwart MJ, Wilkinson KF, Fisher JF, Hidalgo IJ, Borchardt RT: Evaluation of the bile acid transporter in enhancing intestinal permeability to renin-inhibitory peptides. *J Drug Target* 1993, 1(4):347-359.
107. Swaan PW, Szoka FC, Jr., Oie S: Molecular modeling of the intestinal bile acid carrier: a comparative molecular field analysis study. *J Comput Aided Mol Des* 1997, 11(6):581-588.
108. Kagedahl M, Swaan PW, Redemann CT, Tang M, Craik CS, Szoka FC, Jr., Oie S: Use of the intestinal bile acid transporter for the uptake of cholic acid conjugates with HIV-1 protease inhibitory activity. *Pharm Res* 1997, 14(2):176-180.
109. Zheng X, Pan Y, Acharya C, Swaan PW, Polli JE: Structural requirements of the ASBT by 3D-QSAR analysis using aminopyridine conjugates of chenodeoxycholic acid. *Bioconjug Chem*, 21(11):2038-2048.
110. Balakrishnan A, Wring SA, Coop A, Polli JE: Influence of charge and steric bulk in the C-24 region on the interaction of bile acids with human apical sodium-dependent bile acid transporter. *Mol Pharm* 2006, 3(3):282-292.
111. Rais R, Gonzalez PM, Zheng X, Wring SA, Polli JE: Method to screen substrates of apical sodium-dependent bile acid transporter. *AAPS J* 2008, 10(4):596-605.
112. Gonzalez PM, Acharya C, Mackerell AD, Jr., Polli JE: Inhibition requirements of the human apical sodium-dependent bile acid transporter (hASBT) using aminopiperidine conjugates of glutamyl-bile acids. *Pharm Res* 2009, 26(7):1665-1678.
113. Rais R, Acharya C, Mackerell AD, Polli JE: Structural determinants for transport across the intestinal bile acid transporter using C-24 bile acid conjugates. *Mol Pharm*, 7(6):2240-2254.
114. Rais R, Acharya C, Tririya G, Mackerell AD, Polli JE: Molecular switch controlling the binding of anionic bile acid conjugates to human apical sodium-dependent bile acid transporter. *J Med Chem*, 53(12):4749-4760.
115. Zheng X, Diao L, Ekins S, Polli JE: Why we should be vigilant: drug cytotoxicity observed with *in vitro* transporter inhibition studies. *Biochem Pharmacol* 2009, 80(7):1087-1092.
116. Zhang EY, Phelps MA, Banerjee A, Khantwal CM, Chang C, Helsper F, Swaan PW: Topology scanning and putative three-dimensional structure of the extracellular binding domains of the apical sodium-dependent bile acid transporter (SLC10A2). *Biochemistry* 2004, 43(36):11380-11392.
117. Carpenter EP, Beis K, Cameron AD, Iwata S: Overcoming the challenges of membrane protein crystallography. *Curr Opin Struct Biol* 2008, 18(5):581-586.

118. Banerjee A, Swaan PW: Membrane topology of human ASBT (SLC10A2) determined by dual label epitope insertion scanning mutagenesis. New evidence for seven transmembrane domains. *Biochemistry* 2006, 45(3):943-953.
119. Hussainzada N, Banerjee A, Swaan PW: Transmembrane domain VII of the human apical sodium-dependent bile acid transporter ASBT (SLC10A2) lines the substrate translocation pathway. *Mol Pharmacol* 2006, 70(5):1565-1574.
120. Banerjee A, Hussainzada N, Khandelwal A, Swaan PW: Electrostatic and potential cation-pi forces may guide the interaction of extracellular loop III with Na⁺ and bile acids for human apical Na⁺-dependent bile acid transporter. *Biochem J* 2008, 410(2):391-400.
121. Hussainzada N, Da Silva TC, Zhang EY, Swaan PW: Conserved aspartic acid residues lining the extracellular loop 1 of sodium-coupled bile acid transporter ASBT Interact with Na⁺ and 7alpha-OH moieties on the ligand cholestane skeleton. *J Biol Chem* 2008, 283(30):20653-20663.
122. Hussainzada N, Khandewal A, Swaan PW: Conformational flexibility of helix VI is essential for substrate permeation of the human apical sodium-dependent bile acid transporter. *Mol Pharmacol* 2008, 73(2):305-313.
123. Khantwal CM, Swaan PW: Cytosolic half of transmembrane domain IV of the human bile acid transporter hASBT (SLC10A2) forms part of the substrate translocation pathway. *Biochemistry* 2008, 47(12):3606-3614.
124. Hussainzada N, Claro Da Silva T, Swaan PW: The cytosolic half of helix III forms the substrate exit route during permeation events of the sodium/bile acid cotransporter ASBT. *Biochemistry* 2009, 48(36):8528-8539.
125. Ekins S, Boulanger B, Swaan PW, Hupcey MA: Towards a new age of virtual ADME/TOX and multidimensional drug discovery. *J Comput Aided Mol Des* 2002, 16(5-6):381-401.
126. Ray A, Banerjee A, Chang C, Khantwal CM, Swaan PW: Design of novel synthetic MTS conjugates of bile acids for site-directed sulfhydryl labeling of cysteine residues in bile acid binding and transporting proteins. *Bioorg Med Chem Lett* 2006, 16(6):1473-1476.
127. Claro da Silva T, Hussainzada N, Khantwal CM, Polli JE, Swaan PW: Transmembrane helix I contributes to substrate translocation and protein stability of bile acid transporter SLC10A2. *J Biol Chem*.
128. Saeki T, Munetaka Y, Ueda K, Iwami K, Kanamoto R: Effects of Ala substitution for conserved Cys residues in mouse ileal and hepatic Na⁺-dependent bile acid transporters. *Biosci Biotechnol Biochem* 2007, 71(8):1865-1872.
129. Sun AQ, Salkar R, Sachchidanand, Xu S, Zeng L, Zhou MM, Suchy FJ: A 14-amino acid sequence with a beta-turn structure is required for apical membrane sorting of the rat ileal bile acid transporter. *J Biol Chem* 2003, 278(6):4000-4009.

130. Sun AQ, Balasubramaniyan N, Chen H, Shahid M, Suchy FJ: Identification of functionally relevant residues of the rat ileal apical sodium-dependent bile acid cotransporter. *J Biol Chem* 2006, 281(24):16410-16418.
131. Saeki T, Mizushima S, Ueda K, Iwami K, Kanamoto R: Mutational analysis of uncharged polar residues and proline in the distal one-third (Thr130-Pro142) of the highly conserved region of mouse Slc10a2. *Biosci Biotechnol Biochem* 2009, 73(7):1535-1540.
132. Kubinyi H: Comparative Molecular Field Analysis (CoMFA). In *Handbook of Chemoinformatics. Volume 4*. Edited by Gasteiger J. Weinheim: Wiley-VCH; 2003:1555-1574.
133. Klebe G, Abraham U, Mietzner T: Molecular similarity indices in a comparative analysis (CoMSIA) of drug molecules to correlate and predict their biological activity. *J Med Chem* 1994, 37(24):4130-4146.
134. Ekins S, Boulanger B, Swaan PW, Hupcey MA: Towards a new age of virtual ADME/TOX and multidimensional drug discovery. *Mol Divers* 2002, 5(4):255-275.
135. Izzat NN, Deshazer ME, Loose-Mitchell DS: New molecular targets for cholesterol-lowering therapy. *J Pharmacol Exp Ther* 2000, 293(2):315-320.
136. Oldfield CJ, Ulrich EL, Cheng Y, Dunker AK, Markley JL: Addressing the intrinsic disorder bottleneck in structural proteomics. *Proteins* 2005, 59(3):444-453.
137. Andreeva A, Murzin AG: Structural classification of proteins and structural genomics: new insights into protein folding and evolution. *Acta Crystallogr Sect F Struct Biol Cryst Commun*, 66(Pt 10):1190-1197.
138. Cormier CY, Park JG, Fiacco M, Steel J, Hunter P, Kramer J, Singla R, Labaer J: PSI: Biology-materials repository: a biologist's resource for protein expression plasmids. *J Struct Funct Genomics*, 12(2):55-62.
139. Palczewski K, Kumasaka T, Hori T, Behnke CA, Motoshima H, Fox BA, Le Trong I, Teller DC, Okada T, Stenkamp RE *et al*: Crystal structure of rhodopsin: A G protein-coupled receptor. *Science* 2000, 289(5480):739-745.
140. Lucke C, Zhang F, Ruterjans H, Hamilton JA, Sacchettini JC: Flexibility is a likely determinant of binding specificity in the case of ileal lipid binding protein. *Structure* 1996, 4(7):785-800.
141. Oelkers P, Kirby LC, Heubi JE, Dawson PA: Primary bile acid malabsorption caused by mutations in the ileal sodium-dependent bile acid transporter gene (SLC10A2). *J Clin Invest* 1997, 99(8):1880-1887.
142. Montagnani M, Love MW, Rossel P, Dawson PA, Qvist P: Absence of dysfunctional ileal sodium-bile acid cotransporter gene mutations in patients with adult-onset idiopathic bile acid malabsorption. *Scand J Gastroenterol* 2001, 36(10):1077-1080.
143. Wong MH, Oelkers P, Dawson PA: Identification of a mutation in the ileal sodium-dependent bile acid transporter gene that abolishes transport activity. *J Biol Chem* 1995, 270(45):27228-27234.

144. Ho RH, Leake BF, Urquhart BL, Gregor JC, Dawson PA, Kim RB: Functional Characterization of Genetic Variants in the Apical Sodium-Dependent Bile Acid Transporter (ASBT; SLC10A2). *J Gastroenterol Hepatol*.
145. Hallen S, Branden M, Dawson PA, Sachs G: Membrane insertion scanning of the human ileal sodium/bile acid co-transporter. *Biochemistry* 1999, 38(35):11379-11388.
146. Mareninova O, Shin JM, Vagin O, Turdikulova S, Hallen S, Sachs G: Topography of the membrane domain of the liver Na⁺-dependent bile acid transporter. *Biochemistry* 2005, 44(42):13702-13712.
147. Harvey Lodish AB, S Lawrence Zipursky, Paul Matsudaira, David Baltimore, and James Darnell.: *Molecular Cell Biology, 4th edition*. 4th edition. New York: W. H. Freeman and Company.; 2000.
148. van Geest M, Lolkema JS: Membrane topology and insertion of membrane proteins: search for topogenic signals. *Microbiol Mol Biol Rev* 2000, 64(1):13-33.
149. Grunewald M, Kanner BI: The accessibility of a novel reentrant loop of the glutamate transporter GLT-1 is restricted by its substrate. *J Biol Chem* 2000, 275(13):9684-9689.
150. Brocke L, Bendahan A, Grunewald M, Kanner BI: Proximity of two oppositely oriented reentrant loops in the glutamate transporter GLT-1 identified by paired cysteine mutagenesis. *J Biol Chem* 2002, 277(6):3985-3992.
151. Seal RP, Amara SG: A reentrant loop domain in the glutamate carrier EAAT1 participates in substrate binding and translocation. *Neuron* 1998, 21(6):1487-1498.
152. Iwamoto T, Uehara A, Imanaga I, Shigekawa M: The Na⁺/Ca²⁺ exchanger NCX1 has oppositely oriented reentrant loop domains that contain conserved aspartic acids whose mutation alters its apparent Ca²⁺ affinity. *J Biol Chem* 2000, 275(49):38571-38580.
153. Kast C, Canfield V, Levenson R, Gros P: Transmembrane organization of mouse P-glycoprotein determined by epitope insertion and immunofluorescence. *J Biol Chem* 1996, 271(16):9240-9248.
154. Karlin A, Akabas MH: Substituted-cysteine accessibility method. *Methods Enzymol* 1998, 293:123-145.
155. Mueckler M, Makepeace C: Analysis of transmembrane segment 10 of the Glut1 glucose transporter by cysteine-scanning mutagenesis and substituted cysteine accessibility. *J Biol Chem* 2002, 277(5):3498-3503.
156. Shi L, Simpson MM, Ballesteros JA, Javitch JA: The first transmembrane segment of the dopamine D2 receptor: accessibility in the binding-site crevice and position in the transmembrane bundle. *Biochemistry* 2001, 40(41):12339-12348.
157. Slotboom DJ, Konings WN, Lolkema JS: Cysteine-scanning mutagenesis reveals a highly amphipathic, pore-lining membrane-spanning helix in the glutamate transporter GltT. *J Biol Chem* 2001, 276(14):10775-10781.

158. Barneaud-Rocca D, Borgese F, Guizouarn H: Dual transport properties of anion exchanger 1: the same transmembrane segment is involved in anion exchange and in a cation leak. *J Biol Chem*, 286(11):8909-8916.
159. Zarrabi T, Cervenka R, Sandtner W, Lukacs P, Koenig X, Hilber K, Mille M, Lipkind GM, Fozzard HA, Todt H: A molecular switch between the outer and the inner vestibules of the voltage-gated Na⁺ channel. *J Biol Chem*, 285(50):39458-39470.
160. Pajor AM, Sun NN, Joshi AD, Randolph KM: Transmembrane helix 7 in the Na⁺/dicarboxylate cotransporter 1 is an outer helix that contains residues critical for function. *Biochim Biophys Acta*, 1808(6):1454-1461.
161. Kaback HR, Sahin-Toth M, Weinglass AB: The kamikaze approach to membrane transport. *Nat Rev Mol Cell Biol* 2001, 2(8):610-620.
162. Stroud RM: Transmembrane transporters: an open and closed case. *Proc Natl Acad Sci U S A* 2007, 104(5):1445-1446.
163. Kaback HR: Structure and mechanism of the lactose permease. *C R Biol* 2005, 328(6):557-567.
164. Abramson J, Smirnova I, Kasho V, Verner G, Kaback HR, Iwata S: Structure and mechanism of the lactose permease of Escherichia coli. *Science* 2003, 301(5633):610-615.
165. van Iwaarden PR, Pastore JC, Konings WN, Kaback HR: Construction of a functional lactose permease devoid of cysteine residues. *Biochemistry* 1991, 30(40):9595-9600.
166. Kulkarni AA, Haworth IS, Uchiyama T, Lee VH: Analysis of transmembrane segment 7 of the dipeptide transporter hPepT1 by cysteine-scanning mutagenesis. *J Biol Chem* 2003, 278(51):51833-51840.
167. Mueckler M, Makepeace C: Transmembrane segment 6 of the Glut1 glucose transporter is an outer helix and contains amino acid side chains essential for transport activity. *J Biol Chem* 2008, 283(17):11550-11555.
168. Nebane NM, Hurst DP, Carrasquer CA, Qiao Z, Reggio PH, Song ZH: Residues accessible in the binding-site crevice of transmembrane helix 6 of the CB2 cannabinoid receptor. *Biochemistry* 2008, 47(52):13811-13821.
169. Chen JG, Liu-Chen S, Rudnick G: External cysteine residues in the serotonin transporter. *Biochemistry* 1997, 36(6):1479-1486.
170. Kulkarni AA, Haworth IS, Lee VH: Transmembrane segment 5 of the dipeptide transporter hPepT1 forms a part of the substrate translocation pathway. *Biochem Biophys Res Commun* 2003, 306(1):177-185.
171. Loo TW, Clarke DM: Defining the drug-binding site in the human multidrug resistance P-glycoprotein using a methanethiosulfonate analog of verapamil, MTS-verapamil. *J Biol Chem* 2001, 276(18):14972-14979.

172. Loo TW, Bartlett MC, Clarke DM: Methanethiosulfonate derivatives of rhodamine and verapamil activate human P-glycoprotein at different sites. *J Biol Chem* 2003, 278(50):50136-50141.
173. Henry LK, Adkins EM, Han Q, Blakely RD: Serotonin and cocaine-sensitive inactivation of human serotonin transporters by methanethiosulfonates targeted to transmembrane domain I. *J Biol Chem* 2003, 278(39):37052-37063.
174. Lopez-Corcuera B, Nunez E, Martinez-Maza R, Geerlings A, Aragon C: Substrate-induced conformational changes of extracellular loop 1 in the glycine transporter GLYT2. *J Biol Chem* 2001, 276(46):43463-43470.
175. Pajor AM, Randolph KM: Conformationally sensitive residues in extracellular loop 5 of the Na⁺/dicarboxylate co-transporter. *J Biol Chem* 2005, 280(19):18728-18735.
176. Hussainzada N, Da Silva TC, Zhang EY, Swaan PW: Conserved aspartic acid residues lining the extracellular loop I of sodium-coupled bile acid transporter ASBT interact with Na⁺ and 7 alpha-OH moieties on the ligand cholestane skeleton. *Journal of Biological Chemistry* 2008, 283(30):20653-20663.
177. Hussainzada N, Da Silva TC, Swaan PW: The Cytosolic Half of Helix III Forms the Substrate Exit Route during Permeation Events of the Sodium/Bile Acid Cotransporter ASBT. *Biochemistry* 2009, 48(36):8528-8539.
178. Geyer J, Wilke T, Petzinger E: The solute carrier family SLC10: more than a family of bile acid transporters regarding function and phylogenetic relationships. *Naunyn Schmiedebergs Arch Pharmacol* 2006, 372(6):413-431.
179. Combet C, Blanchet C, Geourjon C, Deleage G: NPS@: network protein sequence analysis. *Trends Biochem Sci* 2000, 25(3):147-150.
180. Absalom NL, Schofield PR, Lewis TM: Pore structure of the Cys-loop ligand-gated ion channels. *Neurochem Res* 2009, 34(10):1805-1815.
181. Jones HM, Hamilton KL, Papworth GD, Syme CA, Watkins SC, Bradbury NA, Devor DC: Role of the NH2 terminus in the assembly and trafficking of the intermediate conductance Ca²⁺-activated K⁺ channel hK1. *J Biol Chem* 2004, 279(15):15531-15540.
182. Perlmutter DH: Chemical chaperones: a pharmacological strategy for disorders of protein folding and trafficking. *Pediatr Res* 2002, 52(6):832-836.
183. Steinmann B, Bruckner P, Superti-Furga A: Cyclosporin A slows collagen triple-helix formation *in vivo*: indirect evidence for a physiologic role of peptidyl-prolyl cis-trans-isomerase. *J Biol Chem* 1991, 266(2):1299-1303.
184. Xu C, Zhang J, Huang X, Sun J, Xu Y, Tang Y, Wu J, Shi Y, Huang Q, Zhang Q: Solution structure of human peptidyl prolyl isomerase-like protein 1 and insights into its interaction with SKIP. *J Biol Chem* 2006, 281(23):15900-15908.
185. van den Berghe PV, Stapelbroek JM, Krieger E, de Bie P, van de Graaf SF, de Groot RE, van Beurden E, Spijker E, Houwen RH, Berger R *et al*: Reduced expression of ATP7B affected by Wilson disease-causing mutations is rescued by pharmacological folding chaperones 4-phenylbutyrate and curcumin. *Hepatology* 2009, 50(6):1783-1795.

186. Zhang Q, Wu J, Pan Z, You G: The Role of Dileucine in the Expression and Function of Human Organic Anion Transporter 1 (hOAT1). *Int J Biochem Mol Biol*, 2(1):31-38.
187. Tuchsien E, Woodward C: Assignment of asparagine-44 side-chain primary amide ¹H NMR resonances and the peptide amide N1H resonance of glycine-37 in basic pancreatic trypsin inhibitor. *Biochemistry* 1987, 26(7):1918-1925.
188. Ivery MT: Immunophilins: switched on protein binding domains? *Med Res Rev* 2000, 20(6):452-484.
189. Kramer W, Girbig F, Glombik H, Corsiero D, Stengelin S, Weyland C: Identification of a ligand-binding site in the Na⁺/bile acid cotransporting protein from rabbit ileum. *J Biol Chem* 2001, 276(38):36020-36027.
190. Zahner D, Eckhardt U, Petzinger E: Transport of taurocholate by mutants of negatively charged amino acids, cysteines, and threonines of the rat liver sodium-dependent taurocholate cotransporting polypeptide Ntcp. *Eur J Biochem* 2003, 270(6):1117-1127.
191. Xu L, Li Y, Haworth IS, Davies DL: Functional role of the intracellular loop linking transmembrane domains 6 and 7 of the human dipeptide transporter hPEPT1. *J Membr Biol*, 238(1-3):43-49.
192. Conseil G, Rothnie AJ, Deeley RG, Cole SP: Multiple roles of charged amino acids in cytoplasmic loop 7 for expression and function of the multidrug and organic anion transporter MRP1 (ABCC1). *Mol Pharmacol* 2009, 75(2):397-406.
193. Yamane K, Akiyama Y, Ito K, Mizushima S: A positively charged region is a determinant of the orientation of cytoplasmic membrane proteins in Escherichia coli. *J Biol Chem* 1990, 265(34):21166-21171.
194. Leatherbarrow RJ, Fersht AR: Investigation of transition-state stabilization by residues histidine-45 and threonine-40 in the tyrosyl-tRNA synthetase. *Biochemistry* 1987, 26(26):8524-8528.
195. Krieger F, Moglich A, Kiefhaber T: Effect of proline and glycine residues on dynamics and barriers of loop formation in polypeptide chains. *J Am Chem Soc* 2005, 127(10):3346-3352.
196. Burns-Hamuro LL, Dalessio PM, Ropson IJ: Replacement of proline with valine does not remove an apparent proline isomerization-dependent folding event in CRABP I. *Protein Sci* 2004, 13(6):1670-1676.
197. Edlich F, Fischer G: Pharmacological targeting of catalyzed protein folding: the example of peptide bond cis/trans isomerases. *Handb Exp Pharmacol* 2006(172):359-404.
198. Schiene C, Fischer G: Enzymes that catalyse the restructuring of proteins. *Curr Opin Struct Biol* 2000, 10(1):40-45.
199. Gothel SF, Marahiel MA: Peptidyl-prolyl cis-trans isomerases, a superfamily of ubiquitous folding catalysts. *Cell Mol Life Sci* 1999, 55(3):423-436.

200. Barik S: Immunophilins: for the love of proteins. *Cell Mol Life Sci* 2006, 63(24):2889-2900.
201. Sauer P, Kloters-Plachky P, Stiehl A: Inhibition of ileal bile acid transport by cyclosporin A in rat. *Eur J Clin Invest* 1995, 25(9):677-682.
202. Hulzebos CV, Wolters H, Plosch T, Kramer W, Stengelin S, Stellaard F, Sauer PJ, Verkade HJ, Kuipers F: Cyclosporin a and enterohepatic circulation of bile salts in rats: decreased cholate synthesis but increased intestinal reabsorption. *J Pharmacol Exp Ther* 2003, 304(1):356-363.
203. Loo TW, Bartlett MC, Clarke DM: Processing mutations located throughout the human multidrug resistance P-glycoprotein disrupt interactions between the nucleotide binding domains. *J Biol Chem* 2004, 279(37):38395-38401.
204. Yoshida Y, Tanaka K: Lectin-like ERAD players in ER and cytosol. *Biochim Biophys Acta*, 1800(2):172-180.
205. Salomons FA, Acs K, Dantuma NP: Illuminating the ubiquitin/proteasome system. *Exp Cell Res*, 316(8):1289-1295.
206. Mita S, Suzuki H, Akita H, Hayashi H, Onuki R, Hofmann AF, Sugiyama Y: Inhibition of bile acid transport across Na⁺/taurocholate cotransporting polypeptide (SLC10A1) and bile salt export pump (ABCB 11)-coexpressing LLC-PK1 cells by cholestasis-inducing drugs. *Drug Metab Dispos* 2006, 34(9):1575-1581.
207. Wolf KK, Vora S, Webster LO, Generaux GT, Polli JW, Brouwer KL: Use of cassette dosing in sandwich-cultured rat and human hepatocytes to identify drugs that inhibit bile acid transport. *Toxicol In Vitro*, 24(1):297-309.
208. Kullak-Ublick GA, Stieger B, Hagenbuch B, Meier PJ: Hepatic transport of bile salts. *Semin Liver Dis* 2000, 20(3):273-292.
209. Yasumiba S, Tazuma S, Ochi H, Chayama K, Kajiyama G: Cyclosporin A reduces canalicular membrane fluidity and regulates transporter function in rats. *Biochem J* 2001, 354(Pt 3):591-596.
210. Shenoy SK: Seven-transmembrane receptors and ubiquitination. *Circ Res* 2007, 100(8):1142-1154.
211. Alpini G, Glaser S, Baiocchi L, Francis H, Xia X, Lesage G: Secretin activation of the apical Na⁺-dependent bile acid transporter is associated with cholehepatic shunting in rats. *Hepatology* 2005, 41(5):1037-1045.
212. Mittal S, Ganesh S: Protein quality control mechanisms and neurodegenerative disorders: Checks, balances and deadlocks. *Neurosci Res* 2010, 68 (3): 159-66.